

One ring to rule them all

Identification and characterization of the type IV pili secretin associated protein TsaP
and analysis of the type IV secretion system of *Neisseria gonorrhoeae*

Philipps



Universität
Marburg

Dissertation

zur Erlangung des Doktorgrades der Naturwissenschaften

(Dr. rer. nat.)

dem Fachbereich Biologie

der Philipps-Universität Marburg

vorgelegt von

Katja Siewering

aus Münster

Marburg an der Lahn, August 2014

“Let me tell you the secret that has led me to my goal.
My strength lies solely in my tenacity.”

Louis Pasteur (1822-1895)

Die Untersuchungen zur vorliegenden Arbeit wurden von Februar 2011 bis April 2014 am Max-Planck-Institut für terrestrische Mikrobiologie unter der Leitung von Dr. Christiaan van der Does durchgeführt.

Vom Fachbereich Biologie der Philipps-Universität Marburg (Hochschulkenziffer:1180) als
Dissertation angenommen am: XX.XX.2014

Erstgutachter: Prof. Dr. Lotte Søgaard-Andersen

Zweitgutachter: Prof. Dr. Erhard Bremer

Weitere Mitglieder der Prüfungskommission:

Prof. Dr. Susanne Önel

Prof. Dr. Stefan Bauer

Tag der mündlichen Prüfung: 25.11.2014

Die während der Promotion erzielten Ergebnisse sind zum Teil in folgenden Originalpublikationen veröffentlicht:

Katja Siewering, Samta Jain, Carmen Friedrich, Mariam T. Webber-Birungi, Dmitry A. Semchonok, Ina Binzen, Alexander Wagner, Stuart Huntley, Jörg Kahnt, Andreas Klingl, Egbert J. Boekema, Lotte Søggaard-Andersen, and Chris van der Does (2014), Peptidoglycan-binding protein TsaP functions in surface assembly of type IV pili. PNAS

Pachulec E., **Siewering K.**, Bender T., Heller E.-M., Salgado-Pabon W., Schmoller S.I., Dillard J.P. and van der Does C. (2014), Functional analysis of the Gonococcal Genetic Island of *Neisseria gonorrhoeae*. Submitted to PLoS ONE

Zweig M., Schork S., Koerdt A., **Siewering K.**, Sternberg C., Thormann K., Albers S.-V., Molin S. and van der Does C. (2013), Secreted single-stranded DNA is involved in the initial phase of biofilm formation by *Neisseria gonorrhoeae*. Environmental Microbiology.

Jain S., Zweig M., Peeters E., **Siewering K.**, Hackett K.T., et al. (2012) Characterization of the Single Stranded DNA Binding Protein SsbB Encoded in the Gonococcal Genetic Island. PLoS ONE 7(4): e35285

I Table of Content

I Table of Content	I
II Table of Figures	V
III List of Tables	VII
IV Abbreviations	IX
Abstract	XI
Zusammenfassung	XIII
1. Introduction	1
1.1 <i>Neisseria gonorrhoeae</i>	1
1.2 Bacterial secretion systems	2
1.2.1 Type IV secretion systems	3
1.2.2 Type IV secretion system of <i>Neisseria gonorrhoeae</i>	6
1.3 Type IV pili system	8
1.3.1 Type IV pili assembly machinery	10
1.3.2 LysM domain containing proteins in Type IV pili systems	13
1.3.3 Secretin	14
2. Scope of the thesis	18
3. Material and Methods	19
3.1 Material	19
3.1.1 Strains	19
3.1.2 Plasmid	20
3.1.3 Oligonucleotides	23
3.1.4 Media and Media supplements	26
3.1.5 Antibiotics	27
3.1.6 Buffer and solutions	28
3.1.6 DNA & Protein Ladder	32
3.1.7 Kits	32
3.2 Microbiological and molecular biological methods	32
3.2.1 Cultivation <i>E. coli</i>	32
3.2.2 Cultivation of <i>N. gonorrhoeae</i>	33
3.3 Molecular methods	33

3.3.1 Isolation of genomic DNA from <i>N. gonorrhoeae</i>	33
3.3.2 Isolation of plasmid DNA	33
3.2.3 Agarose gel electrophoresis	33
3.3.4 Polymerase Chain Reaction	33
3.3.4.1 Standard PCR	33
3.3.4.2 Colony PCR	34
3.3.5 RNA isolation	34
3.3.6 First Strand cDNA Synthesis	34
3.3.7 Transcriptional mapping	35
3.3.8 Real-Time PCR	35
3.3.9 Restriction enzyme digestion	36
3.3.10 Ligation	36
3.3.11 Transformation of <i>E. coli</i>	36
3.3.12 Transformation of <i>N. gonorrhoeae</i>	37
3.3.12.1 Natural transformation of <i>N. gonorrhoeae</i>	37
3.3.12.2 Electroporation of <i>N. gonorrhoeae</i>	37
3.3.13 Preparation of <i>N. gonorrhoeae</i> membranes	37
3.3.14 Phenol treatment of <i>N. gonorrhoeae</i> membranes	38
3.3.15 Bacterial adenylate cyclase two-hybrid system	38
3.4 Analytical and biochemical methods	38
3.4.1 SDS-Polyacrylamid-Gel electrophoresis	38
3.4.2 Blue-Native gel electrophoresis	38
3.4.3 Western Blotting	39
3.4.4 Coomassie-Staining	39
3.4.5 Peptidoglycan isolation, binding and zymography	39
3.4.6 Outer membrane detachment assay	40
3.4.7 Outer membrane solubilization	40
3.4.8 Mass spectrometry of non-solubilized fractions	40
3.4.9 Electron microscopy	40
3.4.10 Purification of TsaP	41
3.4.11 Purification of TsaP Δ A33-R83	41

3.4.12 Purification of HA-PilQ(B1/B2)-CPD-His ₁₀	41
3.4.13 Purification of- MalE-TsaP _{MX}	42
3.4.14 Purification of His ₆ -PilQ _{MX} aa20-656	42
3.4.15 Protein-Protein Interaction Assay	42
3.5. Bioinformatical methods	42
3.5.1 Reciprocal BlastP analysis	42
4. Results	44
4.1 Analysis of the Gonococcal Genetic Island	44
4.1.1 Transcriptional mapping of the Gonococcal Genetic Island	44
4.1.2 Analysis of the expression of the single stranded binding protein SsbB	45
4.1.3 DNA secretion facilitates biofilm formation	46
4.2 The peptidoglycan-binding protein TsaP functions in surface assembly of type IV pili	48
4.2.1 Identification of a protein associated with secretin complexes of type IV pili in <i>N. gonorrhoeae</i>	48
4.2.2 Analysis of TsaP in membranes	52
4.2.3 His ₁₀ -TsaP can be purified as a highly stable monomer	53
4.2.4 TsaP binds to peptidoglycan	55
4.2.5 Lack of TsaP affects surface assembly of T4P	56
4.2.6 The peripheral structure of the secretin complex is lost in the $\Delta tsaP$ mutant	57
4.2.7 TsaP homologs are specifically found in bacteria encoding T4aPS	58
4.3 Analysis of TsaP domains and their function	60
4.3.1 Domain prediction	60
4.3.2 Lack of the gonococcal linker domain of TsaP affects surface assembly of T4P	62
4.3.3 The peripheral structure of the secretin complex is lost in the <i>tsaP</i> Δ S213-V245 mutant	63
4.4 Interaction of TsaP with other components of the type IV pili system	64
4.4.1 Identification of protein-protein interaction between TsaP and PilQ using a bacterial adenylate cyclase two-hybrid system	64
4.4.2 PilQ(B1/B2) can be purified as a stable dimer	65
4.4.3 TsaP Δ LysM forms a SDS stable multimer	67
4.4.4 PilQ _{MX} and TsaP _{MX} can be purified as stable dimers	70
4.4.5 Identification of protein-protein interaction between TsaP and PilQ	72
5. Discussion	75

5.1 Analysis of the Gonococcal Genetic Island	75
5.2 The peptidoglycan-binding protein TsaP functions in surface assembly of type IV pili	76
5.3 Analysis of TsaP domains and their function	78
5.4 Interaction of TsaP with other components of the type IV pili system	79
5.5. Conclusion	81
6. Literature	83
V Supplementary Data	97
VI Acknowledgments	98
VII Curriculum Vitae	99
VIII Erklärung	101

II Table of Figures

Figure 1 Schematic representation of the type IV secretion system.....	6
Figure 2 Schematic representation of the genetic map of the GGI of <i>N. gonorrhoeae</i>	7
Figure 3 Schematic representation of the type IV pili system	8
Figure 4 Structure of pilin subunits in the type IV pilus fiber	11
Figure 5 Schematic overview of secretin domain structure	15
Figure 6 Structural comparison of secretin complexes of the type II secretion system and type IV pili system	17
Figure 7 GeneRuler™ 1kb Plus DNA Ladder	32
Figure 8 PageRuler Prestained Protein Ladder Plus.....	32
Figure 9 NativeMark™ Unstained Protein Standard.....	32
Figure 10 Transcription analysis of the genes encoded in the Gonococcal Gentic Island	45
Figure 11 Analysis of the transcription of the <i>yfa-yef</i> region	46
Figure 12 Deletion of the <i>traB</i> gene results in a strong decrease of biofilms formation	47
Figure 13 Solubilization of His ₈ -PliQ containing outer membrane	48
Figure 15 Analysis of purified PilQ by electron microscopy.....	49
Figure 14 Solubilized His ₈ -PilQ purification.....	49
Figure 16 Projection maps of single particle electron microscopy analysis of the PilQ complex from <i>N. gonorrhoeae</i>	50
Figure 17 Identification of TsaP (NGFG_01788)	50
Figure 18 Alignment of TsaP homologs of different organisms.....	51
Figure 19 Membrane binding of TsaP depends on PilQ.....	53
Figure 20 Purification of His ₁₀ -TsaP.....	54
Figure 21 Characterization of binding of TsaP to isolated peptidoglycan sacculi.....	55
Figure 22 TsaP is important for T4P-dependent colony morphology.....	56
Figure 23 Deletion of TsaP leads to formation of membrane protrusions containing T4P in <i>N. gonorrhoeae</i>	56
Figure 24 Projection maps of single particle electron microscopy analysis of the PilQ complex from the <i>N. gonorrhoeae</i> Δ <i>tsaP</i> / <i>tsaP</i> ⁺ strain.....	57
Figure 25 TsaP levels are reduced in membranes of the Δ <i>pilQ</i> strain, but not in the membranes of the Δ <i>pilC</i> , Δ <i>pilF</i> , Δ <i>pilP</i> and Δ <i>pilW</i> strains	58
Figure 26 Identification of genes encoding TsaP homologs and T4aPS related genes in different genomes.....	59

Figure 27 Model prediction for TsaP and TsaP _{MX}	60
Figure 28 Domain architecture of TsaP.....	61
Figure 29 The linker domain of TsaP is important for T4P-dependent colony morphology	62
Figure 30 Deletion of the gonococcal TsaP-linker domain leads to the loss of surface exposed T4P in <i>N. gonorrhoeae</i>	63
Figure 31 Projection maps of single particle electron microscopy analysis of the PilQ complex from <i>N. gonorrhoeae</i>	64
Figure 32 Binary interactions between TsaP and PilQ of <i>N. gonorrhoeae</i> using a bacterial adenylate cyclase two-hybrid (BACTH) system	65
Figure 33 Ni ²⁺ -affinity purification of HA-PilQ(B1B2)-CPD-His ₁₀	66
Figure 34 Size exclusion chromatography of HA-PilQ(B1/B2)-CPD-His ₁₀	67
Figure 35 Ni ²⁺ -affinity purification of His ₁₀ - TsaPΔA33-R83	68
Figure 36 Size exclusion chromatography of His ₁₀ - TsaPΔA33-R83	69
Figure 37 Blue Native PAGE analysis of His ₁₀ -TsaPΔA33-R83	70
Figure 38 Size exclusion chromatography of His ₆ - PilQ _{MX} (aa20-656)	71
Figure 39 Size exclusion chromatography of Male-TsaP _{MX}	72
Figure 40 Analysis of complex formation of TsaP and PilQ by SEC.....	73
Figure 41 Analysis of complex formation of TsaP and PilQ by SEC.....	73
Figure 42 EM analysis of TsaPΔA33-R83 and the high molecular weight complex of the TsaP/PilQ interaction assay	74

III List of Tables

Table 1 <i>Neisseria gonorrhoeae</i> proteins involved in type IV pilus biogenesis.....	9
Table 2 <i>Neisseria gonorrhoeae</i> strains used in this study	19
Table 3 <i>Escherichia coli</i> strains used in this study	20
Table 4 Plasmids used in this study	20
Table 5 Oligonucleotides used in this study	23
Table 6 Lysogeny Broth (LB) medium	26
Table 7 LB agar.....	26
Table 8 GCBL medium.....	26
Table 9 GCB agar.....	27
Table 10 Supplement I (100 x)	27
Table 11 Supplement II (1000 x)	27
Table 12 Sodium bicarbonate (100 x)	27
Table 13 Antibiotics used in this study	27
Table 14 Assay buffer.....	28
Table 15 Coomassie staining solution.....	28
Table 16 Destaining solution.....	28
Table 17 Lysis buffer	28
Table 18 Protein purification buffer A	28
Table 19 Protein purification buffer B	28
Table 20 Protein purification buffer C	29
Table 21 Protein purification buffer D	29
Table 22 Protein purification buffer E.....	29
Table 23 Protein purification buffer F.....	29
Table 24 Protein purification buffer G	29
Table 25 Protein purification buffer H	29
Table 26 Protein purification buffer I	30
Table 27 Protein purification buffer J	30
Table 28 Protein purification buffer K	30
Table 29 Resolving-gel buffer	30
Table 30 Sodium Boric Acid buffer (20x; pH 8,5)	30

Table 31 Stacking-gel buffer	30
Table 32 TBS buffer	30
Table 33 TBST+I buffer	31
Table 34 TGS buffer.....	31
Table 35 Transfer buffer	31
Table 36 6x DNA loading dye	31
Table 37 5x Protein loading dye.....	31
Table 38 Kits used in this study.....	32
Table 39 Pipetting scheme of a 50µl PCR reaction	34
Table 40 Components of reverse transcriptase mixture	35
Table 41 Pipetting scheme of a 50µl transcriptional mapping PCR.....	35
Table 42 Pipetting scheme of a 25 µl qRT-PCR reaction.....	36
Table 43 Pipetting scheme of a 20 µl ligation reaction.....	36
Table 44 Pipetting scheme of Blue native PAGE gels.....	39
Table 45 Nomenclature of TsaP homologs and ATPase and secretin proteins of T4P assembly systems and T2SS of different organisms	59
Table 46 Reciprocal blast analysis of the 450 genomes of proteobacteria	97

IV Abbreviations

APS	Ammonium persulfate
BN/PAGE	Blue native polyacrylamide gel electrophoresis
bp	base pairs
BSA	Bovine serum albumin
CHAPS	3-[(3-Cholamidopropyl)dimethylammonio]-1-propanesulfonate
CLSM	Confocal laser scanning microscopy
C-terminus	Carboxyl-terminus
CV	Column volume
DDM	n-dodecyl- α -D-maltopyranoside
dot/icm system	defective for organelle trafficking/intracellular multiplication
DTT	Dithiothreitol
DUS	DNA uptake sequence
EM	Electron microscopy
GGI	Gonococcal Genetic Island
Gsp	General secretion pathway
h	Hour(s)
IM	Inner membrane
IMAC	immobilized metal ion affinity chromatography
IPTG	Isopropyl β -D-1-thiogalactopyranoside
LOS	Lipooligosaccharide
min	Minutes
MPF	mating pair formation
N-terminus	Amino-terminus
OD	Optical density
OM	Outer membrane
OPA	Colony opacity-proteins
ORF	Open reading frame
PCR	polymerase chain reaction
pN	piconewton
psig	Pounds per square inch gage
Ptl-system	pertussis toxin liberation system
PVDF	Polyvinylidene fluoride
RT	Room temperature
s	seconds
SBA	Sodium boric acid buffer + EDTA
SDS/PAGE	Sodium dodecyl sulfate polyacrylamide gel electrophoresis
SEC	Size exclusion chromatography
ss	Signal sequence
T4P	Type IV pili
T4PS	Type IV pili system
Tat pathway	Twin-arginine pathway

TCA	Trichloroacetic acid
TGS	Tris-Glycine-SDS buffer
TRiP	transfer DNA immunoprecipitation
TxS	Type X secretion
TxSS	Type X secretion system
WT	Wild type

Abstract

Over the years, *N. gonorrhoeae* has evolved and acquired different mechanisms to protect itself against a variety of antibiotics and chemotherapeutic agents. One reason for the rapid spread of antibiotic resistance in gonococci is the highly effective horizontal gene transfer. The transferred DNA is either provided directly via conjugation, or via the environment via autolysis or the gonococcal type IV secretion system (T4SS), which secretes ssDNA into the extracellular milieu. DNA uptake from the environment in *Neisseria* involves the type IV pili (T4P) and the competence system, transporting the DNA across the outer and the inner membrane, respectively. Functional characterization of the type IV secretion system and DNA uptake system and thus the type IV pili machinery in *N. gonorrhoeae* could provide starting points in the exploration of new therapeutic strategies.

To better understand the transcriptional regulatory network of the type IV secretion system of *N. gonorrhoeae* transcriptional mapping of genes essential for DNA secretion was performed. This revealed that genes essential for DNA secretion are encoded within four different operons. Additional analysis of a region, which is not essential for DNA secretion, encoding the single-stranded DNA binding protein SsbB and the topoisomerase TopB showed that these genes are significantly more highly transcribed than genes that are involved in DNA secretion, such as the coupling protein TraD and the relaxase Tral. To investigate whether the single-stranded DNA, which is secreted via the T4SS encoded within the GG1 facilitates biofilm formation, biofilm formation of *N. gonorrhoeae* strains were analyzed in continuous flow-chamber systems by confocal laser scanning microscopy. This showed that the ssDNA secreted via the T4SS plays a role in the early stages of biofilm formation.

In *Neisseria gonorrhoeae*, the native PilQ secretin ring embedded in OM sheets is surrounded by an additional peripheral structure, consisting of a peripheral ring and seven extending spikes. To unravel proteins important for formation of this additional structure, we identified proteins that are present with PilQ in the OM. One such protein, which was named TsaP, the T4P secretin-associated protein, was identified as a widely conserved component that co-occurs with genes for T4P in Gram-negative bacteria. TsaP contains an N-terminal carbohydrate-binding lysin motif (LysM) domain and a C-terminal domain of unknown function. In *N. gonorrhoeae*, lack of TsaP results in the formation of membrane protrusions containing multiple T4P, concomitant with reduced formation of surface-exposed T4P. Lack of TsaP did not affect the oligomeric state of PilQ, but resulted in loss of the peripheral structure around the PilQ secretin. TsaP binds peptidoglycan and associates strongly with the outer membrane in a PilQ-dependent manner. In addition, we identified that TsaP contains apart from the LysM domain, two FlgT-like domains and a linker region, which is specific for *Neisseria spp.* We could show that the linker domain plays an important role in pilus biogenesis in the β -proteobacterium *N. gonorrhoeae*. In order to determine if TsaP directly interacts with PilQ via the B2 domain, PilQ and TsaP of *N. gonorrhoeae* and *M. xanthus* were heterologously expressed and purified. Characterization of the heterologously expressed and purified proteins showed that TsaP is able to form SDS-stable complexes, resembling a ring-like structure, and that it might interact with PilQ, forming a double ring structure. In general, we propose that TsaP anchors the secretin to the PG to enable the secretin to withstand the forces generated during pilus extension and retraction.

Because T4P play an important role in the pathogenesis of many bacteria and TsaP is found in all bacteria that express T4aP and plays an important role in T4aP biogenesis, it might be an important future drug target.

Zusammenfassung

Im Laufe der Jahre hat *Neisseria gonorrhoeae* verschiedene Mechanismen entwickelt, um sich gegen eine Vielzahl von Antibiotika und Chemotherapeutika zu schützen. Die Hauptursache für diese rasche Ausbreitung von Resistenzen ist ein sehr effizienter horizontaler Gentransfer. Die zu transferierende DNA wird dabei entweder mittels Konjugation direkt übertragen oder durch Autolyse der Gonokokken bzw. durch Sekretion von Einzelstrang DNA durch ein Typ-IV-Sekretionssystem (T4SS) an das extrazelluläre Milieu abgegeben. Die Aufnahme von DNA aus dem extrazellulären Milieu erfolgt in *N. gonorrhoeae* durch Typ-IV-Pili (T4P) sowie das Kompetenz-System, welche DNA über die äußere und die innere Membran transportieren. Die funktionelle Charakterisierung des Typ-IV-Sekretionssystems und des DNA-Aufnahme-Systems und somit der Typ-IV-Pili-Maschinerie könnte neue Anhaltspunkte für die Entwicklung therapeutischer Strategien liefern.

Um das Transkriptionsnetzwerk des Typ-IV-Sekretionssystems in *N. gonorrhoeae* besser zu verstehen, wurden die für die DNA-Sekretion essentiellen Gene transkriptionell kartiert. Dieser Ansatz ergab, dass diese Gene in vier verschiedenen Operons enthalten sind. Die Analyse einer für die DNA-Sekretion nicht essentiellen Region, welche für das Einzelstrang-DNA bindende Protein SsbB sowie die Topoisomerase TopB kodiert, zeigte ferner, dass diese Gene signifikant höher exprimiert wurden als die an der DNA-Sekretion essentiell beteiligten Gene. Um zu untersuchen, ob die Einzelstrang-DNA, welche über das T4SS sekretiert wird, die Bildung von Biofilm erleichtert, wurde die Fähigkeit verschiedener *N. gonorrhoeae*-Stämme zur Biofilm-Bildung mittels konfokaler *Laser Scanning*-Mikroskopie untersucht. Diese Analysen zeigten, dass die durch das T4SS sekretierte Einzelstrang-DNA eine Rolle in den frühen Stadien der Biofilmbildung spielt.

In *N. gonorrhoeae* ist der in der äußeren Membran lokalisierte und durch PilQ gebildete Sekretin-Ring von einer zusätzlichen peripheren Struktur umgeben. Diese besteht aus einem peripheren Ring und sieben davon ausgehenden Zacken. Um Proteine zu identifizieren, die für die Bildung der peripheren Struktur wichtig waren, wurden Proteine analysiert, die mit PilQ in der äußeren Membran lokalisiert sind. Durch dieses Vorgehen konnte ein Protein, das TsaP, kurz für Type-IV-Pilus-Sekretin-assoziiertes Protein, genannt wurde, als stark konservierte T4P-Komponente identifiziert werden. TsaP enthält ein N-terminales Kohlenhydrat bindendes Lysin-Motiv, auch als LysM-Domäne bekannt, und eine C-terminale Domäne mit unbekannter Funktion. In *N. gonorrhoeae* resultierte die Deletion von TsaP in der Bildung von Membranausstülpungen, die mit einer verminderten Bildung von oberflächenexponierten T4P einherging. Ferner konnte gezeigt werden, dass eine Deletion von TsaP keinen Einfluss auf den oligomerisations Zustand von PilQ hatte, jedoch zu einem Verlust der peripheren Struktur um PilQ führte. Weitere Analysen zeigten, dass TsaP an Peptidoglycan band und in Abhängigkeit von PilQ mit der äußeren Membran assoziierte. Darüber hinaus konnten neben der LysM-Domäne zwei FlgT-ähnliche Domänen und eine Linker-Region, die spezifisch für *Neisseria spp.* ist, ermittelt werden. Wir konnten zeigen, dass die Linker-Domäne in *N. gonorrhoeae* eine wichtige Rolle bei der Pilus-Biogenese spielte. Um festzustellen, ob TsaP direkt mit der B2-Domäne von PilQ interagiert, wurden TsaP und PilQ von *N. gonorrhoeae* und *M. xanthus* heterolog überexprimiert und gereinigt. Die Charakterisierung dieser Proteine zeigte, dass TsaP in der Lage war, SDS-stabile Komplexe zu bilden, welche eine ringförmige Struktur aufwiesen, und dass

TsaP wahrscheinlich durch Interaktion mit PilQ eine Doppelringstruktur bildete. Wir vermuten, dass TsaP durch direkte Protein-Protein-Interaktion mit PilQ den Sekretin-Ring in der Peptidoglycan-Zellwand verankert und es dem Sekretin-Ring dadurch ermöglicht, den während der Pilus-Bildung und -Retraktion erzeugten Kräfte standzuhalten. Da T4P eine wichtige Rolle für die Pathogenität vieler Bakterien spielen und TsaP in Bakterien, die T4aP exprimieren, vorkommt und eine wichtige Funktion bei der T4aP-Biogenese hat, könnte TsaP einen neuen Angriffspunkt für zukünftige therapeutische Strategien darstellen.

1. Introduction

1.1 *Neisseria gonorrhoeae*

Neisseria gonorrhoeae, first described by Albert Ludwig Sigismund Neisser in 1879, is a Gram-negative diplococcus, which is 0.6-1.0 µm in diameter, and belongs to the family of Neisseriaceae [1, 2]. The only currently identified human pathogens within this family are *N. gonorrhoeae*, the causative agent of the sexually transmitted infection gonorrhoea, and *Neisseria meningitidis*, an agent of acute bacterial meningitis [2]. In contrast to infections with *N. meningitidis*, gonococcal infections have a high prevalence and low mortality.

Gonococcal infections are acquired by sexual contact and are generally limited to mucosal epithelia of the urethra in men and the endocervix in women, but *N. gonorrhoeae* can also infect tissues like the throat, the rectum and the conjunctiva of the eye [3]. Despite effective antibiotic therapies, there are still about 106 million gonococcal infections occurring worldwide each year [4]. This can be explained by the fact that up to 15 % of infected men and 80 % of infected women remain without symptoms. In addition, individuals infected with *N. gonorrhoeae* do not develop protective antibodies. Reasons for this are the evolved immune evasion strategies, including the production of excess membrane, forming membrane vesicles known as blebs [5] and the consecutively or simultaneously expressed a variety of pathogenicity factors, like colony opacity-proteins (Opa) [6-8], porins [9, 10], outer membrane lipooligosaccharides (LOS) [11] as well as type IV pili (T4P), that frequently undergo antigenic- and phase variation [12].

Over the years *N. gonorrhoeae* has evolved and acquired many mechanisms to protect itself against a variety of antibiotics and chemotherapeutic agents. One reason for the rapid spread of antibiotic resistances in *N. gonorrhoeae* is caused by its ability to rapidly take up and transform DNA from the environment, gaining additional genetic information (e.g. genetic variability and antibiotic marker) that enhances its survival [13]. It has been shown that *Neisseria* preferentially takes up DNA that has a nonpalindromic 10 or 12 bp nucleotide sequence (5'-ATGCCGTCTGAA-3'), termed the DNA uptake sequence (DUS) [14, 15]. The transferred DNA is either provided by autolysis or by the gonococcal type IV secretion system, which secretes ssDNA into the extracellular milieu [16-18]. DNA uptake in *Neisseria* involves the T4P as well as the competence system, transporting the DNA across the outer and the inner membrane, respectively.

The aim of this thesis was to study the operon structure within the regions containing the genes involved in DNA release via the type IV secretion system encoded within the Gonococcal Genetic Island (GGI) of *N. gonorrhoeae* and to analyze the outer membrane components of the type IV pili system. Both systems are involved in the transfer of DNA and will be described in detail in the upcoming sections.

1.2 Bacterial secretion systems

Bacterial secretion systems are multi-subunit complexes that are present in a large number of bacterial species. In Gram-negative bacteria, secretion systems have to span both the inner and outer membrane. Previously, 6 different classes of secretion systems have been identified in Gram-negative bacteria [19]. Within the type I, type III, type IV and type VI secretion systems, macromolecules are transferred in a one-step process, whereas in type II and type V secretion systems macromolecules are first exported via the Sec or twin-arginine (Tat) pathway into the periplasm and are then translocated across the outer membrane. Within this chapter only the type II and the type IV secretion systems will be discussed.

Type II secretion systems (T2SSs), which were first discovered in *Klebsiella oxytoca* [20], are dominantly found in bacterial pathogens of plants, animals and humans. In bacteria, the type II secretion systems secrete folded and/or oligomeric exoproteins in a two-step process. In the initial step, the protein is transported across the inner membrane via the Sec or Tat protein translocation machineries [21, 22]. Once in the periplasm, the effector proteins are folded and transported across the outer membrane by the T2SS. The T2SS, which has also been called the general secretion pathway (*Gsp*) or the secreton, is a multiprotein complex, which spans the inner and outer membrane [23] and is encoded by a set of 12 to 16 genes [24]. The core components, forming this multiprotein complex can be grouped into four subassemblies: the pseudopilus, the outer membrane complex, the inner membrane complex and the secretion ATPase. The pseudopilus, which is formed by five different pseudopilins with multiple copies of the major pseudopilin subunit, is mainly a periplasmic structure. Studies of the major pseudopilin subunit GspG of *P. aeruginosa* and *K. oxytoca* showed that after synthesis as a preprotein, inner membrane insertion of the pseudopilin subunits is mediated by the Sec-system. After inner membrane insertion, the N-terminal positive amino acid sequence is cleaved by the aspartyl prepilin protease GspO. Some species share the prepilin peptidase between the T2SS and the type IV pilus system [25]. Recent studies by Cisneros *et al.* suggested that minor pseudopilin subunits build an initiation complex for polymerization of the major pseudopilin subunits beneath it [26, 27]. The outer membrane complex is composed of GspD and belongs to the family of secretins. Secretins are multidomain proteins forming a multimeric channel, which are also identified in type III secretion systems, filamentous-phage assembly systems and type VI pili systems. Sequence comparison and structural studies of GspD showed that it consists of a variable N-terminal domain and a conserved C-terminal domain. The conserved C-terminal domain that contains several putative transmembrane β -strands forms in its multimeric state a β -barrel, which then forms the actual outer membrane channel. Even though secretins are found in various systems, multimerization as well as outer membrane insertion is still not fully understood. Despite that, the efficient membrane insertion of many bacterial outer membrane proteins depend on the BAM-complex, it could be shown that multimerization and membrane insertion of GspD of *K. oxytoca* does not rely on BAM proteins. Instead, it was shown that these processes depend on a small lipoprotein called GspS [28, 29]. In *K. oxytoca* it was shown that in the absence of GspS, GspD mislocalizes in the inner membrane. Since GspS guides GspD to the outer membrane, GspS and homologs are also named pilotins. In addition, Hardie *et al.* could show that binding of the pilotin to GspD protects the secretin from proteolytic degradation [28]. In contrast to the C-terminal domain of GspD, the N-terminal domain of GspD extends into the

periplasm, forming a possible interaction site with other components of the T2SS. At the cytoplasmic side of this complex locates the inner membrane complex, which consists of GspE, GspF, GspL and GspM. GspE belongs to the secretion ATPase superfamily. Binding, hydrolysis and nucleotide release by GspE causes dynamic structural changes that lead to the conversion of chemical energy to mechanical work [30, 31]. Association of GspE to the T2SS is most likely mediated by an interaction to the polytopic inner membrane protein GspF [32] and the inner membrane protein GspL [33, 34]. Connection between the inner and outer membrane complexes has been suggested to be mediated via the inner membrane protein GspC, which is a bitopic inner membrane protein consisting of an N-terminal cytoplasmic domain, a single membrane spanning helix and a large periplasmic domain.

1.2.1 Type IV secretion systems

Type IV secretion systems (T4SSs) are highly versatile multi-subunit secretion systems that are phylogenetically broadly distributed. In Gram-negative bacteria they are cell envelope-spanning complexes that form a channel through both membranes to enable the secretion of DNA and/or effector proteins. T4SSs mediate the exchange of genetic information among diverse species of bacteria as well as fungal, plant and mammalian cells that facilitates their adaptation to the environment. Despite the wide diversity of secreted substrates and various functions of T4SSs, all of these systems are evolutionary related. Homologous components of the different T4SSs have been given different names in different organisms. Within this thesis, a subscript will be used to indicate the T4SS from which the protein is derived. When no subscript is used or specific T4SS is mentioned, the protein encoded within the GGI is meant. Based on their function T4SSs can be divided into three subfamilies: (i) the conjugation systems, (ii) the effector translocator systems and (iii) the uptake and release systems [35].

The largest subfamily of T4SSs are the conjugation systems that are found in Gram-negative, Gram-positive, wall-less bacteria and archaea. Within these systems single-stranded DNA and protein(s) are transferred via direct cell-to-cell contact from a donor into bacterial or eukaryotic target cells [36]. The best studied conjugative T4SSs are the conjugative F-, R388 and pKM101 plasmid of *Escherichia coli*, as well as the T-DNA transfer system of *Agrobacterium tumefaciens* [37]. Next to plasmids, also integrated conjugative elements are transported via T4SSs. Translocation of the integrative conjugative elements takes place by chromosomal excision by an excisionase. Hfr⁺ strains of *E. coli* that contain integrated F-plasmid DNA in their chromosomes are able to transfer the whole chromosomal DNA in this manner [38].

The second subfamily of T4SSs is the effector and translocator subfamily that is used by many pathogenic bacteria like *Bordetella pertussis*, *Legionella pneumophila*, *A. tumefaciens* and *Helicobacter pylori*. Effector and translocator systems deliver DNA and protein effectors by direct cell-to-cell contact into the target cells to aid bacterial colonization and survival within host cells or tissues [35]. *A. tumefaciens*, the causative agent of crown gall disease, induces tumor growth of infected plant cells. The VirB/VirD4 system of *A. tumefaciens* is encoded on the tumor-inducing plasmid. By transferring, next to T-DNA also, at least four effector proteins this system functions as a conjugation and an effector and translocator system. VirE2, the single stranded DNA binding protein of *A. tumefaciens* binds to the T-DNA to protect it from degradation, and binding of VirE2 to the transported single stranded DNA (ssDNA) in the acceptor cell is also thought to be involved in

'pulling' the DNA to the acceptor cell. The role of the other transported effectors, VirE3, VirD4 and VirF during plant infection is still unknown. However, it is thought that VirE3 is involved in supporting the T-DNA transfer to the nucleus [39]. Another example is given by *Legionella pneumophila*, an intracellular pathogen that causes a form of pneumonia known as Legionnaires' disease. It encodes a T4SS, also known as the dot/icm system (defective for organelle trafficking/intracellular multiplication) that secretes effector proteins to the host cell. Within the host cell these effector proteins remodel the cellular compartment in such a way that the bacterium can survive within the host cell [40, 41].

The DNA uptake and release family is the third and smallest T4SS subfamily. This subfamily has evolved to translocate substrates independently of target cell contact and includes DNA transfer from or to the extracellular environment. At present, this family is found in only three species; *H. pylori* which takes up DNA, *B. pertussis* which exports the multisubunit pertussis toxin and *N. gonorrhoeae* which secretes DNA. The human pathogen *H. pylori* causes gastric diseases like gastritis or gastric cancer. It carries two T4SS: the cag pathogenicity island, which belongs to the effector translocator system, and the ComB system. The ComB T4SS of *H. pylori* is the only characterized T4SS that is able to take up DNA from the extracellular milieu [42]. Even though the ComB system mediates the uptake of DNA, it is not known whether the ComB system secretes any substrates. The T4SS of the whooping cough causing bacterium *B. pertussis* use the Ptl-system (pertussis toxin liberation) to secrete the pertussis toxin into the extracellular milieu of host cells. The Ptl-system encoded proteins show homology to the T4SS of *A. tumefaciens* but interestingly no coupling protein for the T4SS of *B. pertussis* could be identified [43]. The only known T4SS that secretes chromosomal DNA directly into the extracellular milieu is the unique T4SS of *N. gonorrhoeae* [16, 18, 44], which will be discussed below in more detail.

Transport of substrates across the membrane by a T4SS occurs in several steps. The first step is recruitment of the substrate, which generally takes place via the coupling protein, which is located in the (inner) membrane. The coupling protein is an ATPase that is present in most T4SSs. The crystal structure of the soluble domain of TrwB_{R388}, the coupling protein encoded on plasmid R388, shows a homohexameric structure with a diameter of 110 Å [45]. The structure has a central channel with a diameter of 20 Å and connects the cytoplasm with the periplasm [45]. For conjugative T4SSs, the coupling protein recruits the DNA via the relaxase. The relaxase is a protein, which binds and cleaves a specific region on the DNA, the origin of transfer (*oriT*). Several different families of relaxases have been identified and divided into 8 different MOB families (MOB_B, MOB_T, MOB_V, MOB_Q, MOB_P, MOB_H, MOB_F, and MOB_C) [46, 47]. DNA nicking is followed by unwinding of the DNA. This helicase activity can be part of the relaxase, or can be performed by another protein. Optimal nicking and unwinding of the DNA often requires accessory proteins.

After recruitment of the substrate to the coupling protein, the protein is transported via the transport complex. In *A. tumefaciens*, the transfer DNA immunoprecipitation (TRiP) assay, in which components of the translocation machinery are co-immunoprecipitated with translocating DNA, helped to identify T4SS components which come in contact with the transported DNA [48]. This revealed that, after initial cross-links to the coupling protein VirD4_{Ti} and the transport ATPase VirB11_{Ti}, the translocating DNA contacts the inner membrane components VirB6_{Ti} and VirB8_{Ti} [48]. VirB6_{Ti} is an inner membrane protein, which contains multiple transmembrane domains, and VirB8_{Ti}

is a bitopic protein with a large C-terminal periplasmic domain. VirB3_{Ti} is also an inner membrane protein with one transmembrane domain, and deletion of VirB3_{Ti} resulted in the loss of a cross-link to the pilin subunit VirB2_{Ti} in the TRiP assay, suggesting that VirB3_{Ti} does not contact the DNA, but is involved in later steps of the transport process [48]. Homologs of VirB3_{Ti}, VirB6_{Ti} and VirB8_{Ti} are also found in T4SSs of Gram-positive bacteria, suggesting that these proteins form a conserved part of the translocation machinery across the inner membrane in all T4SSs [49].

In Gram-negative bacteria, the substrates are further transported across the outer membrane via the core complex, which in *A. tumefaciens* is formed by VirB7_{Ti}, VirB9_{Ti} and VirB10_{Ti}. The structure of the core complex of the T4SS encoded on plasmid pKM101, formed by the VirB7_{Ti}, VirB9_{Ti}, VirB10_{Ti} homologs TraN_{KM101}, TraO_{KM101} and TraF_{KM101} respectively was solved by both, electron microscopy and X-ray crystallography [50-52]. The structure revealed a cylindrical complex of 14 copies of each of the three proteins, through which the substrate most likely passes. The complex is anchored in the outer membrane by TraN_{KM101} and the C-terminal domains of TraO_{KM101} and TraF_{KM101}. Remarkably, the N-terminal domain of TraF_{KM101} is anchored in the inner membrane via a transmembrane domain, thus connecting both the inner and the outer membranes.

Recently a structure of the core complex together with the inner membrane complex was determined [53]. Below the core complex, the inner membrane complex, which is composed of VirB3, VirB4, VirB6, VirB8 and the N-terminus of VirB10, showed a pseudo two-fold symmetry around the long axis of the particle after reconstruction. At each side of the complex are barrel-like densities which are most likely formed by the VirB4 ATPase. Directly above each barrel-like structure lies the arch, which interconnects the barrel structure and the central stalk. The central stalk most likely forms a binding hub between the inner membrane and the core complex by extending into the I-layer of the core complex [53], connecting the core complex with the inner membrane complex (see Figure 1).

The transport of substrates by T4SS is driven by the hydrolysis of ATP. Next to the coupling protein, the *A. tumefaciens* system contains the VirB4_{Ti} and VirB11_{Ti} ATPases. VirB4-like proteins are the most conserved component of T4SSs, and consist of a C-terminal ATPase domain, along with a less conserved N-terminal domain. VirB4-like proteins most likely function as hexamers [55, 56]. The structure of the C-terminal ATPase domain of VirB4 from *Thermoanaerobacter pseudethanolicus* has been solved recently [57]. Moreover, structures of the *H. pylori* VirB11 homologue HP0525 and *Brucella suis* VirB11 protein have been solved. The crystal structures showed the presence of a hexameric ring of ~100–120 Å in diameter [58, 59]. The mechanism of how the energy generated by these ATPases is used to drive the transport of substrates remains unknown. Remarkably, in some T4SSs found in Gram-negative bacteria, like the T4SS encoded on the F-plasmid and all T4SSs of Gram-positive bacteria, no VirB11-like ATPases could be identified.

Next to the proteins of the core complex, T4SSs can contain additional components that are involved in the formation or function of the functional transport complex. Most systems contain a protein with transglycosylase activity like VirB1_{Ti} [60]. Mutagenesis of the transglycosylase activity of VirB1_{Ti} showed that VirB1_{Ti} is not essential for transport but reduces the transfer of DNA [61]. Many proteins found in T4SSs have only been identified in a subset of the T4SSs [49]. For example, the F-plasmid encodes eighteen proteins that are involved in the assembly of the T4SS, of which ten show

no homology to the VirB1-11/VirD4 proteins [37]. Different families of transport complexes (also termed mating pair formation (MPF) complexes) have been identified, and based on the phylogeny of the VirB4 ATPase, these complexes have been divided into 8 different families (MPF_T, MPF_G, MPF_F, MPF_I, MPF_{FA}, MPF_{bacteroidetes}, MPF_{cyanobacteria}, and MPF_{FATA}) [47]. Although there is a bias of several MPF families to use relaxase of a specific family, (e.g. T4SS of the MPF_H family generally are coupled to a MOB_H family relaxase) many different combinations of relaxase (MOB) and transport complex (MPF) families have been identified. It was proposed that this indicates that the MOB and MPF modules may shuffle over long evolutionary distances [47].

Besides the secretion of substrates, many T4SSs can also extend pili [62]. These T4SS pili play an important role in adhesion to target cells, and in case of the pilus encoded on the F-plasmid, can even retract [63]. Since mutants can be created that are either defective in substrate transfer or pili formation, formation of the pilus seems not to be coupled to substrates transport [64, 65]. T4SSs have been shown to contain two distinct classes of pili: long flexible F-type pili and short rigid P-type pili. The F-type pili are 2–20 µm in length and 8–9 nm in diameter, containing a 2 nm wide central lumen [37] whereas P-type pili are shorter than 1 µm in length and 8–12 nm in diameter [66]. Most pilins of T4SSs are processed before they are inserted into the mating pair formation complex. For example, after pilin insertion into the membrane and processing by leader peptidase, TraA, the pilin subunit encoded on the F-plasmid is acetylated on its amino terminus [67]. In contrast, P-type pili, like the TrbC pilin of the RP4 plasmid and the VirB2 pilin of the Ti plasmid undergo maturation steps leading to the formation of a cyclic protein [68-70].

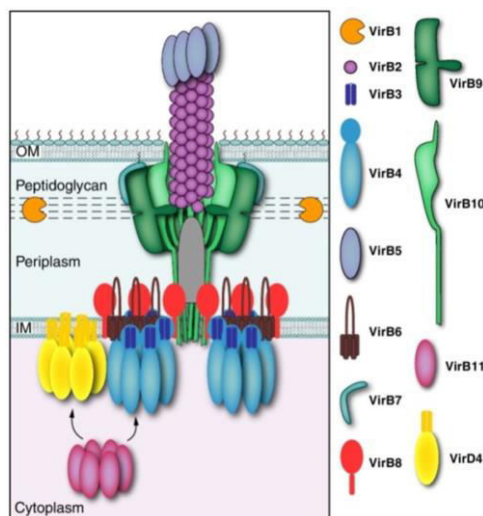


Figure 1 Schematic representation of the type IV secretion system

Subunits on the right, identified with the *A. tumefaciens* VirB/VirD4 nomenclature, assemble as the T4S apparatus/pilus across the Gram-negative cell envelope. Hexameric ATPases establish contacts with the integral inner membrane (IM) subunits to form an inner membrane complex. VirB7, VirB9, and VirB10 form a core complex extending from the IM, periplasm, and outer membrane (OM). A domain of unspecified composition (grey bullet structure) and the pilus assemble within the central chamber of the core complex (adapted from [54])

1.2.2 Type IV secretion system of *Neisseria gonorrhoeae*

Approximately 80 % of the *Neisseria gonorrhoeae* and 17 % of the *Neisseria meningitidis* strains carry a 57 kb large genomic island, which was designated as Gonococcal Genetic Island (GGI). Sequence analysis of the GGI showed a significant lower G+C content (44 %) compared to the rest of the gonococcal chromosome (55 %), suggesting that the GGI is horizontally acquired [17]. As in the case for many horizontally transferred genetic islands, the GGI is integrated near the replication terminus and is flanked by a *difA* and an imperfect *difB* site [18]. The *dif* site is a repeated DNA sequence of 23 bp (AGTTCGCATAATGTATATTATGTTAAAT), which is found at the chromosome

replication terminus among proteobacteria and is recognized by the site specific recombinase XerCD. Usually, XerCD resolve chromosome dimers that arise during cell division. Recently, Domínguez *et al.* could show that substitution of the imperfect *difB* site by another copy of *difA* results in frequent XerD mediated excision and loss of the GGI, indicating that the imperfect *dif* site might be involved in the maintenance of the GGI [71].

The GGI of *N. gonorrhoeae* strain MS11 encodes 62 open reading frames (ORFs) with multiple homologs of T4SS genes. The first 27.5 kb of the GGI encodes 24 open reading frames: 15 of these ORFs show a similar order to those of the well known *E. coli* F-plasmid conjugation system and 18 of these ORFs show significant similarity to the transfer genes of the F-plasmid or other T4SSs (TraD, Tral, LtgX, TraA, TraL, TraE, TraK, TraB, TraV, TraC, Trbl, TraW, TraU, TrbC, TraN, TraF, TraH, and TraG) [18]. 17 genes of the GGI show, like many F-plasmid transfer genes, coding regions which are overlapping or separated by only a few base pairs.

Several studies have shown that the GGI encodes a T4SS that secretes DNA in a contact independent manner directly into the surrounding environment. These studies point out that *N. gonorrhoeae* secretes single stranded DNA during the log-phase, which is protected from the 5' end [72]. Furthermore, Salgado-Pabón *et al.* could show that DNA secretion is higher in piliated than in non-piliated strains [73]. A mutational analysis of genes encoded within the GGI determined the minimal composition of genes that are required for ssDNA secretion (Figure 2) [74].

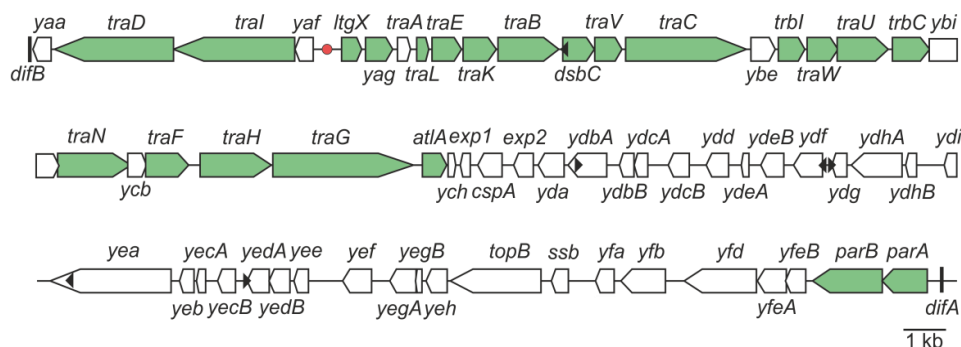


Figure 2 Schematic representation of the genetic map of the GGI of *N. gonorrhoeae*

In green are the genes known to be essential for DNA secretion and in white are the genes not required for DNA secretion. DNA uptake sequences and the putative origin of transfer (*oriT*) are indicated by black triangles and red dot, respectively.

Sequence analysis demonstrated that the GGI consists of three divergently arranged gene regions by which the GGI can be divided into three predicted gene regions. The first part of the GGI includes the relaxase TraI, the coupling protein TraD and two hypothetical proteins (Yaa and Yaf). A study by Salgado-Pabón *et al.* revealed that DNA secretion might be regulated at the transcriptional level of TraD and TraI, while the second part of the GGI is constitutively expressed. The *ltgX-ycH* region encodes proteins that are involved in the structural biology of the T4SS apparatus homologous to mating pair formation (Mpf) proteins of T4SSs. Most of the proteins encoded within the third region are of unknown function or have homologies to DNA processing and modifying proteins.

The role of the secreted ssDNA is currently unclear. The secreted DNA can be used for natural transformation of other *N. gonorrhoeae* cells and contributes to horizontal gene transfer [17, 18, 75]. The role of the GGI in pathogenesis is currently still unclear. Different forms of the GGI have

A list of proteins involved in T4P biogenesis is provided in Table 1. Although many of these components are conserved in type IV pili systems they have been named differently throughout these systems. Here mainly the nomenclature adapted for *N. gonorrhoeae* is used.

Table 1 *Neisseria gonorrhoeae* proteins involved in type IV pilus biogenesis

Protein involved in type IV pili biogenesis	Proposed localization and function of T4aP component	Reference
PilC1 /PilC2	Outer membrane or pilus associated adhesin	[90-94]
PilD	Inner membrane pre-pilin peptidase	[95, 96]
PilE	Fiber-forming major pilin subunit	[97]
PilF	Cytoplasmic pilin polymerase/ATPase	[98]
PilG	Inner membrane platform protein	[99, 100]
PilH	Harbours a N-terminus conserved in prepilins, is cleaved by PilD	[101]
PilK	Harbours a N-terminus conserved in prepilins, is cleaved by PilD	[101]
PilM	Cytoplasmic FtsA-like assembly protein	[102]
PilN	Inner membrane assembly protein; interacts with PilM via its N terminus, PilO and PilP via its C-terminus	[102-104]
PilO	Assembly protein; interacts with PilN and PilP via its C-terminus	[103, 104]
PilP	Assembly lipoprotein; interacts with PilN, PilO, and PilQ	[104]
PilQ	Secretin monomer; forms outer membrane pore	[105]
PilS	Silent minor pilin subunit	[106]
PilT	Cytoplasmic pilin depolymerase/ATPase	[84, 98, 107, 108]
PilU	Cytoplasmic ATPase; regulation of pilus retraction	[109]
PilV	Minor pilin subunit; involved in assembly	[110]
PilW	Minor pilin subunit; involved in assembly	
PilX	Minor pilin subunit; involved in assembly	[111, 112]
PilZ	Harbours a N-terminus conserved in prepilins, is cleaved by PilD	[101]
ComP	Minor pilin subunit; DUS-receptor	[113, 114]
NGFG_01202, (PilWa)	Outer membrane pilotin; required for secretin outer membrane localization and oligomerization	[115]

1.3.1 Type IV pili assembly machinery

The type IV pilus fiber is a dynamic structure consisting of more than 1000 subunits of the major pilin subunit. The major pilin subunit PilE is a small structural protein (15-20 kDa) with a conserved, hydrophobic α -helical N-terminus that acts as both a transmembrane (TM) domain and a protein-protein interaction domain [97]. Type IV pilin subunits are synthesized as prepilin subunits and although they are divergent in sequence, a defining characteristic is a positively charged N-terminal type III signal sequence [116]. This positively charged signal sequence is most likely involved in correct orientation of the pilin subunits during Sec-dependent membrane insertion. After membrane insertion with the C-terminal domain outside the cytoplasmic membrane the bifunctional aspartic protease PilD proteolytically removes the signal sequence and methylates the newly created N-terminal amino acid [117, 118]. Due to their polar nature of the type III signal sequence, the processed pilin subunits remain within the cytoplasmic membrane, forming an inner membrane pool. Once extruded from the inner membrane pool, the pilin subunits assemble into a helical fiber.

Based on the length of the leader peptide in the prepilin and the length of the mature protein, type IV pilin proteins have been divided into type IVa pili and type IVb pili [119]. Type IVa pili, which are present in a variety of bacteria (e.g. *Myxococcus xanthus*, *P. aeruginosa* and *Neisseria spp.*), have a short signal peptide, consisting of 6 to 7 residues. Type IVb pili, which are commonly found in enteric species (e.g. enteropathogenic *E. coli*), on plasmids and other mobile genetic elements have a longer signal peptide (15-30 residues) [120]. Sequence analyses showed that the methylated N-terminal residue, which is phenylalanine for T4aP, varies for T4b pilins. In addition, type IVa proteins share greater N-terminal homology among themselves than with type IVb pili [121]. Although both types of pili share an overall architecture, the topology of the β -sheets differs, resulting in different protein folds. Despite of the different topologies, pilins from many different bacteria share the same design that allows them to assemble into pilus filaments.

Structural analysis of pilin subunits of *N. gonorrhoeae*, *P. aeruginosa* and *V. cholerae* revealed that these proteins share a common architecture, resembling a needle-like structure consisting of an N-terminal α -helix and a globular C-terminal domain (Figure 4A) [97, 122, 123]. The N-terminus, which forms an extended α -helix, can be divided into two subdomains: (i) α 1-N and (ii) α 1-C. The α 1-N domain, which protrudes from the globular C-terminal domain, acts as a transmembrane segment, keeping the pilin subunits within the cytoplasmic membrane prior membrane extrusion [121]. The amphipathic α 1-C domain is embedded in the C-terminal part of the globular domain and packed against the head domain; which generally consist of a 4-stranded β -sheet oriented 45° or more relative to the long axis of the α 1 helix (Figure 4A) [124]. Full-length structures of *P. aeruginosa* and *N. gonorrhoeae* pilins showed that the two N-terminal helix-disrupting residues Pro22 and Gly/Pro42 cause a shallow S-shaped kink, which is suggested to result in flexibility of the α -helix [122, 124]. The antiparallel four-stranded β -sheet of the globular domain is flanked by two variable regions: (i) the $\alpha\beta$ -loop and (ii) the D-region. The $\alpha\beta$ -loop is located on one side of the globular head domain and connects the N-terminal α -helix to the β -sheet. In addition, this partial surface exposed domain is involved in subunit-subunit interaction within the pilus fiber. The second variable domain, the D-region is bound by two conserved C-terminal cysteines that link the D-region, opposite of the $\alpha\beta$ -domain, to the conserved structural core of the head domain. In *P. aeruginosa* this region is of biomedical interest, as it was shown to be involved in binding to epithelial receptors [125]. In

addition, it was shown that the D-region of the T4bP of *V. cholerae* is involved in pilus-pilus interaction and microcolony formation [126].

Cryo-electron microscopy reconstruction and crystallographic analysis of the pilin monomer of *N. gonorrhoeae* showed that the assembled pilus is arranged as a helical fiber with an outer diameter of ~ 60 Å, which is consistent with the ~ 65 Å diameter opening of the secretin, through which the fiber passes to the extracellular milieu [124]. Three-dimensional cryo-EM reconstruction by Craig *et al.* suggested an arrangement of a 3-start left handed helix, which alternatively can be viewed as a 1-start right handed or 4-start right handed helix, with ~ 3.6 subunits per turn (see Figure 4B) [124]. Reconstruction in radial distance coloring highlighted a tightly packed filament interior with a narrow central channel. The surface was shown to contain deep grooves that run along a repeating donut-shaped mass with a central depression. Fitting the crystal structure of the gonococcal pilin into the cryo-EM reconstruction of the pilus revealed that upon placing the hydrophobic N-terminal α -helices almost parallel to the filament axis within the filament core, the pilin globular head domain aligns with the repeating donut-shaped structure. The variable $\alpha\beta$ -loop and D-regions aligned to protruding ridges of the donut-like structure, implicating a role in receptor binding and antigenic variation [124]. Recently, Biais *et al.* could demonstrate that T4aP of *N. gonorrhoeae* undergoes force-induced stretching with dramatic and reversible conformational changes. Stretching not only narrowed the pili by 40 % but exposed residues that were hidden in the unstretched form [127].

In addition to the major pilin subunit PilE, some T4P systems contain a number of prepilin-like proteins, named minor pilin subunits, containing the defining N-terminal prepilin signal sequence. These minor pilin subunits are, like PilE, processed by the prepilin peptidase and assemble into the pilus fibre that influence pilus assembly or function [27, 110, 128].

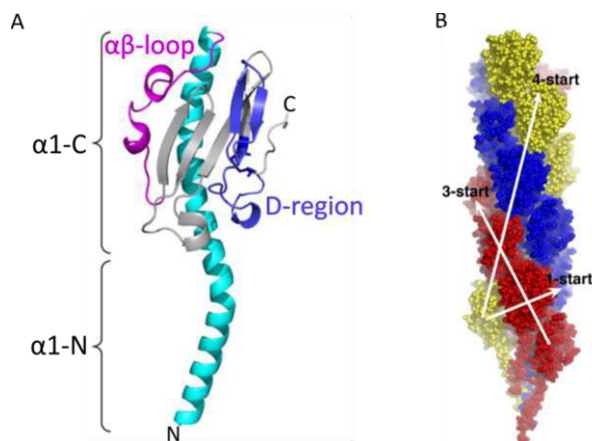


Figure 4 Structure of pilin subunits in the type IV pilus fiber

(A) Secondary structure of the pilin subunit from *N. gonorrhoeae*. (B) Subunits traced along a right-handed 1-start helix, along three strands of a left-handed 3-start helix (colored red, blue, and yellow), and along four strands of a right-handed 4-start helix. (adapted from [123, 124])

T4P systems have two, and sometimes three, cytoplasmic motor ATPases (PilF, PilT and PilU), belonging to the superfamily of secretion ATPases, which are required for rotational extension and retraction of the pilus fiber [129]. Based on homology with type II secretion ATPases, it is expected that the ATPases of the T4P system are composed of two major structural domains. An N-terminal domain which is required for membrane association and localization [130] and a C-terminal domain that contains the Walker A phosphate binding loop and the Walker B motif, that is involved in the formation and stabilization of the nucleoside binding fold by interacting with Mg^{2+} . In addition,

contains the C-terminal domain aspartate and histidine boxes which are only found in ATPases of the T2SS and T4P system [131, 132]. The aspartate box and the histidine-box contain two invariant residues, that are involved in twitching motility [133, 134]. Structural analysis of ATPases belonging to the secretion ATPase superfamily showed that they share a biloped structure, consisting of a PAS-like domain which is joined by a flexible linker to a RecA fold C-terminal domain [135]. Structural data by Satyshur *et al.* showed that upon ATP binding, the N-terminal domain will tilt towards the center of the hexamer that results in a flip of the C-terminal domain towards the outside [135]. Thus, ATP binding lead to substantial movement that could translate bound proteins during pilus assembly and/or retraction [135]. Transposon mutagenesis studies of PilF, PilT and PilU, which are found as homologs in T2SSs, T3SSs and T4P systems and members of the secretion ATPase family, showed that transposon insertions in the ATPase PilF result in a non-piliated phenotype, suggesting that PilF is required for pilus assembly. In contrast, transposon mutagenesis in PilT and its paralogue PilU show a hyperpiliated phenotype [84, 98, 107, 108, 129, 136], suggesting that they are involved in pilus retraction. Optical tweezer experiments showed that retraction of a single pilus filament of *N. gonorrhoeae* can exert forces of 50-100 piconewtons. These forces which are equal to 100.000 times the bacterial bodyweight, and make T4P the strongest microscale elements known to date [137].

The T4P and T2S systems contain a highly conserved polytopic inner membrane protein. Its broad distribution and high level of conservation led to the suggestion that this protein might play an essential role as a platform for pilus and pseudopilus assembly [99, 128, 129]. However, the specific function of members of this family within T2SSs and T4P systems still remains undefined. Despite the high conservation of PilG, relatively little is known about the structures of members of the PilG family. Transmembrane helix prediction methods predict 3 transmembrane helices with two large cytoplasmic loops. Structural analysis of PilG revealed that the protein forms dimers or possibly tetramers and that the cytoplasmic N-terminus forms an α -helical bundle [138-140]. Because of sequence similarities of the N-terminus and the C-terminus a similar fold of the C-terminus is suggested [140]. A systematic genetic analysis of inner membrane proteins of the T4P system of *P. aeruginosa* showed that the polytopic inner membrane protein PilG is essential for pilus polymerization and depolymerization through its potential association with the cytoplasmic ATPases PilB and PilT [141]. In *N. meningitidis* pili determination of a PilG/PilT double mutant showed that T4P could still be detected by immuno fluorescence microscopy, suggesting that PilG is not an essential assembly factor in *N. meningitidis* [101]. The result that PilG is not essential for T4P assembly in *N. meningitidis* by Carbonelle *et al.* is in conflict with results published by Tønjum *et al.* Using transposon mutagenesis Tønjum *et al.* showed that various PilG mutants in *N. gonorrhoeae* and *N. meningitidis* displayed non-piliated colony morphologies and when examined by transmission electron microscopy were devoid of pili [99]. In addition, deletion of the PilG homolog in the Gram-negative δ -proetobacterium *Myxococcus xanthus* caused type IV pili dependent social-motility defects [142]. Based on the contradictory results of PilG, the exact role during T4P still needs to be clarified.

Protein interaction studies of the T4P systems revealed an inner complex that might be involved in the physical interaction between components in the outer and inner membrane [143, 144]. The complex consisting of PilM, PilN, PilO and PilP was shown to be critical for T4P assembly in many

bacteria, like *N. meningitidis* [101], *Thermus thermophilus* [145] and *M. xanthus* [144]. PilM is a cytoplasmic protein with sequence similarities to the actin-like proteins MreB and FtsA [146, 147]. Structural studies by Karupphiah *et al.* revealed that PilM adopts an actin-like fold [102]. Similar to other bacterial actin-like proteins, PilM shows a two domain structure, where each domain can be subdivided into two subdomains. The electron density map showed the presence of ATP, demonstrating that PilM can, similar to MreB and FtsA, bind ATP. However, no evidence for ATP hydrolysis by PilM has been shown up to now. In the structural studies by Karupphiah *et al.*, PilM was co-crystallized with a synthetic peptide, corresponding to the highly conserved region of PilN. The highly conserved N-terminus of PilN bound in a hydrophobic cleft between two subdomains [102]. Mapping sequence conservation onto the PilM surface shows sequence conservation around the PilN interaction site. In addition, this analysis revealed a second conserved patch, opposite of the PilM-PilN interaction cleft, which might be involved in binding to other components of the T4P system [102]. In general Karupphiah *et al.* proposed that PilM first binds ATP and then interacts with PilN and possibly to another cytoplasmic T4P biogenesis protein [102]. In 2009, Sampaleanu *et al.* provided the first evidence that PilN, which has a conserved N-terminal transmembrane helix and a sequence variable periplasmic C-terminal domain [103], not only interact with PilM but also interacts with the periplasmic lipoprotein PilO, forming a stable heterodimer [103]. Even though it is predicted that PilN and PilO have a similar secondary structure, a comprehensive bioinformatic analysis of PilN and PilO proteins showed that proteins of the PilO family, have in contrast to PilN, a high sequence conservation in the periplasmic domain and a more variable cytoplasmic N-terminus [103]. To understand PilN and PilO at the molecular level, the periplasmic domains of PilN and PilO were crystallized [103, 148]. PilO was found to crystallize as dimers where the monomer has two distinct structural domains. An N-terminal coiled-coil domain, a highly versatile α -helical structure that in general is involved in oligomerization, protein-protein interaction and protein-DNA interactions [103]. The second domain is a compact C-terminal core domain, which secondary structure represents a cyclic permutation of the ferredoxin fold that has been previously seen for EpsM, the PilO homolog of the T2SS of *V. cholerae* [103, 138]. Recent structural data of the periplasmic part of PilN revealed that PilN forms a dimer with a ferredoxin-like fold, similar to PilO [148]. The last component of the physical connection complex is the lipoprotein PilP. PilP is a periplasmic lipoprotein that can localize to the inner membrane, even in the absence of its putative lipidation signal [104]. Co-purification experiments, with the inner membrane components PilN and PilO showed that these three proteins form a stable complex. Recently, Georgadiou *et al.* and Friedrich *et al.* could show that loss of either PilN, PilO or PilP in *N. meningitidis* and *M. xanthus* had a negative effect on the stability of the other gene products, indicating an interaction between these proteins [144, 149]. Chemical shift assays, using recombinant PilP and part of the secretin PilQ identified that the C-terminal domain of PilP interacts with the NO domain of the secretin PilQ. Suggesting that this forms the connection between on one hand the inner membrane lipoproteins PilN and PilO and on the other hand with the outer membrane secretin PilQ [150].

1.3.2 LysM domain containing proteins in Type IV pili systems

Since the size of the T2SSs and T4P systems by far exceeds the experimentally determined permeability of 50-100 kDa of the peptidoglycan sacculi, bacteria containing these systems may

need to remodel their peptidoglycan layer. Up to now only a few peptidoglycan-associated or peptidoglycan modifying enzymes associated with these systems have been identified.

It has been shown that the cytoplasmic protein complex, formed by ExeA and ExeB, of *A. hydrophila* might help translocation of the secretin ExeD from the inner membrane to the outer membrane [151, 152]. Indeed, the deletion of *exeA* and *exeB* results in monomeric and inner membrane localized ExeD. Interestingly, it is hypothesized that ExeA facilitates secretin formation by binding to peptidoglycan via a LysM domain [153]. Binding of ExeA to peptidoglycan causes multimerization into a ring-like structure that could act as scaffold to direct secretin assembly [154]. Another PG-associated protein that affects/promotes secretin formation is the inner membrane protein FimV of *P. aeruginosa*. PG pulldown assays with FimV showed that it binds to PG in a LysM motif-dependent manner; the deletion of the LysM domain results in reduced motility, secretin levels and surface piliation. Wehbi *et al.* could show that FimV promotes secretin formation, which depends on the PG-binding domain LysM [155, 156]. LysM domains are used by bacteria to keep specific proteins at the cell surface by attaching them in a non-covalently manner to the peptidoglycan. The LysM domain was discovered as a repeat of 44 amino acids in the lysozyme of the Bacillus phage $\phi 29$ [157]. Now that many genomes have been sequenced, the LysM domain has been identified in many proteins like bacterial lysins, bacteriophage proteins, bacterial peptidoglycan hydrolases, peptidases, chitinases, esterases, reductases and nucleotidase and even in some eukaryotic proteins. They have not been identified in archaeal proteins [158]. The number of this domain per protein and the position(s) within the proteins differ. A Hidden Markov model showed that the LysM sequence is conserved over the first 16 amino acids and less conserved over the last 10 residues. The first solved LysM structure was the LysM domain of the outer membrane-bound lytic murein transglycosylase MltD of *E. coli*. The structure of MltD showed a $\beta\alpha\alpha\beta$ secondary structure with the two α -helices packing onto the same side of an antiparallel β -sheet [159]. In general LysM containing proteins can be classified into two categories, (i) PG-binding proteins and (ii) PG-hydrolyzing proteins. So far, most of the proteins encoding a LysM domain belong to the PG-hydrolyzing category. Nevertheless, PG-binding proteins have been identified, such as FimV of *P. aeruginosa* or AcmA of *Lactococcus lactis* [156, 160].

1.3.3 Secretin

The secretin family of outer membrane proteins is found in T2SSs, T3SSs, filamentous-phage assembly systems and type IV pili systems. Three-dimensional reconstructions of secretin structures by electron microscopy revealed that they adopt multimeric structures, characterized by the formation of large chambers with a central cavity that ranges from 50 to 90 Å in diameter [150, 161-163]. Sequence comparison and limited proteolysis showed that secretins consist of a conserved C-terminal (CTD) and variable N-terminal domains (Figure 5) [162]. The conserved C-terminal region that is responsible for oligomerization and membrane spanning contains several transmembrane β -sheets forming a β -barrel upon multimerization [164-166]. Different experiments showed that this CTD is protease resistant and stays in its homomultimeric form after protease treatment [162]. The more variable N-terminal domain extends into the periplasm forming the sides of the chamber and is involved in interaction with other components [150, 167]. Structural studies showed that the N-terminal domain of secretins consist of three to four subdomains, named N0 to N5, each exhibiting a

α/β -type fold. Crystallographic studies of N0-N2 of GspD, the secretin of the T2SS from ETEC, and NON1, the secretin EscC from the T3SS, showed that these periplasmic domains are arranged into two lobes [168, 169]. In this structure the N0 domain interacts with the N1 domain via an antiparallel pair of β -strands. Sequence alignment showed that the hydrophobic interface residues are conserved throughout secretins of the T2SS, suggesting that the compact NON1 lobe is a common feature in T2SS [168]. The recently solved structure of NON1 of *N. meningitidis* by NMR showed that these periplasmic domains adopt a similar fold to the N0 domains identified for GspD and EscC. In addition, Berry *et al.* could show that the N0 domain of *N. meningitidis* possesses a strikingly novel feature. The C-terminus of the *N. meningitidis* N0 domain contains a long random coiled region, which forms a linker region between N0 and N1, and this feature is conserved throughout T4P dependent secretins [150]. Bioinformatic studies of T4P, T2SS and T3SS dependent secretins showed that the extreme N-terminal region of T4P dependent secretins contain one or two β -rich domains, named B1 and B2 (Figure 5). Sequence comparison of the second β -domain from PilQ revealed a high degree of conservation. Mapping 63 different T4P dependent secretin sequences onto the protein structure revealed that the conserved residues form a single patch on the domain, indicating that this conserved patch might form a binding site to an unidentified T4P biogenesis protein [150].

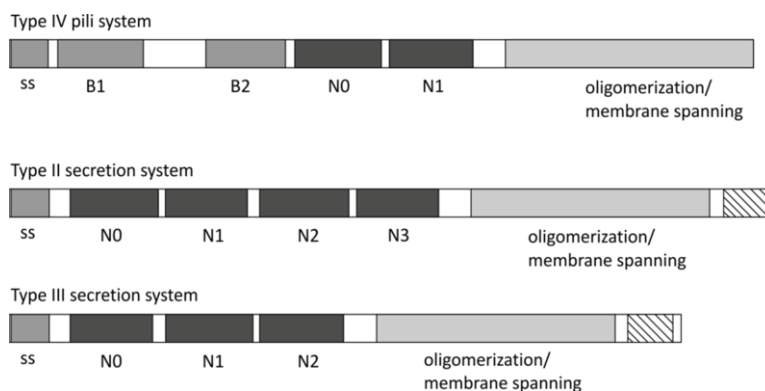


Figure 5 Schematic overview of secretin domain structure

Domain architecture of secretins from the T4P system, T2SS and the T3SS. Members of the secretin superfamily contain a C-terminal secretin core homology domain (light grey). Two to four periplasmic subdomains, termed N0–N3 (black). The T4P system specific B1 and B2 regions (dark grey), which are located at the N-terminus, are predicted to be rich in β -structure. A T2SS and T3SS-specific domain, termed the S-domain (striped), is located at the very C terminus (adapted from [150]).

Over the last years, secretin complexes from T2SS, T3SS, T4P and filamentous phage extrusion systems have been studied intensively [167, 170, 171]. Electron microscopy analysis of secretins revealed that they share special features including a cylindrical structure with a 12-15 fold symmetry and a central cavity with a wide opening at one end and a periplasmic gate at the other. Analysis of the secretin PulD of the T2SS from *K. oxytoca* showed a cylindrical dodecameric arrangement with peripheral radial spokes, which are most likely formed by the pilotin PulS [166]. End- and side-view averages were used for 3D mapping and revealed that the cylindrical complex shows a two-ring structure from which the radial spokes extend from one of these rings. The first ring is present in the outer leaflet of the outer membrane with weak connections to the second ring, which is present in the periplasm and inner leaflet of the outer membrane (Figure 6A) [164]. The secretin complex that was shown to be open at its periplasmic side was closed off from the outer membrane by a continuous density [164]. Nouwen *et al.* could show that a fusion of proteoliposomes containing the purified PulD-PulS complex with a lipid bilayer results in a small voltage-activated, ion-conducting

channel. Analysis of the PulD secretin channel in the presence of its corresponding substrate, pullulanase, showed no change in channel conductivity, indicating that the interaction between secreted proteins and the secretin might not be sufficient for channel opening [166]. Recent cryo-EM studies on the secretin of the T2SS from *V. cholerae* showed that GspD assembles into a complex which is ~ 155 Å in diameter and ~ 200 Å in length. The channel of the secretin complex has a periplasmic opening of approximately 75 Å in diameter is narrowed by a constriction to ~ 55 Å in diameter. Placing modeled dodecameric ring structures of N0-N1, N2 and N3 in the density map of EspD revealed that the N0-N1 ring fits into the widest area at the bottom of the periplasmic part of the secretin. The N2 and N3 rings can be positioned directly above the N0-N1 ring in the map. Surprisingly, the N3 ring fits to the constriction site of the cryo-EM map (Figure 6B) [167]. Studies by Collins *et al.* showed that the T4P secretin PilQ from *N. meningitidis* showed a doughnut-like structure with one open end. Single-particle averaging showed that this complex has a 12-fold rotational symmetry with a funnel-shaped cavity of 6.5 nm in diameter [172]. Since the cavity tapers to a closed point which effectively blocks the formation of a continuous pore, lead to the hypothesis that the secretin complex has to undergo conformational changes in order to allow passage of the assembled fiber [172]. In order to dock the recently solved structures of the N0, N1, B1 and B2 domain into the PilQ secretin structure, a 3D reconstruction of the complete PilQ dodecamer was performed by Berry *et al.* Single particle reconstruction of $\sim 20,000$ particles showed that, in contrast to previously published *N. meningitidis* secretin complexes a chamber of 155 Å in height and 110 Å in diameter which is closed at both ends [150]. Docking of PilQ domain structures into the cryoelectron microscopy map showed that the N0-N1 domain might line the chamber wall. Since Berry *et al.* ascribed the flattened disc density at the top of the 3D reconstruction to the membrane spanning C-terminal domain, the β -domains would therefore be part of the density, closing the secretin chamber at the bottom. Docking the β -domains into the 3D reconstruction additionally revealed that the PilQ oligomer could accommodate 12 copies of B2 but not B1, suggesting that the B1 domain adopts a partially unfolded state in the assembled oligomer (Figure 6C) [150]. Recent transmission EM analysis of the T4P secretin PilQ from *N. gonorrhoeae* by Jain *et al.* showed that the secretin complex in its native lipid environment forms a double ring structure with seven extending spikes (Figure 6D) [105]. Single particle averaging revealed a 14-fold symmetry for the peripheral ring and a 14-15 fold symmetry for the central ring, most likely corresponding to PilQ. Improvement of the obtained structure suggested that the structure is flexible between the central and peripheral ring. Single particle analysis of secretin structures from *N. meningitidis* showed that the spikes were absent and that the peripheral ring was partly or completely lacking. The results of Jain *et al.* demonstrate that the secretin complex contain unidentified flexible extra domains [105].

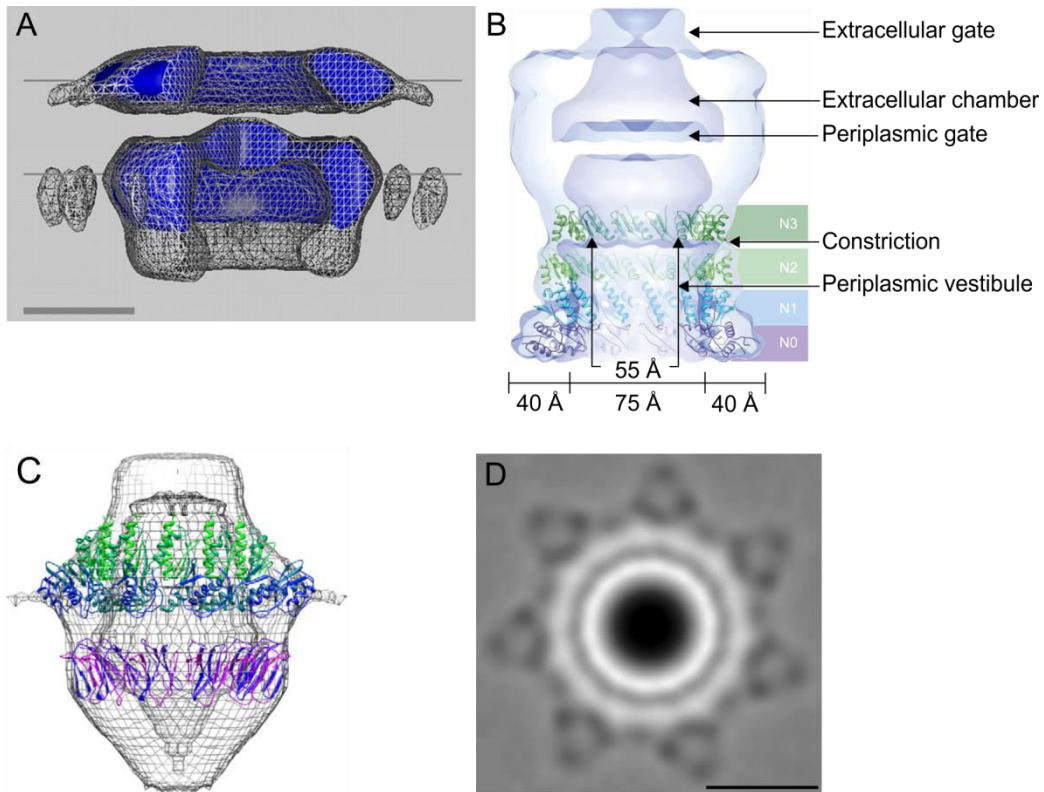


Figure 6 Structural comparison of secretin complexes of the type II secretion system and type IV pili system

(A) Calculated volumes and back-projections of PulD complex. The *horizontal lines* represent the outer limits of the lipopolysaccharide/phospholipid outer membrane. Scale bar equal 5 nm. (B) Fitting of 12-member ring models of the GspD N-terminal periplasmic domains (N0–N3) into the GspD density map. The N0 domain (dark blue) and N1 domain (light blue) are anchored at the bottom of the GspD density map. This places the N2 domain (light green) into the central periplasmic domain density and the N3 domain (dark green) into the periplasmic constriction. (C) Docking of the B2 domain (purple) and N0/N1 domain (blue-green) into the PilQ cryoelectron density map. (D) Projection map of the secretin complex of *N. gonorrhoeae*. Scale bar equals 100 Å. (adapted from [105, 150, 164, 167])

2. Scope of the thesis

Over the years, *N. gonorrhoeae* has evolved and acquired different mechanisms to protect itself against a variety of antibiotics and chemotherapeutic agents. One reason for the rapid spread of antibiotic resistance in gonococci is the highly effective horizontal gene transfer that is promoted by the type IV pili. The transforming DNA is either provided by autolysis or by the gonococcal type IV secretion system, which secretes ssDNA into the extracellular milieu [16-18]. DNA uptake in *Neisseria* involves the T4P and the competence system, transporting the DNA across the outer and the inner membrane, respectively. Functional characterization of the type IV secretion system and DNA uptake system and thus the type IV pili machinery in *N. gonorrhoeae* could provide starting points in the exploration of new therapeutic strategies.

In this thesis, components of the type IV secretion system and outer membrane components of the type IV pili system of *Neisseria gonorrhoeae* are described.

Chapter 4.1 describes the analysis of the type IV secretion system of *N. gonorrhoeae* encoded by the Gonococcal Genetic Island. Mutational analysis of genes encoded within the GGI determined the minimal composition of genes, encoded within the GGI, which are required for ssDNA secretion [74]. Mapping of the operon structure within these regions was used to gain insights into the transcriptional regulatory network of the T4SS. To determine whether DNA secretion is regulated at the transcription level of TraD and TraI, which are involved in targeting the secreted DNA to the secretion apparatus [36], or additionally at the transcription level of the *ssbB-yegA* operon, the expression level of the *ssbB-yegA* operon was analyzed qRT-PCR. To investigate if the single stranded DNA, which is secreted via the T4SS encoded within the GGI facilitates biofilm formation, biofilm formation of different *N. gonorrhoeae* strains were compared by Maria Zweig. A complementation of a *traB* deletion strain by transformation with chromosomal DNA from *N. gonorrhoeae* MS11 WT strain showed that the ssDNA which is secreted via the T4SS within the GGI facilitates initial attachment of *N. gonorrhoeae* to surfaces.

In **Chapter 4.2**, the secretin complex of the type IV pili system is analyzed. Based on the fact that the PilQ secretin complex of *N. gonorrhoeae* interacts with other proteins in the peripheral membrane to form a large multi-domain complex and that the functions of these extra domains are currently unknown, the aim was to identify the protein within the extra domains, to characterize their function and to determine whether these domains can also be found in Type II secretion systems and in the Type IV pili systems of other organisms.

In **Chapter 4.3**, the identification of TsaP domains and their functional characterization is described. To study the effect of these domains, mutants carrying deletions of different domains were used to determine their effect on T4P and the secretin complex embedded in its native lipid environment.

In **Chapter 4.4**, the interaction of TsaP with other components of the type IV pili system of *N. gonorrhoeae* and *M. xanthus* is described. To identify protein-protein interaction of TsaP and PilQ, fragments of TsaP and PilQ of *N. gonorrhoeae* were tested *in vivo*, using the bacterial adenylate cyclase two-hybrid (BACTH) system. As an alternative method to the BACTH system, size exclusion chromatography (SEC) of mixed proteins was used to study the interaction of TsaP with other components of the type IV pili system.

3. Material and Methods

3.1 Material

Buffers and solutions were prepared using ELGA H₂O. Reagents were purchased from Difco (Heidelberg), Merck (Darmstadt), Roth (Karlsruhe), Fermentas (Sankt Leon-Roth) and Sigma-Aldrich (Steinheim) unless indicated otherwise.

3.1.1 Strains

Table 2 *Neisseria gonorrhoeae* strains used in this study

Strain	Genotype	Source or references
MS11	<i>N. gonorrhoeae</i> clinical isolate	[173]
FA1090	<i>N. gonorrhoeae</i> clinical isolate	[174]
ND500	derivative of <i>N. gonorrhoeae</i> strain MS11 with GGI deleted	[18]
KS031	derivative of <i>N. gonorrhoeae</i> strain MS11; <i>tsaP</i> ΔS213-V245	This thesis
KS035	Δ <i>tsaP</i> /Plac- <i>tsaP</i>	This thesis
KS036	derivative of <i>N. gonorrhoeae</i> strain KS031; <i>tsaP</i> ΔS213-V245/Plac- <i>tsaP</i>	This thesis
KS037	derivative of <i>N. gonorrhoeae</i> strain SJ082; Δ <i>tsaP</i> /Plac- <i>tsaP</i> ΔA33-R83	This thesis
SJ001-MS	derivative of <i>N. gonorrhoeae</i> strain MS11 with <i>pilQ</i> truncation	[105]
SJ004-MS	<i>pilQ</i> with insertion encoding internal His-tag	[175]
SJ006-FA1090	FA1090 strain transformed with PCR product to introduce an in frame deletion of aa 1 to 31 of <i>pilE</i>	[105]
SJ030-MS	MS11 strain transformed with pSJ030; non polar insertion in <i>pilC</i> , Erm ^R	[105]
SJ031-MS	MS11 strain transformed with PCR product to introduce in frame deletion of aa M1 to N181 of <i>pilP</i>	[105]
SJ032-MS	MS11 strain transformed with pSJ032; non polar insertion of <i>pilW</i> , Erm ^R	[105]
SJ082-MS	derivative of <i>N. gonorrhoeae</i> strain MS11 with <i>TsaP</i> deleted	[175]
EP006	derivative of <i>N. gonorrhoeae</i> strain MS11 with <i>RecA</i> deleted	[176]
EP060	derivative of <i>N. gonorrhoeae</i> strain MS11 with <i>PilF</i> deleted	[105]

N. gonorrhoeae mutants were created by homologous recombination into the chromosome. Either plasmid DNA or PCR products were introduced by natural transformation or electroporation as

described in chapter 3.3.12.1 and 3.3.12.2 or previously [177]. MS11 was used as the WT strain. To generate SJ004-MS, in which a sequence encoding a His₈-tag was inserted between P154 and F155 of the small basic repeat region of PilQ. 2 PCR products were generated with primers 552 and 572 and primers 573 and 553 respectively. These products were mixed and used as a template for a third PCR using primers 552 and 553. This PCR product was transformed to strain MS11. To generate strain SJ082-MS, in which *tsaP* is disrupted by the insertion of plasmid pIND3, MS11 was transformed with pSJ082. To generate strain KS035, in which the *tsaP* deletion in strain SJ082-MS is complemented by a copy of *tsaP* behind the *lac* promoter of plasmid pSJ023 inserted between the *lctP* and *aspC* genes, SJ082-MS was transformed with pKS007. To generate strain KS031, in which amino acids S213-V245 of *tsaP* are deleted, MS11 was transformed with linearized pKS004. To generate strain KS036, in which the *tsaP*ΔS213-V245 deletion in strain KS031 is complemented by a copy of *tsaP* behind the *lac* promoter of plasmid pSJ023 inserted between the *lctP* and *aspC* genes, KS031 was transformed with pKS007. To generate strain KS037, in which the *tsaP* deletion in strain SJ082-MS is complemented by a copy of *tsaP*ΔA33-R83 behind the *lac* promoter inserted between the *lctP* and *aspC* genes, SJ082-MS was transformed with pKS036. All chromosomal mutations were confirmed by DNA sequence analysis.

Table 3 *Escherichia coli* strains used in this study

Strain	Genotype	Source or references
DH5α	F ⁻ Φ80 <i>lacZ</i> ΔM15 Δ(<i>lacZYA-argF</i>) U169 <i>recA1 endA1 hsdR17</i> (rK ⁻ , mK ⁺) <i>phoA supE44 λ- thi-1 gyrA96 relA1</i>	Invitrogen
BL21 (DE3) Star	F ⁻ <i>ompT hsdS_B</i> (r _B ⁻ , m _B ⁻) <i>gal dcm rne131</i> (DE3)	Invitrogen
Rosetta 2 (DE3)	F ⁻ <i>ompT hsdS_B</i> (r _B ⁻ m _B ⁻) <i>gal dcm</i> (DE3) pRARE2 (Cm ^R)	Novagen/Merck
BTH101	F ⁻ <i>cya-99 araD139 galE15 galK16 rpsL1</i> (Str ^r) <i>hsdR2 mcrA1 mcrB1</i>	EUROMEDEX

3.1.2 Plasmid

Table 4 Plasmids used in this study

Plasmid	Properties	Source or references
pIND3	Insertion duplication mutagenesis vector for <i>N. gonorrhoeae</i> ; Erm ^R	[16]
pET20b(+)	Expression vector, T7 promoter; Amp ^R	Merck Millipore
pKS001	Plasmid, which is used as template to construct different <i>tsaP</i> mutants by site directed mutagenesis	This study
pKS004	Plasmid to construct <i>tsaP</i> ΔS213-V245 deletion created by site-directed mutagenesis using primers 1007 and 1008	This study
pKS007	pSJ023- <i>tsaP</i> ; Cm ^R	This study
pKS011	Plasmid used for BACTH analysis. Contains PCR product encoding TsaP(aa23-407) created with primers 1066 and 1067, cloned in KpnI and PstI site of pKT25; Kan ^R	This study

pKS012	Plasmid used for BACTH analysis. Contains PCR product encoding Tsap(aa152-407) created with primers 1074 and 1067, cloned in KpnI and PstI site of pKT25; Kan ^R	This study
pKS013	Plasmid used for BACTH analysis. Contains PCR product encoding Tsap(aa23-151) created with primers 1066 and 1069, cloned in KpnI and PstI site of pKT25; Kan ^R	This study
pKS014	Plasmid used for BACTH analysis. Contains PCR product encoding Tsap(aa23-407) created with primers 1068 and 1067, cloned in KpnI and PstI site of pKNT25; Kan ^R	This study
pKS015	Plasmid used for BACTH analysis. Contains PCR product encoding Tsap(aa152-407) created with primers 1065 and 1067, cloned in KpnI and PstI site of pKNT25; Kan ^R	This study
pKS016	Plasmid used for BACTH analysis. Contains PCR product encoding Tsap(aa23-151) created with primers 1068 and 1069, cloned in KpnI and PstI site of pKNT25; Kan ^R	This study
pKS017	Plasmid used for BACTH analysis. Contains PCR product encoding Tsap(aa23-407) created with primers 1068 and 1067, cloned in KpnI and PstI site of pUT18C; Amp ^R	This study
pKS018	Plasmid used for BACTH analysis. Contains PCR product encoding Tsap(aa152-407) created with primers 1065 and 1067, cloned in KpnI and PstI site of pUT18C; Amp ^R	This study
pKS019	Plasmid used for BACTH analysis. Contains PCR product encoding Tsap(aa23-151) created with primers 1068 and 1069, cloned in KpnI and PstI site of pUT18C; Amp ^R	This study
pKS020	Plasmid used for BACTH analysis. Contains PCR product encoding Tsap(aa23-407) created with primers 1068 and 1067, cloned in KpnI and PstI site of pUT18; Amp ^R	This study
pKS021	Plasmid used for BACTH analysis. Contains PCR product encoding Tsap(aa152-407) created with primers 1065 and 1067, cloned in KpnI and PstI site of pUT18; Amp ^R	This study
pKS022	Plasmid used for BACTH analysis. Contains PCR product encoding Tsap(aa23-151) created with primers 1068 and 1069, cloned in KpnI and PstI site of pUT18; Amp ^R	This study
pKS023	Plasmid used for BACTH analysis. Contains PCR product encoding PilQ(aa25-715) created with primers 1070 and 1071, cloned in KpnI and BamHI site of pKT25; Kan ^R	This study
pKS024	Plasmid used for BACTH analysis. Contains PCR product encoding PilQ(aa25-300) created with primers 1070 and 1072, cloned in KpnI and BamHI site of pKT25; Kan ^R	This study

pKS025	Plasmid used for BACTH analysis. Contains PCR product encoding PilQ(aa301-715) created with primers 1073 and 1071, cloned in KpnI and BamHI site of pKT25; Kan ^R	This study
pKS026	Plasmid used for BACTH analysis. Contains PCR product encoding PilQ(aa25-715) created with primers 1070 and 1071, cloned in KpnI and BamHI site of pKNT25; Kan ^R	This study
pKS027	Plasmid used for BACTH analysis. Contains PCR product encoding PilQ(aa25-300) reated with primers 1070 and 1072, cloned in KpnI and BamHI site of pKNT25; Kan ^R	This study
pKS028	Plasmid used for BACTH analysis. Contains PCR product encoding PilQ(aa301-715) reated with primers 1073 and 1071, cloned in KpnI and BamHI site of pKNT25; Kan ^R	This study
pKS029	Plasmid used for BACTH analysis. Contains PCR product encoding PilQ(aa25-715) created with primers 1070 and 1071, cloned in KpnI and BamHI site of pUT18C; Amp ^R	This study
pKS030	Plasmid used for BACTH analysis. Contains PCR product encoding PilQ(aa25-300) created with primers 1070 and 1072, cloned in KpnI and BamHI site of pUT18C; Amp ^R	This study
pKS031	Plasmid used for BACTH analysis. Contains PCR product encoding PilQ(aa301-715) created with primers 1073 and 1071, cloned in KpnI and BamHI site of pUT18C; Amp ^R	This study
pKS032	Plasmid used for BACTH analysis. Contains PCR product encoding PilQ(aa25-715) created with primers 1070 and 1071, cloned in KpnI and BamHI site of pUT18; Amp ^R	This study
pKS033	Plasmid used for BACTH analysis. Contains PCR product encoding PilQ(aa25-300) created with primers 1070 and 1072, cloned in KpnI and BamHI site of pUT18; Amp ^R	This study
pKS034	Plasmid used for BACTH analysis. Contains PCR product encoding PilQ(aa301-715) created with primers 1073 and 1071, cloned in KpnI and BamHI site of pUT18; Amp ^R	This study
pKS035	Vector for overexpression of 10x his-tagged TsaPΔA33-R83; Amp ^R	This study
pKS036	Plasmid to construct <i>tsaPΔA33-R83</i> deletion. Created	This study

	by site-directed mutagenesis on pKS007 using primers 1107 and 1108; Cm ^R	
pAW001	Vector for overexpression of 10x his-tagged TsaP; Amp ^R	Alexander Wagner
pAW003	Vector for overexpression of HA-tagged PilQ(B1/B2); Amp ^R	Alexander Wagner
pSJ023	Vector for overexpression of OneSTrEP tagged SsbB (derived from pKH37 vector); Cm ^R	Samta Jain
pSJ082	Plasmid to construct <i>tspP</i> deletion vis insertion-duplication mutagenesis; Erm ^R	Samta Jain
pSC108	Vector for overexpression of 6x his-tagged PilQ _{mx} aa20-656; Kan ^R	Carmen Friedrich
pSC121	Vector for overexpression of MalE-tagged TsaP _{mx} ; Amp ^R	Carmen Friedrich
pKNT25	Bacterial Adenylate Cyclase Two-Hybrid System vector; Kan ^R	EUROMEDEX
pKT25	Bacterial Adenylate Cyclase Two-Hybrid System vector; Kan ^R	EUROMEDEX
pUT18	Bacterial Adenylate Cyclase Two-Hybrid System vector; Amp ^R	EUROMEDEX
pUT18C	Bacterial Adenylate Cyclase Two-Hybrid System vector; Amp ^R	EUROMEDEX

3.1.3 Oligonucleotides

Table 5 Oligonucleotides used in this study

Oligonucleotide name	Sequence ¹	Description
418F-GGI	5'-AAGCATGATGAGGGCTATGG-3'	<i>traH-exp1-C-For</i>
472R-GGI	5'-GATATGCCCGAGTCTGAAGC-3'	<i>traD</i>
473F-GGI	5'-CCCAATGCGTCAATAAGAGG-3'	<i>traD</i>
474R-GGI	5'-GTCTATCCAACCGGTGACAG-3'	<i>tral</i>
475F-GGI	5'-CCCGTTCTTTAGCTTTCTC-3'	<i>tral</i>
476F-GGI	5'-TGGTCGGACGGAACACAGAG-3'	<i>ItgX-traF-H-For</i>
477R-GGI	5'-CGACCTGCGTACCAATAGGG-3'	<i>ItgX-traF-H-Rev</i>
478F-GGI	5'-GGCCTGCTGCAATAGTGATG-3'	<i>ItgX-traF-C-For</i>
479R-GGI	5'-ACCGCACTAGCGGACTTTAC-3'	<i>ItgX-traF-C-Rev</i>
480F-GGI	5'-CAGCTTGGACAGTCGATATG-3'	<i>ItgX-traF-I-For</i>
481R-GGI	5'-TTGGCCGCTGTCTTGTTTAG-3'	<i>ItgX-traF-I-Rev</i>
482F-GGI	5'-AGACAGCGGCAAAGCATTTC-3'	<i>ItgX-traF-J-For</i>

483R-GGI	5'-CCGGCTACGATTACATTGCG-3'	<i>ItgX-traF</i> -J-Rev
484F-GGI	5'-AGGGAGGCATCCGTTAATGG-3'	<i>ItgX-traF</i> -K-For
485R-GGI	5'-GATGGAAGTCCTTGCTAGAG-3'	<i>ItgX-traF</i> -K-Rev
486F-GGI	5'-ATGTCCGGCTTCGGTATAGG-3'	<i>ItgX-traF</i> -E-For
487F-GGI	5'-ATCAAGCAGCACGCATTTGG-3'	<i>traH-exp1</i> -D-For
488R-GGI	5'-CGCACTTGCGGATTATGAAC-3'	<i>traH-exp1</i> -D-Rev
489F-GGI	5'-TAGCGTATTCCC GCCCTGTC-3'	<i>ItgX-traF</i> -LM-For
491F-GGI	5'-TACAGCCGAGGCCATTGAAG-3'	<i>ItgX-traF</i> -G-For
492R-GGI	5'-CAAGGCTGCCAATGAAACC-3'	<i>ItgX-traF</i> -G-Rev
493F-GGI	5'-TAAGGTCTTCCC GG TAGTTG-3'	<i>ItgX-traF</i> -F-For
494R-GGI	5'-ATGGCAGTCGGGAATAACTC-3'	<i>ItgX-traF</i> -F-Rev
495F-GGI	5'-CCGCTAGTGCGGTTGCATTG-3'	<i>ItgX-traF</i> -D-For
496R-GGI	5'-GATACCGGCACATGATAATCTC-3'	<i>ItgX-traF</i> -D-Rev
498R-GGI	5'-GACGGAATGCGACTATTGAG-3'	<i>Ssb-yegA</i> -E-Rev
499F-GGI	5'-ACTTCCAGTATGCTGGTAGAGGGC-3'	<i>Ssb-yegA</i> -D-For
701R-GGI	5'-GTGGTTGAACACCGACAATC-3'	<i>Ssb-yegA</i> -D-Rev
702F-GGI	5'-TTACGGTAGCCACAGTAGTC-3'	<i>Ssb-yegA</i> -B-For
703R-GGI	5'-CTGAGCGTGTAGAAGCTATC-3'	<i>Ssb-yegA</i> -B-Rev
704F-GGI	5'-TGAGACTGCTCACGTTTAGG-3'	<i>Ssb-yegA</i> -A-For
705R-GGI	5'-TTCTGTGCCGATGACTGTCC-3'	<i>Ssb-yegA</i> -A-Rev
706R-GGI	5'-GCCGTATGTCGAGAAAGAAG -3'	<i>parA-yfa</i> -G-Rev
707R-GGI	5'-GCAGCATAGGGAGCCATTTCC-3'	<i>ItgX-traF</i> -E-Rev
708R-GGI	5'-ATGTCTGTCCGACCTGTAAG-3'	<i>Ssb-yegA</i> -C-Rev
709F-GGI	5'-CTTCAGGATTGTCGGTGTTCC-3'	<i>Ssb-yegA</i> -C-For
710F-GGI	5'-TGTGTCAACACCGAACTACC-3'	<i>yaf-yaa</i> -E-For
711R-GGI	5'-AACGCATTTACGGAGGGAAG-3'	<i>yaf-yaa</i> -E-Rev
712F-GGI	5'-TTCCAGATAACCGCTAGCAC-3'	<i>yaf-yaa</i> -AB-For
713F-GGI	5'-CGGCCACTGGAAGAAACAAC-3'	<i>parA-yfa</i> -F-For
714R-GGI	5'-GAGACCAGGGCTATCAAGAG-3'	<i>parA-yfa</i> -F-Rev
716R-GGI	5'-GAAAGCGCTCTCGGTTAATG-3'	<i>ItgX-traF</i> -AB-Rev
717R-GGI	5'-AAACGGGAGCTAAGAGTGAG-3'	<i>parA-yfa</i> -D-Rev
718F-GGI	5'-TTGGGCAAGGCTATAATCGG-3'	<i>parA-yfa</i> -D-For
721R-GGI	5'-TCTGTGACAATTCTAATTAATAAAC-3'	<i>yaf-yaa</i> -B-Rev
722F-GGI	5'-AGGGAAGGGCATCCTTACTC-3'	<i>yaf-yaa</i> -C-For
723R-GGI	5'-GCCACTGCCGATAGATATTG-3'	<i>yaf-yaa</i> -C-Rev
724F-GGI	5'-GGCAGTAAGGGCATAATAGG-3'	<i>yaf-yaa</i> -D-For
725R-GGI	5'-CATACAGCCAGGTTCAAGAC-3'	<i>yaf-yaa</i> -D-Rev
726F-GGI	5'-GGTTAAGTTGCGGCTTTCAC-3'	<i>Ssb-yegA</i> -E-For
728F-GGI	5'-ATATCTAGCTAAAATGCCACGGACAG-3'	<i>parA-yfa</i> -G-For

730R-GGI	5'-TGTTGGCCATGATGCGTTTC-3'	<i>yaf-yaa-FG-Rev</i>
733F-GGI	5'-GAGGTAACGATCTAGTATCC-3'	<i>traH-exp1-EF-For</i>
734R-GGI	5'-TGCTCAAGTAGTGATTTAGG-3'	<i>traH-exp1-E-Rev</i>
739R-GGI	5'-GCCGGTTCAGATATACCAGG-3'	<i>traH-exp1-F-Rev</i>
743R-GGI	5'-ATTGGCTTCCGCTCCCATTG-3'	<i>traH-exp1-AB-Rev</i>
744F-GGI	5'-GCTATAACCGCTTCATGGAG-3'	<i>traH-exp1-A-Rev</i>
746F-GGI	5'-GACAACGCGGATATTTCCAGG-3'	<i>traH-exp1-B-Rev</i>
748R-GGI	5'-AATATCCGCGTTGTCAACCG-3'	<i>ltgX-traF-L-For</i>
750R-GGI	5'-GCCGGCTTCGAAAAGATGTG-3'	<i>ltgX-traF-M-For</i>
766R-GGI	5'-ATCGTGATGCTGCCCATCTC-3'	<i>ssbB</i>
767F-GGI	5'-ACGCTCAGTTGGAACAATGAATAC-3'	<i>ssbB</i>
769F-GGI	5'-CCTGCCACAGTGTAGTAAAC-3'	<i>topB</i>
770R-GGI	5'-TCGATCGGACGGATTCAAAC-3'	<i>topB</i>
774R-GGI	5'-GGCAGCATTATACCTTATAAATC-3'	<i>yaf-yaa-B-Rev</i>
775R-GGI	5'-TCAAGGGAAAAAGGGTAAAAG-3'	<i>yaf-yaa-A-Rev</i>
776R-GGI	5'-GCAACAGCAAGAGTGACCAG-3'	<i>traH-exp1-C-Rev</i>
778F-GGI	5'-GCCTTTACCTTATCGTATTC-3'	<i>ltgX-traF-B-For</i>
779F-GGI	5'-CTTGAACCCTTCTTTAACCC-3'	<i>ltgX-traF-A-For</i>
784F-GGI	5'-AGCCAAAGCAGCACGAGCCATATC-3'	<i>parA-yfa-E-For</i>
785R-GGI	5'-TAACCTATGCCCCTGCGCTTC-3'	<i>parA-yfa-E-Rev</i>
786F-GGI	5'-ATTGTCGAGCGGATGATTTTC-3'	<i>parA-yfa-ABC-For</i>
592	5'-gagt ggtacc TACAGCCCGTGGAATGGTG-3'	<i>tsaP</i> -KpnI
593	5'-cat ggATCc AAGGATGGGTGCGGGTGTAG-3'	<i>tsaP</i> -BamHI
697	5'-GCTTACGGCGTTGCTTATTG-3'	<i>secY</i>
698	5'-CCCGCCCTACCATTAAACTG-3'	<i>secY</i>
914	5'-ACCGGCTACACGTACAACCTG-3'	<i>yaf-yaa-F-For</i>
915	5'-GCTGGGACATATTGGAATGG-3'	<i>parA-yfa-B-Rev</i>
926	5'-CAGACGCTCCATTCTCGAAG-3'	<i>yaf-yaa-G-For</i>
1001	5'-gcg cggtacc ATGCAACGTCGTATTATAACCCTGCTCTGC GCGGCAGGTATGGCATTCTC-3'	<i>tsaP</i> -KpnI
1002	5'-gcg gaattc TTATTGGAAAGGGTTCGGAATCG-3'	<i>tsaP</i> -EcoRI
1007	5'-TCGGAAATGGCGGTTTCGACGCGTTGTTTCGAGGGCGG AGTC-3'	<i>tsaPΔS231-V245</i>
1008	5'-GTCGAAACCGCCATTTCCGAAATACAGCAGGGCGACT ACCTGATG -3'	<i>tsaPΔS231-V245</i>
1048	5'-GATTGCGGATGTTTTTCTCTTTATAAATC-3'	<i>parA-yfa-C-Rev</i>
1050	5'-GCAATGGCGGAGGAATTCAC-3'	<i>parA-yfa-A-Rev</i>
1052	5'-cggcgtata catatg caccatcaccaccatcatcaccatcaccacGC AAATCTGGAGGTGCGCCC-3'	<i>tsaP</i>

1057	5'-gcgcca TATG CAACGTCGTATTATAACCCTGCTCTGCG CGGCAGGTATGGCATTCTC-3'	<i>tsaP</i> -NdeI
1058	5'-gcgcgcca agctt TTATTGGAAAGGGTCGGAATCG-3'	<i>tsaP</i> -HindIII
1061	5'-gcgcg ctcga GTTATTGGAAAGGGTCGGAATC-3'	<i>tsaP</i> -PstI
1065	5'-tcgcg ctcag GCTGTACACCAAAGGCGCCAGGG-3'	<i>tsaP</i> -PstI
1066	5'-tcgcg ctcag GGCAAATCTGGAGGTGCGCCC-3'	<i>tsaP</i> -PstI
1067	5'-gcgcg ggtagc CGTTGGAAAGGGTCGGAATCGAC-3'	<i>tsaP</i> -KpnI
1068	5'-tcgcg ctcag GGCAAATCTGGAGGTGCGCCC-3'	<i>tsaP</i> -PstI
1069	5'-gcgcg ggtagc CGCAGCTGCCTTCCGGGCCCGAGAG-3'	<i>tsaP</i> -KpnI
1070	5'-gcgcg ggatcc CGGAAACATTACAGACATCAAAG-3'	<i>pilQ</i> -PstI
1071	5'-gcgcg ggtagc CGATAGCGCAGGCTGTTGCC-3'	<i>pilQ</i> -KpnI
1072	5'-gcgcg ggtagc CGCCGGCCTGTGAAGGTTTTGG-3'	<i>pilQ</i> -KpnI
1073	5'-gcgcg ggatcc CAAAATCTCCCTTGACTTCCAAGATG-3'	<i>pilQ</i> -PstI
1074	5'-tcgcg ctcag GGCTGTACACCAAAGGCGCCAGGG-3'	<i>tsaP</i> -PstI
1107	5'-GAGGCGCGGTTTCGCCCAACGTACGCCAAAGTTTGT GTTGAGAATG-3'	<i>tsaP</i> Δ A33-R83
1108	5'-CTCAACACAAACTTTGGCGTACGTTGGCGGCGAACCG CGCCTC-3'	<i>tsaP</i> Δ A33-R83

¹ Sequences in bold display restriction sites used for cloning. Sequences in upper case indicate sequences complementary to the respective genes. Sequences in lower case show added sequences required for cloning purposes.

3.1.4 Media and Media supplements

Table 6 Lysogeny Broth (LB) medium

Component	
Yeast Extract	15 g
Tryptone	10 g
NaCl	10 g
H ₂ O	add to a total volume of 1 L

Table 7 LB agar

Component	
Agar	15 g
LB medium	add to a total volume of 1 L

Table 8 GCBL medium

Component	
Protease peptone	15 g
Dipotassium phosphate	4 g

Potassium dihydrogen phosphate	1 g
NaCl	1 g
H ₂ O	1 L

Before use, add 1 % supplement I (100x) and 0.1 % supplement II (1000x) and 10 % Sodium bicarbonate (100x)

Table 9 GCB agar

Component	
GC medium base	36.25 g
Agar	1.25 g
H ₂ O	1 L

After autoclaving add 1 % supplement I (100x), 0.1 % supplement II (1000x)

Table 10 Supplement I (100 x)

Component	
Glucose	40 g
Glutamine	1 g
Thiamine pyrophosphate	2 mg
H ₂ O	add to a total volume of 100 ml

Table 11 Supplement II (1000 x)

Component	
Iron (III) nitrate	50 mg
H ₂ O	add to a total volume of 100 ml

Table 12 Sodium bicarbonate (100 x)

Component	
Sodium bicarbonate	0.42 g
H ₂ O	add to a total volume of 100 ml

3.1.5 Antibiotics

Table 13 Antibiotics used in this study

Antibiotic	Stock concentration [mg/ml]	Final concentration [µg/ml]		Solvent
		<i>E. coli</i>	<i>N. gonorrhoeae</i>	
Chloramphenicol	34	34	10	EtOH
Erythromycin	50	450	20	EtOH
Kanamycin	50	50	-	H ₂ O
Ampicillin	34	34	-	H ₂ O

3.1.6 Buffer and solutions

Table 14 Assay buffer

Component	
Tris/HCl; pH 10	100 mM
NaCl	100 mM
MgCl ₂	1 mM

Table 15 Coomassie staining solution

Component	
Ethanol	125 ml
Acetic acid	100 ml
Coomassie Blue R250	0.5 g
CuSO ₄ 5 H ₂ O	0.5 g
H ₂ O	add to a total volume of 250 ml

Table 16 Destaining solution

Component	
CuSO ₄ 5 H ₂ O	0.5 % (w/v)
Acetic-acid	7 % (v/v)
2-n-Propanol	12 % (v/v)

Table 17 Lysis buffer

Component	
Triton X-100	1 % (v/v)
EDTA; pH 8.0	2 mM
Tris/HCl	20 mM

Table 18 Protein purification buffer A

Component	
HEPES/NaOH; pH 7.5	50 mM
NaCl	100 mM
Imidazole	15mM
Glycerol	10 % (v/v)

Table 19 Protein purification buffer B

Component	
HEPES/NaOH; pH 7.5	50 mM
NaCl	100 mM
Imidazole	400 mM

Glycerol	10 % (v/v)
----------	------------

Table 20 Protein purification buffer C

Component	
HEPES/NaOH; pH 7.5	50 mM
NaCl	100 mM
Glycerol	10 % (v/v)

Table 21 Protein purification buffer D

Component	
Tris/HCl; pH 7.5	20 mM
NaCl	200 mM
Imidazole	15 mM
Glycerol	10 % (v/v)

Table 22 Protein purification buffer E

Component	
Tris/HCl; pH 7.5	20 mM
NaCl	200 mM
Imidazole	400 mM
Glycerol	10 % (v/v)

Table 23 Protein purification buffer F

Component	
Tris/HCl; pH 7.5	20 mM
NaCl	200 mM
Glycerol	10 % (v/v)
DTT	1 mM

Table 24 Protein purification buffer G

Component	
HEPES/NaOH; pH 7.5	50 mM
NaCl	400 mM
Imidazole	100 mM
Glycerol	10 % (v/v)

Table 25 Protein purification buffer H

Component	
HEPES/NaOH; pH 7.5	50 mM
NaCl	400 mM

Imidazole	500 mM
Glycerol	10 % (v/v)

Table 26 Protein purification buffer I

Component	
HEPES	50 mM
NaCl	400 mM
Glycerol	10 % (v/v)

Table 27 Protein purification buffer J

Component	
Tris/HCl; pH 7.5	20 mM
NaCl	200 mM
DTT	1 mM
EDTA	1 mM

Table 28 Protein purification buffer K

Component	
Tris/HCl; pH 7.5	20 mM
NaCl	200 mM
DTT	1 mM
EDTA	1 mM
Maltose	1 mM

Table 29 Resolving-gel buffer

Component	
Tris/HCl; pH 6.8	500 mM
SDS	0.4 % (w/v)

Table 30 Sodium Boric Acid buffer (20x; pH 8,5)

Component	
NaOH	200 mM
EDTA; pH 8.0	40 mM

Table 31 Stacking-gel buffer

Component	
Tris/HCl; pH 8.8	1.5 M
SDS	0.4 % (w/v)

Table 32 TBS buffer

Component	
Tris/HCl; pH 7.5	38 mM
NaCl	15 mM

Table 33 TBST+I buffer

Component	
TBS	1 x concentrated
I-Block	0.1 % (w/v)
Tween 20	0.1 % (w/v)

Table 34 TGS buffer

Component	
Tris base	30.28 g
SDS	10 g
Glycine	144.13 g
H ₂ O	add to a total volume of 1000 ml

Table 35 Transfer buffer

Component	
Tris base	20 mM
Glycine	200 mM
Methanol	20 % (v/v)

Table 36 6x DNA loading dye

Component	
Tris/HCl; pH 7.6	10 mM
Bromophenol blue	0.03 % (w/v)
EDTA	60 mM
Glycerol	60 % (v/v)

Table 37 5x Protein loading dye

Component	
SDS	10 % (w/v)
Bromophenol blue	0.04 % (w/v)
DTT	500 mM
Glycerol	50 % (v/v)
Tris/HCl; pH 6.8	300 mM

3.1.6 DNA & Protein Ladder

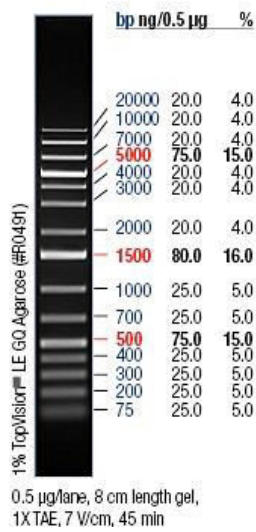


Figure 7 GeneRuler™ 1kb Plus DNA Ladder

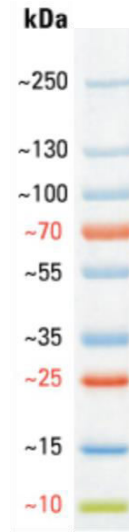


Figure 8 PageRuler Prestained Protein Ladder Plus



Figure 9 NativeMark™ Unstained Protein Standard

3.1.7 Kits

Table 38 Kits used in this study

Name	Reagents
First Strand cDNA Synthesis Kit	M-MuLV Reverse Transcriptase; RiboLock RNase Inhibitor; 5x Reaction buffer; 10 mM dNTP Mix; 100 µM random Hexamer Primer; nuclease free H ₂ O
Dnase I	RNase-free DNase I; 10x Reaction Buffer with MgCl ₂ ; 50 mM EDTA
peqGOLD TriFast™	peqGOLD TriFast™
GenElute™ PCR Clean-Up Kit	Column Preparation Solution; Binding Solution; Wash Solution
GenElute™ HP Plasmid Miniprep Kit	Column Preparation Solution; Resuspension Solution; Lysis Buffer; Neutralization/Binding Buffer; Wash Solution 1, Wash Solution 2;

3.2 Microbiological and molecular biological methods

3.2.1 Cultivation *E. coli*

E. coli strains were cultivated on LB agar plates, containing the appropriate antibiotic. For overnight cultures, single colonies were inoculated in 3 ml LB medium. Cells were grown 37 °C in a shaking incubator.

3.2.2 Cultivation of *N. gonorrhoeae*

N. gonorrhoeae strains were grown on GCB agar plates, containing the appropriate antibiotic. Incubation was performed at 37 °C and 5 % CO₂. The colony morphology, which indicates whether cells are piliated or non-piliated was checked under the light microscope before daily restreaking. Under the microscope piliated colonies of *N. gonorrhoeae* are small with sharp edges. In contrast, non-piliated *N. gonorrhoeae* colonies are flat and bigger in size with “fuzzy” edges. Liquid cultures of *N. gonorrhoeae* were inoculated from cell material of one fully grown agar plate and incubated 1.5 h in 3 ml of pre-warmed GCBL medium. After measuring the optical density at 600 nm (OD₆₀₀), the liquid culture was diluted to OD₆₀₀ 0.3. For further experiments the diluted culture was incubated at 37 °C (shaking) until the cells reached an OD₆₀₀ ~1.0. 3 ml cells were pelleted in a 2 ml tube and stored at -80 °C for further use.

3.3 Molecular methods

3.3.1 Isolation of genomic DNA from *N. gonorrhoeae*

Cell pellets derived from a 3 ml liquid culture of *N. gonorrhoeae* cells were used to isolate genomic DNA according to the instruction manual of the ZR Genomic DNA II Kit. DNA concentrations were measured using the PeqLab Nanodrop ND-1000 spectrophotometer.

3.3.2 Isolation of plasmid DNA

Plasmid DNA was isolated from 5 ml liquid cultures of *E. coli* according to the instruction manual of the GenElute™ HP Plasmid Miniprep Kit. Plasmid DNA concentrations were measured using the PeqLab Nanodrop ND-1000 spectrophotometer.

3.2.3 Agarose gel electrophoresis

DNA fragments or PCR products were separated according to their molecular sizes in 1.5 % agarose in 1x SBA-buffer. Staining of nucleic acids was achieved by the intercalating fluorescent dye ethidium bromide which was added to the agarose gel with a final concentration of 1 µg/ml to the agarose gel. The samples were mixed with 6x DNA loading dye before loaded on the agarose gel. The voltage and gel running buffer were adjusted according to the demanded separation characteristics. To estimate the size of a DNA fragment the 1 kb Plus DNA Ladder was also loaded on the gel. DNA fragments were visualized by illuminating at 365 nm and then photographed using the UVP Bio-Doc Imaging System and Mitsubishi Electronic P93 printer.

3.3.4 Polymerase Chain Reaction

3.3.4.1 Standard PCR

Standard PCR amplification of DNA was performed using Phusion polymerase. After an initial denaturation step of 30 sec at 98 °C, 35 cycles of denaturation (98 °C for 10 sec), annealing (30 sec) and elongation (30 sec/kb) were performed, followed by a final elongation at 72 °C for 10 min. The annealing temperature was chosen depending on the melting temperature of the primer as provided by the primer manufacturer or calculated by Clone Manager (normally in the range of 50-65 °C). The

elongation time was chosen depending on the length of the PCR product. The composition of a 50 μ l PCR reaction is shown in Table 39.

Table 39 Pipetting scheme of a 50 μ l PCR reaction

PCR reaction mixture	Volumes per reaction
H ₂ O	36.3 μ l
5x Phusion HF-Buffer	10 μ l
dNTPs (10 mM)	0.5 μ l
Primer (10 μ M)	1.0 μ l each
Template DNA	1.0 μ l
Phusion DNA polymerase	0.2 μ l

3.3.4.2 Colony PCR

Colony PCR was used to identify bacterial clones containing the correct insertion. Single colonies were picked and transferred to PCR tubes containing 50 μ l Lysis buffer (Table 17) followed by heating to 95 °C and incubation for 10 min. The lysate was kept for additional 10 min at room temperature and centrifuged for 10 min at 17,000 x *g*. 4 μ l of the lysate was used as a PCR template. PCR amplification of DNA was performed as described in 3.3.4.1.

3.3.5 RNA isolation

After thawing cell pellets of piliated and non-piliated *N. gonorrhoeae* strains, the pellet was resuspended in 1 ml TriFast™ buffer per reaction tube. To allow for the complete dissociation of the nucleoprotein complexes, the samples were kept for about 10 minutes at room temperature. After addition of 200 μ l of chloroform, the samples were shaken vigorously for 15 sec and kept again at room temperature for 10 minutes. The red phenol-chloroform phase, the interphase and the colorless RNA containing aqueous phase were separated by centrifugation for 10 min at 12,000 x *g*. The RNA containing aqueous phase was transferred to a new 1.5 ml reaction tube containing 500 μ l of isopropanol. The RNA was precipitated by incubating the tube for 15 min on ice. After centrifugation at 4 °C for 10 minutes at 12,000 x *g*, RNA was pelleted at the side of the tube. After removal of the supernatant the RNA pellet was washed twice with 1ml ice-cold ethanol (75 % (v/v)) by vortexing and subsequent centrifugation at 4 °C for 10 minutes at 12,000 x *g*. The supernatant was removed carefully after the second washing step and the RNA pellet was air-dried. After resuspending the pellet in 20 μ l diethylidicarbonate (DEPC) treated water the RNA concentration was measured using the PeqLab Nanodrop ND-1000 spectrophotometer.

3.3.6 First Strand cDNA Synthesis

Total RNA was (0.2 μ g) mixed with DEPC treated H₂O up to a final volume of 10 μ l and 1 μ l random hexamer primer (0.2 μ g/ μ l) was added in a sterile reaction tube. The tubes were heated at 65 °C for 10 min in the PCR cycler. After preparation of the reverse transcriptase mixture according to Table 40, 9 μ l of the mixture were pipette into each reaction tube containing RNA. The sample was

incubated for 5 min at 25 °C, followed by 60 min incubation at 37 °C. The reaction was terminated by incubation for 5 min at 70 °C. A control of cDNA synthesis was performed without the addition of Reverse transcriptase. The cDNA was stored at -80 °C was used as a template for polymerase chain reaction (PCR) and real-time PCR amplification reactions.

Table 40 Components of reverse transcriptase mixture

Reverse transcriptase mixture	Volumes per reaction
5x Reaction Buffer	4 µl
RiboLock RNase Inhibitor (20 U/µl)	1 µl
dNTP Mix (10mM)	2 µl
M-MuLV Reverse Transcriptase (20 U/µl)	2 µl

3.3.7 Transcriptional mapping

The most general applied operon prediction method is a PCR based on intergenic distances. Total RNA from pilated and non-piliated *N. gonorrhoeae* strains was isolated and transcribed into cDNA according to 3.3.5 and 3.3.6. After cDNA synthesis PCR was performed as described in 3.3.4.1. A typical reaction composition for transcriptional mapping is shown in Table 41. If the intergenic distance between two genes was found to be ≥ 10 nucleotides the region was selected for transcriptional analysis and oligonucleotides were designed for this region according to the GGI sequence.

Table 41 Pipetting scheme of a 50µl transcriptional mapping PCR

Reverse transcription reaction mixture	Volumes per reaction
H ₂ O	35.3 µl
5x Phusion HF-Buffer	10 µl
dNTPs (10 mM)	0.5 µl
Primer (10 µM)	1.0 µl each
Template DNA	2.0 µl
Phusion DNA polymerase	0.2 µl

3.3.8 Real-Time PCR

To determine the transcript levels of genes encoded within the GGI the Maxima SYBR Green/ ROX qPCR Master Mix was used. After an initial denaturation step of 2 min at 95 °C, 40 cycles of amplification, with 15 sec at 95 °C and 1 min at 60 °C, followed by melting curve analysis (15 sec at 95 °C, 30 sec at 60 °C and 15 sec at 95 °C), was performed using a 7300 Real Time PCR System of Applied Biosystems. Results were depicted as the level of transcript compared with the *secY* gene ($2^{-\Delta Ct}$). A typical 25 µl qRT-PCR reaction mixture is shown in Table 42. For each gene, six biological replicates were performed.

Table 42 Pipetting scheme of a 25 μ l qRT-PCR reaction

qRT-PCR reaction mixture	Volumes per reaction
Maxima SYBR Green/ ROX qPCR Master Mix	12.5 μ l
Primer A (0.3 μ M)	4.0 μ l
Primer B (0.3 μ M)	1.0 μ l
cDNA	2.0 μ l
H ₂ O	10.0 μ l

3.3.9 Restriction enzyme digestion

The purified vectors and PCR products were mixed with the corresponding restriction enzymes and digested as recommended by the manufacturer. In most cases the reaction mix was incubated in a double digest reaction for 1 h at 37 °C and inactivated as recommended by the manufacturer. The digested DNA was purified with the GenElute™ PCR Clean-Up Kit as described in the instruction manual. The DNA concentration was measured with PeqLab Nanodrop ND-1000 spectrophotometer.

3.3.10 Ligation

T4-ligase was used for DNA ligation. T4-ligase catalyzes the formation of phosphodiester bonds between neighbouring 3'-OH and 5'-phosphate ends. The amount (ng/ μ l) of insert, which was added into the reaction, was double the amount (ng/ μ l) of vector. A typical ligation reaction which is incubated for 1 hour at RT is shown in Table 43.

Table 43 Pipetting scheme of a 20 μ l ligation reaction

Ligation reaction mixture	Volumes per reaction
H ₂ O	9.0 μ l
5x Rapid Ligation Buffer	4.0 μ l
T4 DNA-Ligase	1.0 μ l
Insert	4.0 μ l
Vector	2.0 μ l

3.3.11 Transformation of *E. coli*

For transformation of *E. coli* cells, a 50 μ l aliquot of chemical competent cells were thawed on ice and 1 μ l plasmid DNA was added. After an incubation time of 30 min on ice the cells were subjected to a heat shock at 42 °C for 90 sec. The cells were immediately placed on ice for 2 min and 800 μ l of LB medium was added. The cells were incubated at 37 °C for 1 h while shaking vigorously. The transformed cells were either used to inoculate LB medium or were grown on LB agar plates. To obtain single colonies on LB agar plates 50 μ l of the culture was plated on LB agar plates supplemented with appropriate antibiotics. The plates were incubated overnight at 37 °C. For liquid cultures, 50 mL of LB medium supplemented with appropriate antibiotics was inoculated with the transformed cell suspension and incubated at 37 °C overnight.

3.3.12 Transformation of *N. gonorrhoeae*

3.3.12.1 Natural transformation of *N. gonorrhoeae*

In the presence of high concentrations of DNA, *N. gonorrhoeae* can be transformed at high efficiency by growing bacteria on agar plates. To insert a construct into the chromosome by double-crossover event, 10 to 20 μl of linearized plasmid or purified PCR products were spotted on GCB agar plates, whereas for insertion duplication mutagenesis 10 to 20 μl of non linearized plasmid were used. After DNA was soaked into the agar plate, a piliated *N. gonorrhoeae* colony was streaked through the DNA spots. Subsequently the plate was incubated over night at 37 °C and 5 % CO₂. For transformation without selectable markers, the individual colonies were screened onto GCB plates using an inoculation loop. The GCB agar plates were incubated overnight at 37 °C and 5 % CO₂ and the individual transformants were screened for non-selectable mutations by PCR (see chapter 3.3.4.2). For transformations using fragments containing selectable marker, cells that grew on the DNA spots were transferred onto a GCB plate with appropriate antibiotics. After the GCB agar plates were incubated overnight at 37 °C and 5 % CO₂, colonies were picked and screened for transformants as described above for transformation without selectable marker.

3.3.12.2 Electroporation of *N. gonorrhoeae*

N. gonorrhoeae strains were grown on GCB agar plates, supplemented with appropriate antibiotics. Incubation was performed at 37 °C in the presence of 5 % CO₂. To prepare the cells for electroporation, cell material of one fully grown agar plate was transferred into 1 ml pre-warmed sucrose (0.3 M) and centrifuged for 30 sec at 17,000 x *g* at 37 °C. After two more washing steps with pre-warmed 0.3 M sucrose the pellet was resuspended in 100 μl of 0.3 M sucrose and mixed with 1-5 mg DNA solution. The cell/DNA mixture was transferred into a 2 mm electroporation cuvette and electroporated with the pulse controller set at 2500 V, 25 μF , 200 Ω . Subsequently, cells were resuspended in 1 ml pre-warmed GCBL medium without antibiotics and transferred to a GCB agar plate without antibiotics. After incubating the plate right-side up for 6 h at 37°C and 5 % CO₂, cells were washed off the plate with 1 ml GCBL medium. 50 μl of the cell suspension was plated onto a GCB agar plate containing the appropriate antibiotic. When required multiple plates were used. GCB agar plates were incubated at 37 °C and 5 % CO₂ until colonies were observed.

3.3.13 Preparation of *N. gonorrhoeae* membranes

Cells of selected *N. gonorrhoeae* strains were grown overnight in 1 liter GCBL medium and harvested by centrifugation at 4,302 x *g* for 10 min. After resuspension of the pellet in 50 mM Tris/HCl pH 7.5 cells were broken by 3 shots of a high-pressure Cell Disrupter (Constant Cell Disruption Systems) at 1.9 kbar. Cell debris was removed by centrifugation for 10 min at 4,300 x *g*. Subsequently, membranes were sedimented by centrifugation at 178,000 x *g* for 1 hour. After the membrane fractions were resuspended in 1 ml 50 mM Tris/HCl pH 7.5, total membrane fractions were subfractionated on a discontinuous sucrose gradient consisting of 1 ml 54 %, 1.8 ml 51 %, 0.8 ml 45 % and 0.8 ml 36 % sucrose. Adjacent, centrifugation for 30 min at 44,400 x *g* the lower two fractions were collected, diluted in 50 mM Tris/HCl pH 7.5 and centrifuged for 1 hour at 178,000 x *g*.

The final membrane preparation was resuspended in 50 mM Tris/HCl pH 7.5 and used for membrane-stripping, immuno-blotting, SDS/PAGE and EM analysis.

3.3.14 Phenol treatment of *N. gonorrhoeae* membranes

To dissociate secretin complexes embedded in its native lipid environment, outer membrane samples were individually treated with an equal volume of phenol at 70 °C for 10 min. After incubating the samples for 10 min at 4 °C the phenol-protein suspension was centrifuged at 5,000 x *g* for 10 min. After discarding the upper aqueous layer, the interface and phenol layer was treated with 1 ml chilled acetone. After the incubation overnight at -20 °C the protein was collected by centrifugation for 10 min at high speed (4°C). To improve sharpness of the protein bands on SDS/PAGE gels, the pellet was washed twice with 1 ml chilled acetone. After collecting the proteins by centrifugation for 5 min at high speed and 4 °C, the supernatant was discarded and the pellet was dried at 37 °C. The final preparation was resuspended in 5x protein loading dye.

3.3.15 Bacterial adenylate cyclase two-hybrid system

Chemical competent BTH101 cells were co-transformed with BACTH plasmids. Serial dilutions of the transformants were plated on LB/X-Gal/IPTG agar plates and incubated at 30 °C for 2 days in order to obtain about 100-200 colonies per plate. If the proteins interact with each other the resulting β -galactosidase activity results in blue colonies. As a positive control, competent cells were co-transformed with the control plasmids pKT25-*zip* and pUT18C-*zip* whereas in the negative control cells were co-transformed with the plasmids pKT25 or pKNT25 and pUT18 or pUT18C. After two days, three clones per transformation were picked and used as inoculum for 2ml LB/IPTG. After an incubation time of 4 h, 2 μ l of the liquid cultures were applied on LB/X-Gal/IPTG plates for comparison of the color change.

3.4 Analytical and biochemical methods

3.4.1 SDS-Polyacrylamid-Gel electrophoresis

SDS/PAGE analyses were performed using the Bio-Rad Mini-PROTEAN Electrophoresis System Minigel-system (Biorad) with 0.75 mm or 1.5 mm gels. SDS-PAGE-gels consisting of a 12 % separating gel and a 4 % stacking gel were used. Before loading, the samples were mixed with 5x protein-loading dye. SDS/PAGE was performed in 1x TBE buffer at 30 mA/gel for 50 min. For further analysis the gels were either pre-equilibrated for immunoblot analysis or stained with coomassie staining solution (Table 15). Gels were destained by heating up with destaining solution (Table 16).

3.4.2 Blue-Native gel electrophoresis

Blue native PAGE analysis were performed with the Minigel-system from Biorad with 0.75 mm gels. these were cast as gradient gels with 4-13 % acrylamide. 4 % stacking gels were layered on top of the native gel. The compositions for 4 % and 13 % gels are given in Table 44. The gels were cast at room temperature with a gradient-casting system. The cathode buffer A was stirred overnight at room temperature to completely dissolve the coomassie. The sample buffer was made of cathode buffer A and 10 % glycerol (v/v). The gels were run at 4-7 °C. As long as the samples were in the stacking gel,

gels were run with cathode buffer A at a constant voltage of 100 V. After entering the native gel the voltage was changed to 150 V. When 1/3 of the gels were reached the cathode, the buffer was changed to cathode buffer B and the voltage was adjusted to 200 V. The molecular masses of the protein samples were calculated based on the migration rates of the marker proteins and the sample.

Table 44 Pipetting scheme of Blue native PAGE gels

Component	4 % gel	13 % gel
Acrylamide 40%	0.6 ml	3.25 ml
Gel buffer	2.0 ml	3.33 ml
Glycerol	-	2.0 ml
APS (10 % w/v)	50 μ l	60 μ l
TEMED	5 μ l	7 μ l
ddH ₂ O	6 ml	10 ml

3.4.3 Western Blotting

To identify proteins via immuno blotting, electrophoresed proteins were transferred onto a polyvinylidene difluoride membrane using the mini trans-blot electrophoretic transfer cell. After the membrane was blocked for 1 h with TBST-I buffer (Table 33), the membrane was incubated for 1.5 h with anti-PilQ, anti-TsaP or anti-PilE antibody (1:5000 dilution in TBST-I buffer). Before the membrane was incubated for 1.5 h with AP conjugated secondary antibody, the membrane was washed twice for 10 min. Subsequently, the membrane was washed 3 times for 10 min with TBST-I buffer. Finally, the membrane was equilibrated twice for 5 min with assay buffer (Table 14) followed by 5 min incubation with CDP-star solution. The chemiluminescence signal was detected using the LAS-4000 Fujifilm analyser.

3.4.4 Coomassie-Staining

Polyacrylamide gels, covered with coomassie staining solution, were heated in a microwave until boiling. The gels were incubated in the hot coomassie staining solution for 5-10 min on a platform shaker and then washed twice in H₂O. The gels were again heated in water and incubated for 5 min with constant shaking. A final destaining step was performed by incubating the gel in hot destaining solution until the background turned colorless. In a final step the gels were washed with H₂O and scanned with an Epson Perfection V700 Photo scanner.

3.4.5 Peptidoglycan isolation, binding and zymography

Murein sacculi of *N. gonorrhoeae* were purified from three liters of an exponentially growing culture as described previously [178]. The purification of the sacculi was confirmed by EM. To test for binding to peptidoglycan, 5 μ g purified *N. gonorrhoeae* TsaP or 5 μ g *E.coli* Exonuclease I was incubated with or without 1 mg peptidoglycan in a volume of 150 μ l for 1 h at 15 °C in protein-purification buffer D. Samples were spun down in an airfuge (Beckman Coulter) at 20 pounds per

square inch gage (psig) for 10 min. The supernatant (unbound fraction) was collected while the pellet was resuspended in protein purification buffer C. The samples were spun down again at 20 psig for 10 min. The supernatant (wash fraction) was collected and the pellet fraction was resuspended in 4 % SDS in buffer C, incubated for 2 h at 15 °C and centrifuged for 5 min at 15 psig. The supernatant (bound fraction) was collected. All fractions were precipitated with trichloroacetic acid and analyzed by immunoblotting. To test for PG hydrolysis activity of TsaP, 5 µg purified TsaP was loaded on 12 % SDS/PAGE gels containing 0.04 % (w/v) PG and zymography was performed essentially as described [178]. 5 µg BSA, lysozyme and mutanolysin were loaded as negative and positive controls, respectively.

3.4.6 Outer membrane detachment assay

Outer membranes were treatment with 7.5 M urea for 30 min at 4 °C on a rotary shaker. Following membrane treatment, samples were centrifuged for 30 min at 10,000 x *g* at 4 °C. Proteins in the soluble fractions were collected. The insoluble proteins were treated once more with 7.5 M urea and collected by centrifugation. Supernatant and pellet fractions were then analyzed by SDS/PAGE and immunoblotting using α-TsaP peptide-antibody. Before loading, soluble fractions were precipitated with trichloroacetic acid.

3.4.7 Outer membrane solubilization

1 mg of outer membranes were solubilized in 950 µl solubilization buffer (4 % SB3-12, 50 mM Tris pH 7.4, 250 mM NaCl) overnight at 4 °C. After centrifugation at 100,000 x *g* for 30 min, the solubilized proteins and non solubilized fractions were phenol treated as described before [105, 179] and analyzed on a 12 % SDS/PAGE.

3.4.8 Mass spectrometry of non-solubilized fractions

Membranes were solubilized for 2 h in buffer A with different detergents (1 % DDM, 2 % CHAPS, 1 % Triton, 4 % SB3-10, 4 % SB3-12 and 5 % SB3-14) at 4 °C. After centrifugation at 100,000 x *g* for 30 min at 4 °C, the supernatant was removed and the pellet was resuspended in 250 mM NaCl, 50 mM Tris; pH 7.4. After dissociation of the multimeric PilQ complex, samples were loaded on SDS/PAGE. Mass spectrometry to identify the proteins excised from SDS/PAGE gels was performed as described [180]. Mass spectrometry analysis was performed by Jörg Kahnt.

3.4.9 Electron microscopy

To analyze purified PilQ, elution fractions of the purification were applied on carbon coated copper grids and negatively stained with 2 % uranyl acetate by the droplet method as described previously [105]. EM and single particle analysis of secretin complexes from purified PilQ fractions or in isolated membranes was performed as described [105, 179]. For *N. gonorrhoeae*, transmission electron microscopy of whole cells and T4P was essential done as described [181]. Transmission electron microscopy was performed on a JEOL JEM-2100 at an acceleration voltage of 120 kV and images captured with a 2k x 2k fast scan CCD camera F214.

3.4.10 Purification of TsaP

E. coli BL21 star (DE3) cells transformed with pAW001 were grown to an OD₆₀₀ of 0.5 in Lysogeny Broth medium at 37 °C and induced with 0.5 mM IPTG. After incubation for another 3 h, cells were harvested by centrifugation at 4 °C for 10 min at 7,500 x *g*. Cells were resuspended in 10 ml protein purification buffer A containing Protease Inhibitor Cocktail (Roche) and 10 µg/ml DNase I and lysed by three passages through a French press at 1,000 psi. The suspension was centrifuged at 4 °C for 10 min at 12,000 x *g* followed by ultracentrifugation for 30 min at 180,000 x *g*. The supernatant was loaded on a HiTrap Chelating HP column (GE Healthcare) equilibrated with protein purification buffer A. After washing the column with protein purification buffer B containing 20, 40 and 50 mM imidazole, TsaP was eluted with a gradient from 50-400 mM imidazole in buffer B. Fractions containing TsaP were collected. These fractions were applied to a Superdex 75 HiLoad 16/60 column equilibrated with protein purification buffer C or protein purification buffer F if the protein is used for interaction assays. Fractions containing TsaP were collected and frozen.

3.4.11 Purification of TsaP Δ A33-R83

E. coli BL21 star (DE3) cells transformed with pKS035 were grown to an OD₆₀₀ of 0.5 in Lysogeny Broth medium at 37 °C and induced with 0.5 mM IPTG. After incubation for another 3 h, cells were harvested by centrifugation at 4 °C for 10 min at 7,500 x *g*. Cells were resuspended in 10 ml protein purification buffer G containing Protease Inhibitor Cocktail (Roche) and 10 µg/ml DNase I and lysed by three passages through a French press at 1,000 psi. The suspension was centrifuged at 4 °C for 10 min at 12,000 x *g* followed by ultracentrifugation for 30 min at 180,000 x *g*. The supernatant was loaded on a HiTrap Chelating HP column (GE Healthcare) equilibrated with protein purification buffer G. After washing the column with protein purification buffer H containing 20, 40 and 50 mM imidazole, TsaP was eluted with a gradient from 50-500 mM imidazole in buffer H. Fractions containing TsaP were collected. These fractions were applied to a Superdex 75 HiLoad 16/60 column equilibrated with protein purification buffer I. Fractions containing TsaP Δ A33-R83 were collected and frozen.

3.4.12 Purification of HA-PilQ(B1/B2)-CPD-His₁₀

E. coli BL21 star (DE3) cells transformed with pAW003 were grown to an OD₆₀₀ of 0.5 in Lysogeny Broth medium at 37 °C and induced with 0.5 mM IPTG. After incubation for another 3 h, cells were harvested by centrifugation at 4 °C for 10 min at 7,500 x *g*. Cells were resuspended in 10 ml Protein-purification buffer D containing Protease Inhibitor Cocktail (Roche) and 10 µg/ml DNase I and lysed by three passages through a French press at 1,000 psi. The suspension was centrifuged at 4 °C for 10 min at 12,000 x *g* followed by ultracentrifugation for 30 min at 180,000 x *g*. The supernatant was loaded on a HiTrap Chelating HP column (GE Healthcare) equilibrated with protein purification buffer E. After washing the column with Protein-purification buffer A containing 20, 40 and 50 mM imidazole, TsaP was eluted with a gradient from 50-400 mM imidazole in protein purification buffer E. Fractions containing TsaP were collected. These fractions were applied to a Superdex 200 HiLoad 16/60 column equilibrated with Protein-purification buffer D. Fractions containing HA-PilQ(B1/B2)-CPD-His₁₀ were collected and frozen.

3.4.13 Purification of- Male-TsaP_{MX}

E. coli Rosetta 2 (DE3) cells transformed with pSC121 were grown to an OD₆₀₀ of 0.5 in Lysogeny Broth medium at 37 °C and induced with 0.5 mM IPTG. After incubation overnight at 18 °C, cells were harvested by centrifugation at 4 °C for 10 min at 7,500 x *g*. Cells were resuspended in 10 ml protein purification buffer J containing Protease Inhibitor Cocktail (Roche) and 10 µg/ml DNase I and lysed by three passages through a French press at 1,000 psi. The suspension was centrifuged at 4 °C for 10 min at 12,000 x *g* followed by ultracentrifugation for 30 min at 180,000 x *g*. The supernatant was mixed with equilibrated amylose matrix and incubated for 30-60 min at 4 °C. The mixture was loaded on a Pierce centrifuge column. After collecting the flow through, the column was washed twice with 20 ml protein purification buffer J. Bound protein was eluted with 3 times 1 ml protein purification buffer K. These fractions were applied to a Superdex 200 HiLoad 16/60 column equilibrated with Protein-purification buffer F. Fractions containing Male-TsaP were collected and frozen.

3.4.14 Purification of His₆-PilQ_{mx}aa20-656

E. coli Rosetta 2 (DE3) cells transformed with pSC108 were grown to an OD₆₀₀ of 0.5 in Lysogeny Broth medium at 37 °C and induced with 0.5 mM IPTG. After incubation overnight at 18 °C, cells were harvested by centrifugation at 4 °C for 10 min at 7,500 x *g*. Cells were resuspended in 10 ml protein purification buffer D containing Protease Inhibitor Cocktail (Roche) and 10 µg/ml DNase I and lysed by three passages through a French press at 1,000 psi. The suspension was centrifuged at 4 °C for 10 min at 12,000 x *g* followed by ultracentrifugation for 30 min at 180,000 x *g*. The supernatant containing all soluble proteins was mixed with the equilibrated Ni²⁺-NTA agarose and incubated gently shaking at 4°C for 30-60 min. The mixture was loaded on a Pierce centrifuge column. After collecting the flow through, the column was washed twice with 20 ml protein purification buffer D. Bound protein was eluted with 3 times 1 ml protein purification buffer E. These fractions were applied to a Superdex 200 HiLoad 16/60 column equilibrated with Protein-purification buffer F. Fractions containing His₆-PilQ_{mx}aa20-656 were collected and frozen.

3.4.15 Protein-Protein Interaction Assay

To identify direct protein-protein interaction, proteins purified in protein purification buffer F were mixed and incubated for 1 h at 32 °C. As control, each protein was additionally analyzed separately. After concentrating the protein mixture to a volume of 100 µl using an Amicon Ultra-0.5 device, the sample was applied to a Superdex 200 10/300 GL column equilibrated with Protein-purification buffer F.

3.5. Bioinformatical methods

3.5.1 Reciprocal BlastP analysis

Reciprocal BlastP analysis was performed as described previously [182]. BlastP analyses were done with an initial expect value cutoff of 0.1 on 450 selected genomes of proteobacteria. The PilQ (NP_253727.1), PilT (NP_249086.1; Met1-Ser119), PilF (NP_253216.1; Met1-Gly199), PilM (NP_253731.1), PilN (NP_253730.1), PilO (NP_253729.1) and the TsaP (NP_248710.1; Arg90-Pro341),

MltD (PA1812), AmiC (PA4947), FimV (PA3115) proteins of *Pseudomonas aeruginosa* PAO1 were used as the initial query sequences in the analyses. The initial blast data was filtered with a query-specific expect value cutoff (PilQ, E-65; PilT, E-20; PilF, E-5; PilM, E-15; PilN, E-5, PilO, E-5; TsaP, E-3; MltD, E-5; AmiC, E-5; FimV, E-5) to eliminate non-specific results. The reciprocal BlastP analysis was performed by Dr. Stuart Huntley.

4. Results

4.1 Analysis of the Gonococcal Genetic Island

4.1.1 Transcriptional mapping of the Gonococcal Genetic Island

Many Gram-negative bacteria have conserved macromolecule secretion systems. Type IV secretion systems have been found mainly in pathogenic bacteria, such as *Agrobacterium tumefaciens*, *Helicobacter pylori* and *Neisseria gonorrhoeae*. In *N. gonorrhoeae* the type IV secretion system, which is involved in secretion of single stranded DNA into the extracellular milieu is located on a genetic island called the Gonococcal Genetic Island (GGI). Here I describe my contributions to the progress obtained in the understanding of the regulation and function of the genes encoded in the GGI.

To gain insights into the transcriptional regulatory network of the T4SS, I aimed to map the operon structure within the regions containing the genes involved in DNA secretion using RT-PCR. Based on the three divergently transcribed gene regions of the GGI, the GGI has previously been divided into three major parts. PCR analysis of the genes *yaf*, *tral*, *traD*, and *yaa* which are found within the first GGI part, showed that the genes are encoded by the same polycistronic mRNA. The translational coupling of these 4 genes was as expected, based on the small spacing between these genes. Except for the translational coupling of these genes the analysis revealed that the transcription start area is between 130 and 210 bp upstream of the *yaf* gene. To determine the transcription end, oligonucleotides according to the sequence downstream of the *dif* site were designed. Remarkably, agarose gel electrophoresis of the amplified PCR products indicated that the transcript is terminated between 250 and 620 bp after the *dif* site (Figure 10A), demonstrating that the transcription takes place across the *dif* site. The second mapped GGI part was that from *ItgX* to *yeh*, a region in which the genes are oriented in the same direction. Again, many of the genes in this region are located very close together, and the analysis was performed for all the genes which were spaced more than 10 nucleotides apart. For all gene pairs studied, except for the *traF-traH* pair PCR products were obtained, indicating that this region consists of 2 operons, one operon from *ItgX* to *traF* and one region from *traH* to *yeh* (Figure 10B and Figure 10C). Agarose gel electrophoresis of the amplified DNA products was used to determine the transcription start region, which was found to lie between 290 and 200 bp upstream of *ItgX* (see Figure 10B). The operon mapping further demonstrated that the transcription start site for the *traH-yeh* operon lies between 25 and 90 bp before the *traH* gene (see Figure 10C). The third GGI region encodes for proteins with homologies to DNA processing and modifying proteins. However, most of the genes of this region encode for proteins with an unknown function, and are not involved in DNA secretion. It was decided to map the regions including the genes which were shown to be essential for DNA secretion. The RT-PCR analysis demonstrated that the *parA*, *parB*, *yfeB* and *yfb* genes, although they are often found genetically linked to *ssbB* [183], are not encoded in the same operon (Figure 10D). To predict the transcription start of the last operon a more detailed analysis of the region upstream of *parA* was undertaken, which identified that the transcript starts between 320 and 350 bp before the *dif* site.

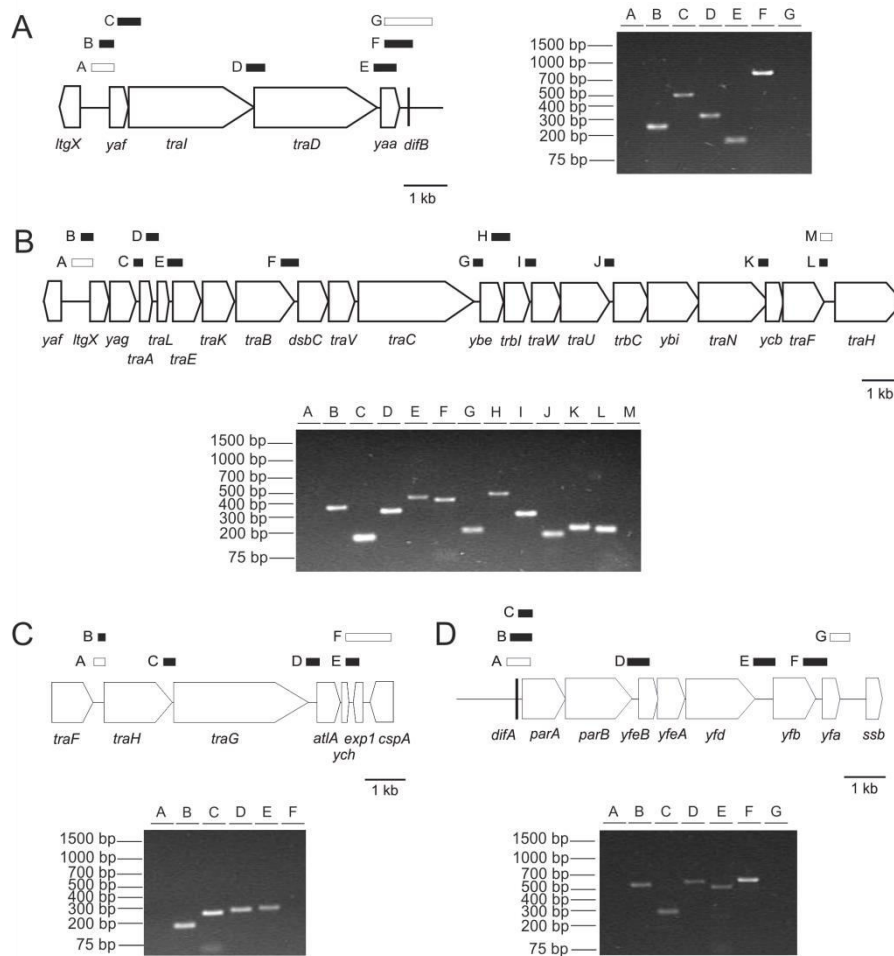


Figure 10 Transcription analysis of the genes encoded in the Gonococcal Genetic Island

PCR with different primer combinations on cDNA generated by reverse transcriptase on RNA isolated from strain MS11, was used to identify operons within the GGI. The results of the transcriptional analysis using different primer pairs within A) the *yaf-yaa*, B) the *ltgX-traF*, C) the *traH-exp1* and D) the *parA-yfa* regions are depicted. The right (A) or lower (B, C, D) agarose gels on which the PCR products obtained with the different primer combinations were loaded. The left (A) or upper (B, C, D) part of the figure shows a representation of the genetic structure of the operon. Genes are indicated by arrows and the expected PCR products by boxes over the genes. Primer combinations for which a PCR product was obtained are indicated by black boxes and primer combinations for which no PCR product was obtained are indicated by white boxes.

4.1.2 Analysis of the expression of the single stranded binding protein SsbB

Currently no information is available about the expression of the SsbB protein encoded within the GGI or any of its close homologs. The *ssbB* gene is located between several genes transcribed in the same direction (Figure 11A). The RT-PCR analysis demonstrated that the *ssbB*, *topB*, *yeh*, *yegB* and *yegA* genes form an operon (Figure 11B). Homologs of the ParA and ParB proteins, the topoisomerase, and the proteins with the DUF2857 (YfeB) and the DUF1845 (Yfb) domains are conserved within the SsbB homologs encoded within genetic islands. The *yegA* gene is followed by a previously unnamed gene (annotated as NgonM_04872 in the MS11 whole genome shotgun sequence) which encodes a 149 amino acids long conserved hypothetical protein with a DUF3577 domain. This gene was named *yef*. Remarkably, my operon mapping data shows that the operon that contains *ssbB* is transcribed during normal growth of *N. gonorrhoeae*. The first operon of the GGI which contains the *traI* and *traD* proteins that are involved in targeting the secreted DNA to the

secretion apparatus is upregulated in piliated cells compared to non-piliated cells [36]. To determine the expression levels of the *ssbB* gene and to test whether a similar upregulation could be observed in the expression of the *ssbB-yegA* operon, a qualitative real time PCR (qRT-PCR) using primers designed against the *ssbB*, *topB*, *tral* and *traD* genes and against the *secY* gene as a control was performed on mRNA isolated from piliated and non-piliated strains (Figure 11). The qRT-PCR revealed relatively low levels of transcription compared to the transcript containing the *secY* gene but higher levels of transcription than the *tral* and *traD* genes. However, no differences in the expression levels of the *ssbB* and *topB* genes were observed between piliated and non-piliated cells. An analysis by S. Jain showed that although the *ssbB* gene is transcribed during growth, it had no significant effect on DNA release. To further validate if SsbB is secreted, different fractions (cytosolic fraction, blebs and medium fraction) were isolated and analyzed by immunoblotting. SsbB could only be detected in the cytosolic fraction but not in the medium fraction, suggestin that SsbB is not secreted. Additionally, it was tested if SsbB plays an important role in DNA uptake and competence. For this, the effect of SsbB on the efficiency of DNA uptake by *N. gonorrhoeae* was tested in co-culture experiments. In general it could be shown that SsbB has no effect on ssDNA secretion and/or DNA uptake.

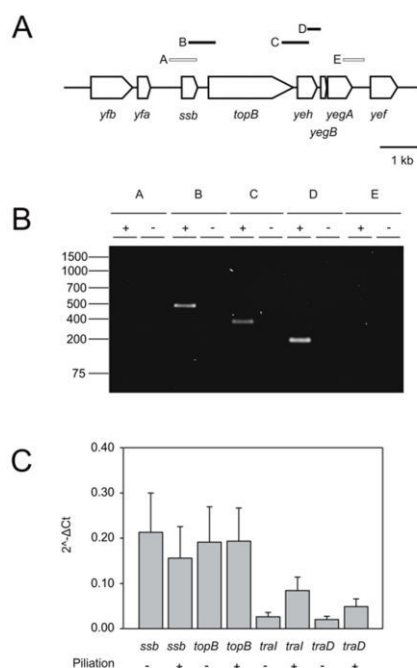


Figure 11 Analysis of the transcription of the *yfa-yef* region

Reverse transcriptase was used to map the operon structure of the *ssb-yegA* region within the GGI of *N. gonorrhoeae* strain MS11. A) Schematic representation of the *yfa-yef* region of the GGI. Genes are indicated by arrows and the expected PCR products by lines over the genes. Primer combinations for which a PCR product was obtained are indicated by black boxes and primer combinations for which no PCR product was obtained are indicated by white boxes. B) Operon mapping of the *ssb-yegA* operon. Transcripts were determined by PCR. (+) indicates reactions on cDNA created in the presence of reverse transcriptase and (-) indicates reactions on cDNA created in the absence of reverse transcriptase. C) Quantitative gene expression levels of *ssbB*, *topB*, *tral* and *traD* of piliated and non-piliated *N. gonorrhoeae* strains were determined by qRT-PCR. The graph shows the mRNA levels as comparative gene expression after normalizing each gene to *secY*. Values depict means \pm standard deviation of six biological replicates.

4.1.3 DNA secretion facilitates biofilm formation

During attachment to surfaces, planktonic bacteria start to produce extracellular substances like exopolysaccharides, secreted proteins, membrane vesicles and extracellular DNA (eDNA). It was demonstrated for many organisms, like *Pseudomonas aeruginosa* [184], *Streptococcus pneumoniae* [185], *Enterococcus faecalis* [186], *Staphylococcus aureus* [187], *N. meningitidis* [188] and *N. gonorrhoeae* [189] that eDNA is an important component of the biofilm. As biofilms of *N. gonorrhoeae* contain large quantities of eDNA, we explored the possibility that the ssDNA, which is secreted by the T4SS, could contribute to biofilm formation. Biofilm experiments in continuous flow-chamber systems, performed by Maria Zweig, could show that the incorporation of the ssDNA degrading enzyme Exonuclease I into the media decreased *N. gonorrhoeae* biofilm formation by ~95

%. Because biofilm formation was influenced by the addition of Exonuclease I, and thus most likely by the presence of ssDNA, it was tested whether the ssDNA secreted via the T4SS encoded within the GGI facilitates biofilm formation.

To investigate if single stranded DNA, which is secreted via the T4SS encoded within the GGI facilitates biofilm formation, biofilm formation of two different *N. gonorrhoeae* strains was compared by Maria Zweig. The strains initially used within this study were the *N. gonorrhoeae* MS11 WT strain and the MS11 $\Delta traB$ deletion strain. The MS11 $\Delta traB$ strain contains a deletion in the *traB* gene. TraB is part of the T4SS core complex and deletion of this gene results in abolishment of DNA secretion. Biofilms of the different strains were grown for 3 days in a continuous flow chamber system and biofilm formation was imaged by Maria Zweig after 24, 48 and 72 hours. Quantification of the biofilms showed that deletion of the *traB* gene influenced biofilms formation (Figure 12). However, *N. gonorrhoeae* strains can undergo both antigenic and phase variation, of especially proteins that are located on the surface of the cell, and are thus exposed to the immune system of the human host. Antigenic and phase variation of e.g. the pilin subunit strongly influence the ability of *N. gonorrhoeae* to form biofilms. Therefore, it was essential to show that the effects of the *traB* deletion on biofilm formation were caused by the *traB* mutation, and were not the result of antigenic variation. Complementation in *N. gonorrhoeae* is usually done by insertion of the gene of interest onto the gonococcal chromosome. The majority of DNA that enters the cell during natural transformation is single stranded and not a target for restriction enzymes and is therefore much more efficiently incorporated than replicating plasmids. For this reason, I restored the *traB* deletion strain by transformation with chromosomal DNA from *N. gonorrhoeae* MS11 wt strain, which results in a strain in which the $\Delta traB$ deletion is replaced by the WT *traB* gene.

Using this strain, Maria Zweig showed that the strain in which the *traB* deletion is replaced by the WT *traB* gene forms biofilms in a similar manner as the WT strain, demonstrating that the effects observed in biofilm formation in the *traB* deletion strain are indeed caused by the *traB* deletion.

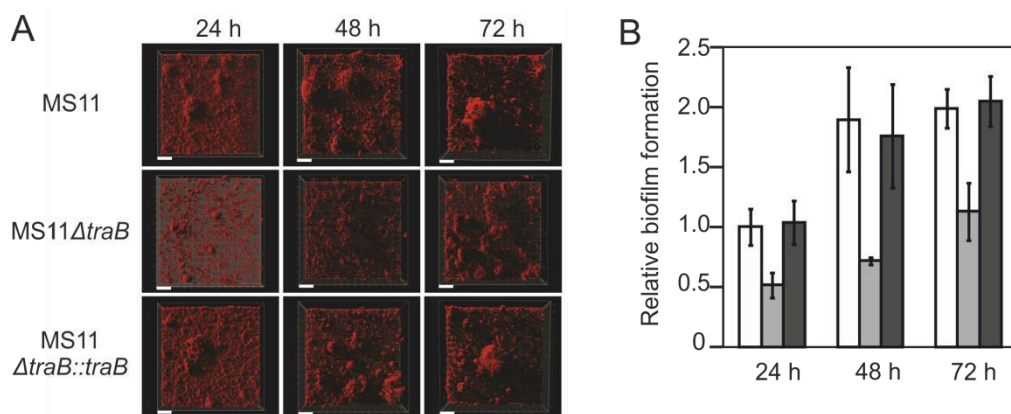


Figure 12 Deletion of the *traB* gene results in a strong decrease of biofilms formation

Confocal laser scanning microscopy in continuous flow chambers inoculated with *N. gonorrhoeae* MS11, MS11 $\Delta traB$ and MS11 $\Delta traB::traB$ imaged 24, 48 and 72 hours after inoculation. (A) Biofilms were stained with Syto62 and visualized by CLSM. Micrographs represent three-dimensional projections. The scale bar equals 20 μ m. (B) Quantification of the amount of biofilms formed by MS11 (white bars), MS11 $\Delta traB$ (light grey) and MS11 $\Delta traB::traB$ (dark grey bars) after 24, 48 and 72 hours. [CLSM and quantification was performed by Dr. M. Zweig, MPI Marburg]

4.2 The peptidoglycan-binding protein TsaP functions in surface assembly of type IV pili

4.2.1 Identification of a protein associated with secretin complexes of type IV pili in *N. gonorrhoeae*

Previous transmission electron microscopic (EM) studies of native secretin complexes of *N. gonorrhoeae* embedded in OM sheets showed that the PilQ secretin ring is surrounded by an additional peripheral structure which consists of a peripheral ring and seven extending spikes (see Figure 16A and Figure 16E) [105]. To identify the protein(s) that form the peripheral structure, we first attempted to solubilize and purify the complex from isolated membranes. As has been done previously for *N. meningitidis* PilQ [190], a His₈-tag was introduced into the small basic repeat region of PilQ of the *N. gonorrhoeae* wild-type (WT) strain MS11, generating strain SJ004-MS. In prior secretin cell envelope extractions studies of PilQ of *N. meningitidis* [172, 191, 192], PulD of *Klebsiella oxytoca* [166], XcpQ of *P. aeruginosa* [161], YscC of *Yersinia enterocolitica* [163, 193] and the filamentous phage pIV [171] a variety of zwitterionic, non-ionic and ionic detergents, which mimic the natural lipid environment, were used and it was found that proteins of the secretin family generally require harsh solubilization conditions. Based on these protocols isolated outer membranes, derived from *N. gonorrhoeae* strain SJ004-MS, were solubilized using the zwitterionic detergents SB3-14 (5 % w/v), SB3-12 (4 % w/v), SB3-10 (4 % w/v), CHAPS (2 % w/v) and the non-ionic detergents DDM (1 % w/v), CHAPS (2 % w/v) and Triton (1 % w/v). Even though SDS was additionally used in previous studies, SDS was not tested for His₈-PilQ extraction, since this harsh detergent most likely would result in protein denaturation and loss of the additional structures. The outer membranes were incubated within the different detergents and subjected to an ultracentrifugation step, aimed to separate solubilized proteins from the non-solubilized pellet fraction. To determine the extraction efficiency of the His₈-PilQ complex, the solubilized and pelleted non-solubilized fractions were phenol treated and analyzed by SDS/PAGE (Figure 13). Similar to what was reported previously; only small amounts of His₈-PilQ could be extracted from outer membranes using zwitterionic and nonionic detergents. Comparing the amount of solubilized and non-solubilized His₈-PilQ demonstrated that PilQ is largely insoluble in nonionic detergents at neutral pH, a phenomenon which is common for secretin complexes [166]. A screen of several detergents showed that only

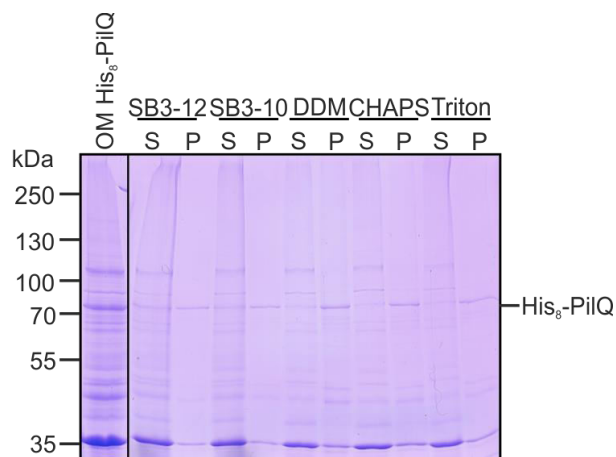


Figure 13 Solubilization of His₈-PilQ containing outer membrane

Outer membranes isolated from His₈-PilQ strain were solubilized by 4 % SB3-12, 4 % SB3-10, 1 % DDM, 2 % CHAPS and 1 % Triton respectively. The solubilized protein fractions (S) and non-solubilized pellet fractions (P) were phenol treated and analyzed by 12 % SDS/PAGE.

small amounts of His₈-PilQ could be solubilized from isolated membranes and purified by Ni²⁺-affinity chromatography. Figure 14 shows the different fractions during purification of the His₈-PilQ complex, analyzed after phenol treatment on a SDS/PAGE. To gain insights into the structure of the His₈-PilQ containing elution fractions, electron microscopy (EM) was applied to negatively stained samples of the elution fraction. Figure 15 shows an overview of isolated particles obtained from a purification using 4% sulfobetaine 3-12 to solubilize and purify the complex. Single particle alignment of these particles showed a structure consisting of a single ring (Figure 16B and Figure 16F) with a diameter (150 Å) similar to that observed for PilQ complexes from *N. meningitidis* [190]. Comparison of these particles with the previously described class average of the secretin complex embedded in OM sheets, i.e. in its native OM environment ([105]; Figure 16A and Figure 16E), showed that isolated His₈-PilQ has the same size and shape as the inner ring of this structure. However, the additional features, i.e. the peripheral ring and the spikes, were lost during solubilization and purification. This observation explains why these features have not been detected in previously described PilQ purifications [191, 192, 194]. At the obtained resolution, individual domains of the His₈-PilQ complex are not well resolved, but, as observed previously [105], after imposing 14-fold symmetry features become more pronounced compared to any other imposed symmetry between 12 and 16, suggesting a 14-fold symmetry for the *N. gonorrhoeae* PilQ multimer (Figure 16F).

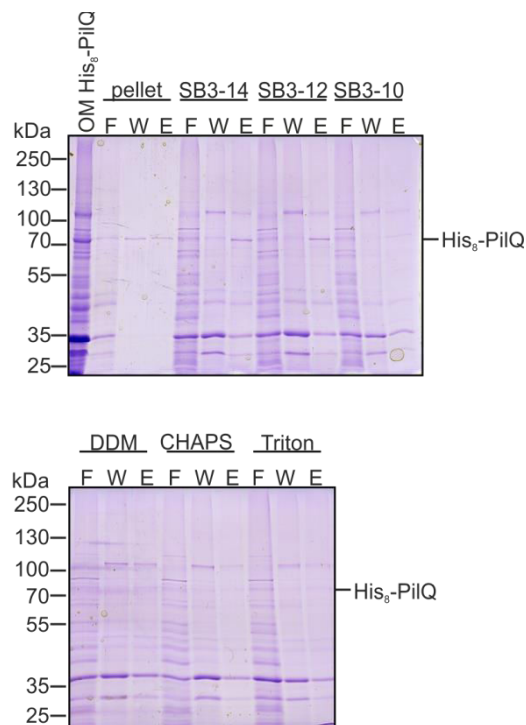


Figure 15 Solubilized His₈-PilQ purification

Outer membranes isolated from His₈-PilQ strain were solubilized by 5 % SB3-14, 4 % SB3-12, 4 % SB3-10, 1 % DDM, 2 % CHAPS and 1 % Triton respectively and His₈-PilQ was purified by Ni²⁺-affinity chromatography. The flowthrough (F), wash (W) and elution (E) fractions were phenol treated and analyzed by 12 % SDS/PAGE.

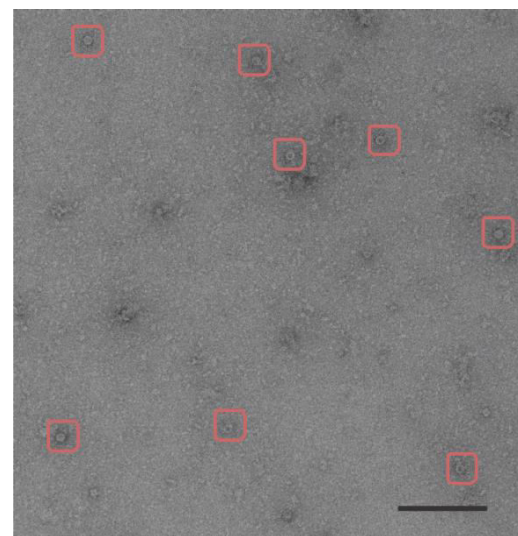


Figure 14 Analysis of purified PilQ by electron microscopy

Elution fractions of the PilQ purification were applied to carbon coated copper grids and negatively stained with 2 % uranyl acetate. PilQ particles are indicated by the red boxes. The scale bar equals 100 nm. [The EM analysis was performed by Dr. M Webber-Birungi Rijksuniversiteit Groningen]

Because the peripheral ring and spikes were lost during solubilization and purification, we analyzed the non-solubilized *N. gonorrhoeae* membrane fractions by SDS-PAGE. These fractions contained significant amounts of His₈-PilQ along with several other proteins (Figure 17A). Identification of these proteins by mass spectrometry (MS) (performed by J. Kahnt) identified EF-Tu, OMP I, OMP III and a peroxiredoxin 2 family protein. These proteins were identified in a proteome study of *N. meningitidis* as 4 of the 5 most abundantly expressed proteins [195]. MS also identified PilQ and the conserved hypothetical protein NGFG_01788, which were not identified as highly abundant proteins in the proteomics study mentioned. NGFG_01788 is a 45.5 kDa protein that contains a type I signal sequence, an N-terminal LysM domain and a C-terminal part of unknown function (Figure 17B). The LysM domain is a widespread protein domain involved in PG binding. BlastP analysis and alignment identified many NGFG_01788 homologs that are conserved over the entire length of NGFG_01788 (Figure 18), and that are found widespread among Gram-negative bacteria. Importantly, as shown in Figure 18 the conserved residues in other LysM domains are also conserved in the LysM domains of homologs of NGFG_01788 [158, 159]. Based on the presence of NGFG_01788 in the non-solubilized membrane fractions together with His₈-PilQ, the presence of the LysM domain, we hypothesized that NGFG_01788 is a component of the secretin complex that might anchor the complex to the PG. From here on, we refer to NGFG_01788 as TsaP, for Type IV pili secretin associated Protein.

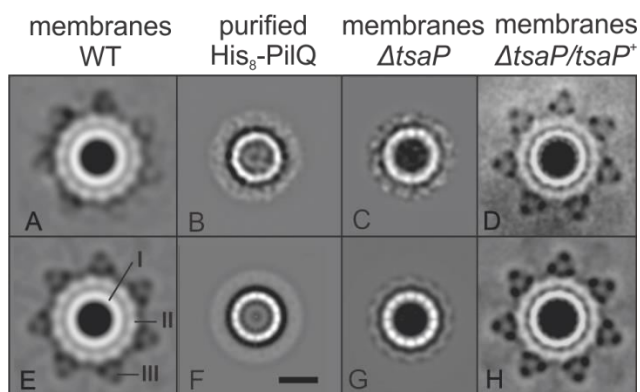


Figure 17 Projection maps of single particle electron microscopy analysis of the PilQ complex from *N. gonorrhoeae*

Projection maps of class averages of single particle EM images obtained from membranes isolated from (A, E) the WT, (C, G) the $\Delta tsaP$ strain and (D, H) the $\Delta tsaP/tsaP^+$ strain grown in the presence of 1 mM IPTG. (B, F) show class averages of single particle EM images of the solubilized and purified His₈-PilQ complex. Projection maps without (A, B, C and D) and with (E, F, G, H) 14-fold imposed symmetry are depicted. I, II and III indicate the inner ring, the peripheral ring and the spikes respectively. Scale bar, 10 nm. [The EM analysis and single particle electron microscopy analysis was performed by D.A. Semchonok, Rijksuniversiteit Groningen]

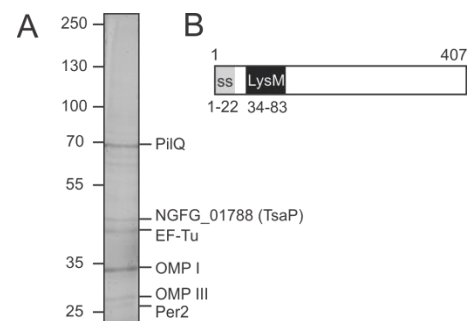


Figure 16 Identification of TsaP (NGFG_01788)

(A) Coomassie stained SDS/PAGE of the non-solubilized fraction of SB3-12 treated OMs. Analysis by mass spectrometry identified PilQ, TsaP (NGFG_01788), elongation factor Tu (EF-Tu), OM protein I (OMP I), OM protein III (OMP III) and a peroxiredoxin 2 family protein (Per2). (B) Domain structure of TsaP. The signal sequence (ss) and LysM domain are depicted.

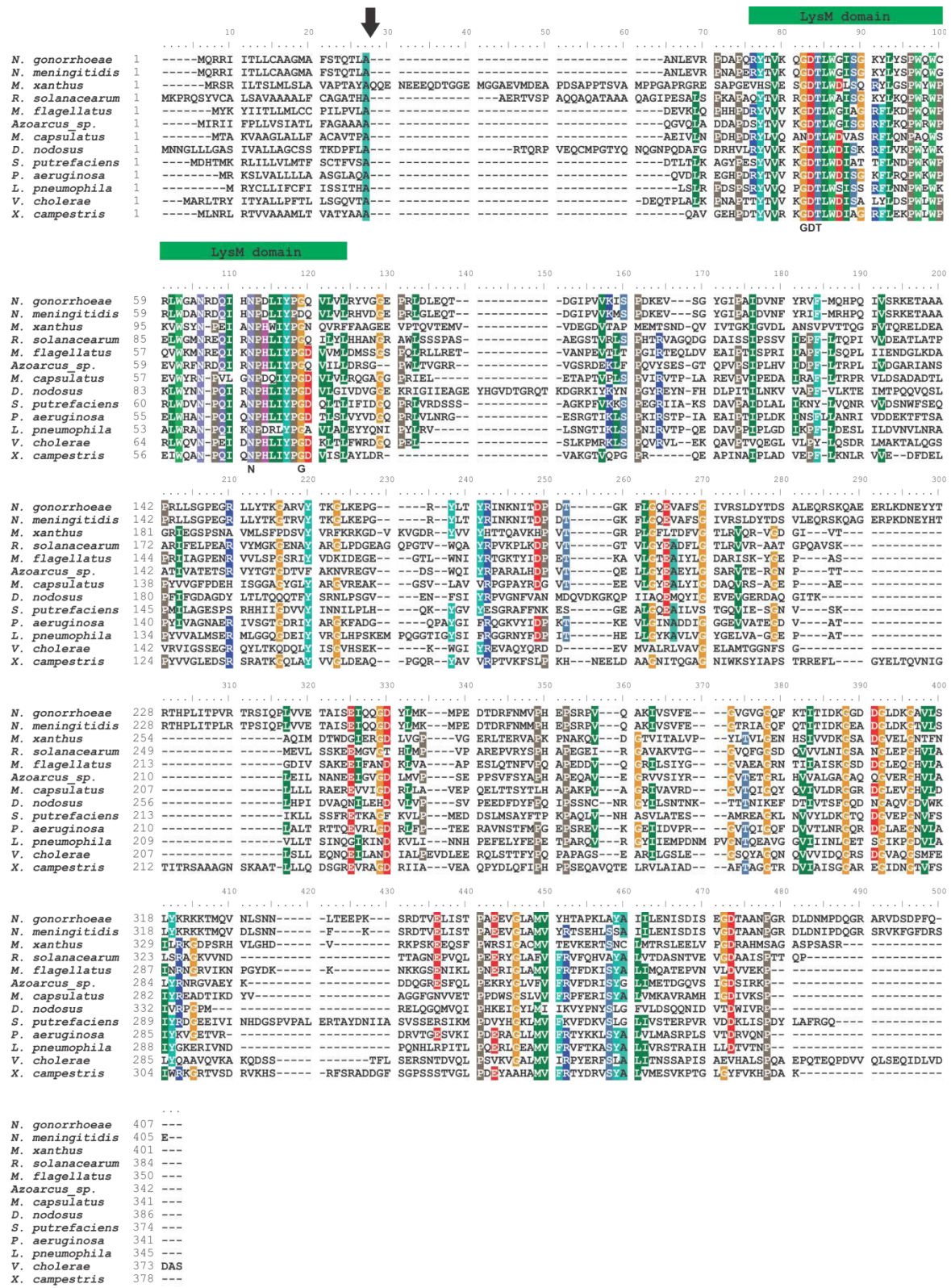


Figure 18 Alignment of Tsap homologs of different organisms

Tsap homologs described in table 46 (supplementary data) were aligned. Colored residues are <50 % conserved. The putative signal sequence cleavage site is indicated with a black arrow, while the LysM domain is indicated with a green box. Residues (G40, D41, T42, N70 and G77) that are highly conserved in LysM domains are indicated in bold below the alignment.

4.2.2 Analysis of TsaP in membranes

To characterize the function of TsaP in *N. gonorrhoeae*, a $\Delta tsaP$ mutant was generated in the WT strain by insertion duplication mutagenesis [16]. Moreover, a $\Delta tsaP$ complementation strain was generated by the ectopic insertion of a copy of *tsaP* under control of the *lac* promoter ($\Delta tsaP/tsaP^+$) [18]. Unless otherwise indicated, the $\Delta tsaP/tsaP^+$ strain was grown in the presence of 1 mM IPTG. Western blot on whole cell extracts using α -TsaP antibodies demonstrated the presence of a protein of the expected size that was not detected in the $\Delta tsaP$ strain demonstrating that the α -TsaP antibodies are specific for TsaP. Moreover, TsaP was present at WT levels in the $\Delta tsaP/tsaP^+$ complementation strain (Figure 19A). Immunoblotting on whole cell extracts using the α -PilE antibodies showed that all three strains accumulated similar amounts of the PilE pilin protein.

To determine directly whether TsaP is associated with membranes, total membranes were isolated from the WT, $\Delta pilQ$, $\Delta tsaP$ and $\Delta tsaP/tsaP^+$ strains. PilQ forms a highly SDS-stable oligomeric complex that migrates as a high molecular weight complex in SDS/PAGE. Coomassie staining of SDS/PAGE gels of isolated membranes showed that the high molecular weight PilQ complex was present in membranes from the $\Delta tsaP$ and $\Delta tsaP/tsaP^+$ strains at similar levels as observed in WT (Figure 19B). Thus, neither the level nor the oligomerization of PilQ are affected in $\Delta tsaP$ and $\Delta tsaP/tsaP^+$ strains. The PilQ oligomer can be dissociated before SDS/PAGE analysis by treatment with hot phenol. Phenol treated membranes were analyzed after SDS/PAGE and western blotting with antibodies raised against TsaP, PilQ and the pilin PilE. These experiments demonstrated that the PilQ monomer accumulated at similar levels in the WT, $\Delta tsaP$ and $\Delta tsaP/tsaP^+$ strains. In isolated total membranes, $\Delta tsaP/tsaP^+$ and WT showed similar levels of TsaP accumulation (Figure 19C); however, the level of TsaP was reduced in the $\Delta pilQ$ mutant, suggesting that either membrane insertion or membrane association of TsaP depends on PilQ. As was observed for whole cell extracts, the level of PilE was comparable in membranes isolated from the WT, $\Delta pilQ$, $\Delta tsaP$ and $\Delta tsaP/tsaP^+$ strains (Figure 19C), again showing that all strains expressed the pilin subunit. To test whether TsaP is more stably associated with membranes containing PilQ, total membranes isolated from the WT and $\Delta pilQ$ strains were incubated with 7.5 M urea. Incubation of membranes with 7.5 M urea is a common method to remove membrane associated but not membrane inserted proteins [196]. Even after two washes, TsaP was only partially dissociated from WT membranes containing PilQ (Figure 19D), suggesting that TsaP is either membrane inserted, or is very tightly bound to the membrane. Remarkably, when membranes derived from the $\Delta pilQ$ mutant were treated with 7.5 M urea, TsaP was fully removed. Thus tight association with or integration of TsaP in the OM depends on PilQ. We speculate that the reduced levels of TsaP observed in total membranes in the $\Delta pilQ$ strain (Figure 19C) either reflects the lack of tight association or integration of TsaP in the OM in the absence of PilQ or that PilQ functions to stabilize TsaP. As shown below, TsaP binds to PG. Therefore, it also remains a possibility that TsaP associates more strongly with PG in the absence than in the presence of PilQ. If that would be the case, less TsaP would be recovered in the membrane fraction in the absence of PilQ.

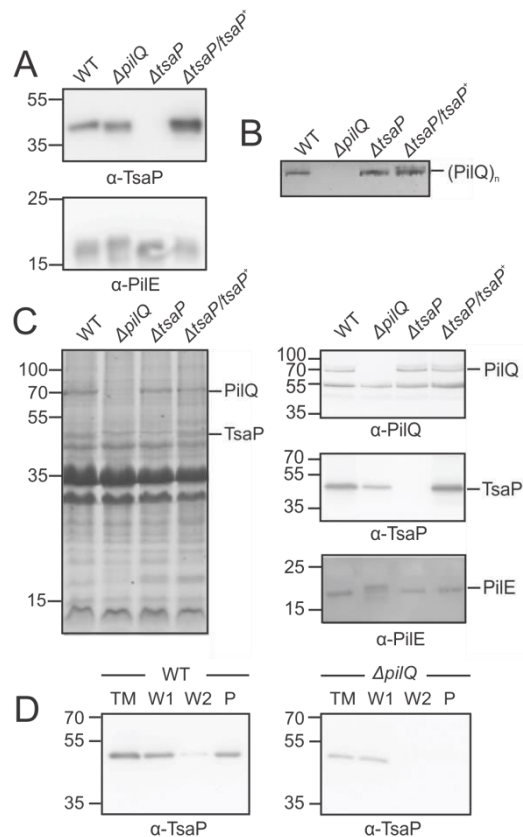


Figure 19 Membrane binding of TsaP depends on PilQ

(A) Immunoblot analysis of equal amounts of total cell extracts of the WT, $\Delta pilQ$, $\Delta tsaP$ and $\Delta tsaP/tsaP^+$ strains grown in the presence of 1 mM IPTG using α -TsaP, and α -PilE antibodies. (B) The panel shows the upper part of a Coomassie stained SDS/PAGE of non-phenol treated OM fractions isolated from the indicated *N. gonorrhoeae* strains. (C) The left panel shows a Coomassie stained SDS-PAGE of phenol treated OM fractions from the indicated strains. The right panels show immunoblot analysis of the same samples using α -TsaP, α -PilQ and α -PilE antibodies. (D) Total membranes (TM) derived from *N. gonorrhoeae* WT (left) and the $\Delta pilQ$ mutant (right) were treated twice for 30 min with 7.5 M urea. After centrifugation, the supernatants (W1 and W2) and the resuspended membrane pellets (P) were analyzed by immunoblot analysis using the α -TsaP antibody.

4.2.3 His₁₀-TsaP can be purified as a highly stable monomer

To further characterize TsaP, His₁₀-TsaP was purified and biochemically characterized. As TsaP contains a type I signal sequence, the first 23 amino acids were removed to prevent transport to the periplasm upon overexpression in *E. coli*. His₁₀-tagged TsaP was cloned under the T7 promoter and the resulting overexpression construct was transformed into *E. coli* BL21 (DE3) star. This overexpression strain carries the T7 polymerase and the IPTG-inducible *lac*-promoter. After overexpression, TsaP could be purified in homogeneity in large amounts using a two step protocol as described in paragraph 3.4.10. TsaP elutes from the Ni²⁺-affinity column at an imidazole concentration of 150 mM. The elution profile is shown in Figure 20A. Each second elution fraction was analyzed by SDS/PAGE. His₁₀-TsaP migrates on SDS/PAGE gels at a position corresponding to the calculated size of 45.5 kDa (Figure 20B). Taking the SDS/PAGE into account the fractions A10-B9 were pooled and loaded on a size exclusion volume. The elution profile showed one distinct peak at an elution volume of 80 ml (see Figure 20B). Correlating the elution volume of the observed protein peak with commercially available molecular weight standards showed that this peak correspond to a molecular mass of 45 kDa, which is in agreement with the calculate mass of monomeric His₁₀-TsaP. The different elution fractions were analyzed by SDS/PAGE and TsaP was detected in each of the fractions (Figure 20D). A second band with a molecular mass of approximately 37 kDa could additionally be detected. This second band could also be detected in immunoblot analysis using an antibody raised against TsaP, indicating that the second band most likely correspond to degraded TsaP protein.

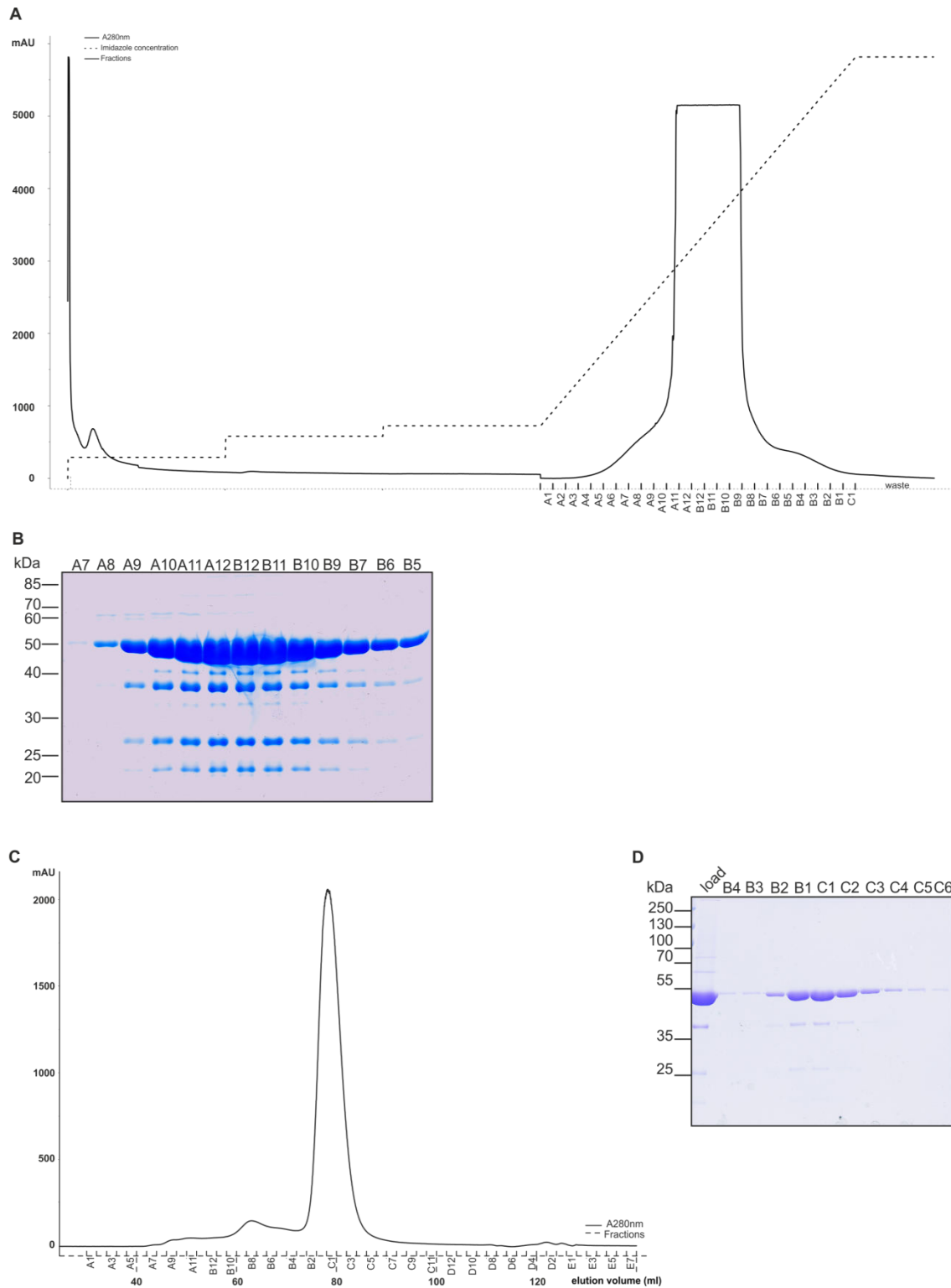


Figure 20 Purification of His₁₀-TsaP

(A) Elution profile of Ni²⁺-affinity chromatography. The protein was detected at 280 nm and is indicated by the solid line. The imidazole concentration is indicated by the dashed line. The intensity is given in mAU. The collected fractions are labeled as indicated. (B) 12 % SDS/PAGE with elution fractions from the Ni²⁺-affinity chromatography. The labeling of the lanes corresponds to the labeling of the elution fractions shown in (A). Molecular masses are indicated on the left side. TsaP migrates at a position corresponding to a molecular mass of 45 kDa. (C) His₁₀-TsaP eluted as a monomer from the SD200 gel filtration column. The protein was detected at 280 nm which is indicated by the solid line. (D) His₁₀-tagged TsaP was essentially pure as assayed by Coomassie staining of a 12 % SDS/PAGE of the purified protein. The labeling of the lanes corresponds to the labeling of the elution fractions shown in (C). The position of various markers for the SDS/PAGE are indicated.

4.2.4 TsaP binds to peptidoglycan

TsaP contains an N-terminal LysM domain. To test whether TsaP is able to bind and/or hydrolyze PG, His₁₀-TsaP and murein sacculi of *N. gonorrhoeae* were purified (Figure 21A and Figure 21B). In a sedimentation assay, TsaP was found in the supernatant in the absence of murein sacculi and was sedimented to the pellet fraction in the presence of murein sacculi (Figure 21C), demonstrating that TsaP binds to isolated murein sacculi. Purified TsaP was also tested in a zymogram assay (Figure 21D), but no hydrolysis of *N. gonorrhoeae* murein could be detected whereas lysozyme and mutanolysin, as expected, show clear zones of hydrolysis. The hydrolysis zone of mutanolysin was observed at a height comparable to proteins with a molecular mass of ~250 kDa. Most likely, mutanolysin is not completely unfolded during the SDS/PAGE and is thus retained by binding to the murein during electrophoresis, an effect which has been seen for other proteins before. Since the high level of O-acetylation of *N. gonorrhoeae* murein inhibits the activity of lysozyme [197], the specific activity of lysozyme was lower than the activity of mutanolysin.

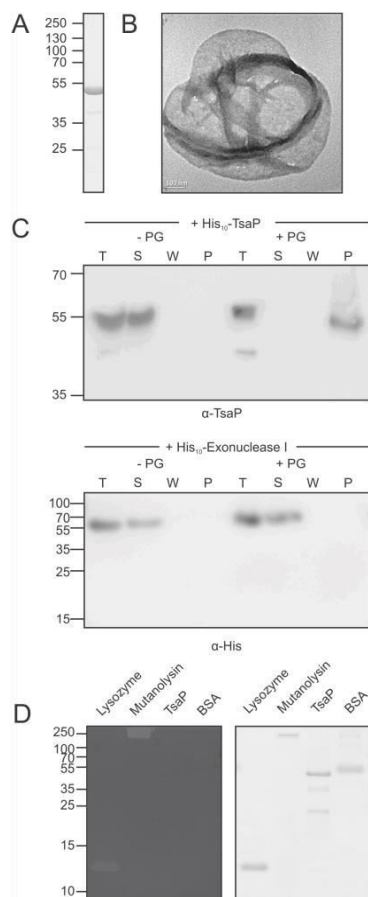


Figure 21 Characterization of binding of TsaP to isolated peptidoglycan sacculi

(A) TsaP was overexpressed and purified from *E.coli*. Fractions eluted from the size exclusion column at a size corresponding to the monomer were analyzed by SDS-PAGE and Coomassie staining. (B) Peptidoglycan sacculi were isolated from *N. gonorrhoeae* and analyzed by electron microscopy. (C) To test for binding of TsaP to peptidoglycan, 5 μ g TsaP were incubated without (upper panel, -PG) or with 1 mg peptidoglycan (upper panel, +PG). Samples were centrifuged, and the supernatant (S1) was collected and the pellet was resuspended. The samples were centrifuged again and the supernatant (S2) was collected and the pellet fraction was resuspended. The different fractions were analyzed by immunoblotting using α -TsaP antibodies. As a control, 5 μ g purified His₁₀-tagged Exonuclease I, was incubated without (lower panel, -PG) or with 1 mg peptidoglycan (lower panel, +PG), treated as described above, and analyzed using an α -His antibody. To test for peptidoglycan hydrolysis, zymography was performed. (D) Lysozyme, mutanolysin, TsaP and BSA (5 μ g each) were applied to SDS gels containing purified murein sacculi. The proteins were stained with Coomassie blue (lrightside). A second gel (left side) was incubated in renaturation buffer to allow for refolding of the proteins and peptidoglycan hydrolysis was detected by staining of sacculi with methylene blue. Clear zones of hydrolysis are observed for mutanolysin and lysozyme, but not for BSA and TsaP.

4.2.5 Lack of TsaP affects surface assembly of T4P

On agar plates, gonococci assembling T4P on their cell surface form small, compact colonies with a sharp edge. Non-piliated cells form flat colonies with a larger diameter and a “fuzzy” edge [177]. To further understand the function of TsaP, the WT, $\Delta pilQ$, $\Delta tsaP$ and $\Delta tsaP/tsaP^+$ strains were analyzed on agar plates (Figure 22). WT and the $\Delta pilQ$ mutant showed colony morphologies corresponding to piliated and non-piliated cells, respectively. The $\Delta tsaP$ mutant and the $\Delta tsaP/tsaP^+$ strain grown in the absence of IPTG showed colony morphologies matching that of non-piliated cells. Importantly, in the presence of IPTG, the $\Delta tsaP/tsaP^+$ strain showed a colony morphology matching that of piliated cells. Thus, deletion of *tsaP* resulted in loss of the piliated colony morphology. The $\Delta tsaP$ and the $\Delta tsaP/tsaP^+$ strains grown in the absence of IPTG also showed slightly decreased growth on plates, but longer incubation did not result in a piliated colony morphology.

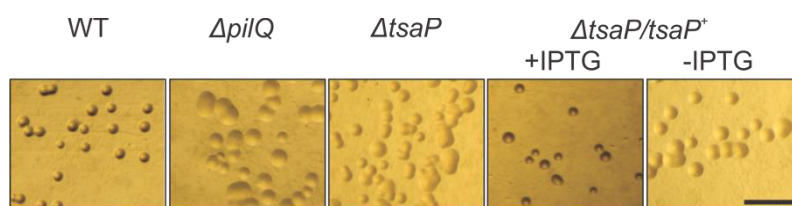


Figure 22 TsaP is important for T4P-dependent colony morphology

The indicated *N. gonorrhoeae* strains were incubated at 37 °C for 24 h on GCB plates. The scale bar equals 1 mm.

In a next step, WT, $\Delta tsaP$ and $\Delta tsaP/tsaP^+$ cells were negatively stained for subsequent EM (Figure 23). All strains showed OM vesicles (blebs) either as single blebs or in longer chains [198, 199]. In WT and the $\Delta tsaP/tsaP^+$ strain, single and bundled T4P were observed. In contrast, in the $\Delta tsaP$ mutant, T4P were only observed in membrane protrusions, which were filled with up to 10 T4P. This strongly resembles the phenotype of the previously described $\Delta pilQ/\Delta pilT$ double mutant, in which T4P are assembled but cannot pass the OM and therefore form OM protrusions. Similar to the $\Delta tsaP$ mutant, the $\Delta pilQ/\Delta pilT$ mutant also showed a slight growth retardation and a colony morphology matching that of non-piliated cells [200]. We conclude that in the $\Delta tsaP$ mutant, T4P are formed, but these T4P are unable to efficiently pass the OM and, therefore, assemble in OM protrusions and are not displayed on the cell surface.

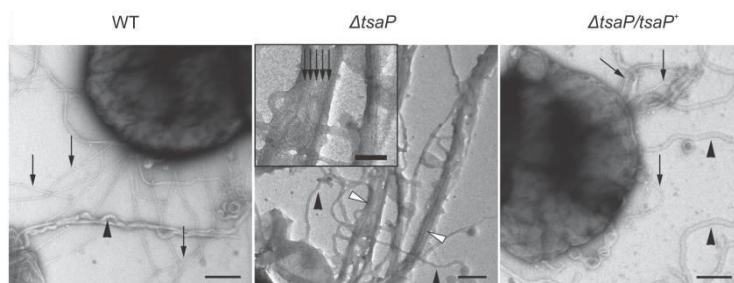


Figure 23 Deletion of TsaP leads to formation of membrane protrusions containing T4P in *N. gonorrhoeae*

EM analysis of WT, $\Delta tsaP$ and $\Delta tsaP/tsaP^+$ strains grown in the presence of 1 mM IPTG. Cells were applied to carbon-coated copper grids, washed twice with double distilled water and subsequently stained with uranyl acetate before investigation via EM. T4P (black arrows) and membrane blebs (black arrow heads). The membrane protrusions (white arrows) observed in the $\Delta tsaP$ mutant are filled with T4P (see inset). Scale bar in main images and inset equal 200 nm and 50 nm, respectively. [The EM analysis was performed by Prof. Dr. Klingl, Philipps-Universität Marburg]

4.2.6 The peripheral structure of the secretin complex is lost in the $\Delta tsaP$ mutant

To determine whether the deletion of *tsaP* affected the structure of the secretin complex in its native OM environment, OMs isolated from the $\Delta tsaP$ and $\Delta tsaP/tsaP^+$ strains were studied by transmission EM followed by single particle averaging [105]. A comparison of the projection maps of the secretin complexes obtained from membranes of the $\Delta tsaP$ (Figure 16C and Figure 16G) and $\Delta tsaP/tsaP^+$ (Figure 16D and Figure 16H) strains with projection maps obtained from WT membranes (Figure 16A and Figure 16E), showed that the peripheral ring and the spikes are lost in the $\Delta tsaP$ mutant, and that they are recovered in the $\Delta tsaP/tsaP^+$ strain. The structures observed in membranes of the $\Delta tsaP$ mutant strongly resemble the structure of the isolated PilQ complex (Figure 16B). The two-dimensional map of the $\Delta tsaP/tsaP^+$ particle was obtained at slightly higher resolution than the map of the WT particle. The structure is seen in a slightly tilted top-view position. A small protein domain is visible inside the inner rings, especially in the lower half. It is present in 14 copies. This becomes even clearer after imposing a high-pass filter on the image (Figure 24). This analysis demonstrates that the *N. gonorrhoeae* PilQ secretin complex has a 14-fold symmetry.

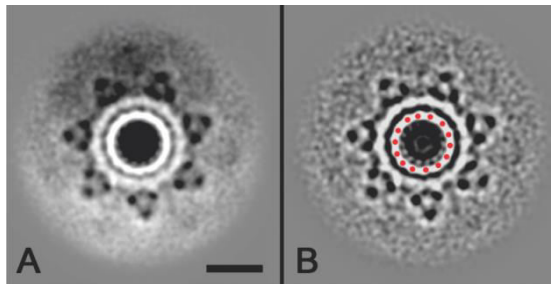


Figure 24 Projection maps of single particle electron microscopy analysis of the PilQ complex from the *N. gonorrhoeae* $\Delta tsaP/tsaP^+$ strain

(A) A two-dimensional map of the $\Delta tsaP/tsaP^+$ particle, seen in a slightly tilted top-view position. A small protein domain is visible inside the inner rings, especially in the lower half. It is present in 14 copies, but some copies in the upper half are partly invisible because of partial overlap with the main body of the ring, which is the effect of tilt on the carbon support film of most of the particles. (B) Fine details become stronger after imposing a high-pass filter on the image in such a way all waves with a frequency representing wavelengths lower than 1.5 nm have been suppressed by 50%. The red dots mark places with a wider part of the inner rings to which the small protein domains are connected. The scale bar is 10 nm. [The EM analysis and single particle electron microscopy analysis analysis was performed by D.A. Semchonok, Rijksuniversiteit Groningen]

Loss of the peripheral structure in the $\Delta tsaP$ mutant, combined with the observations that the membrane association/integration of TsaP depends on PilQ, suggest that PilQ and TsaP interact directly and that at least part of the peripheral structure around the PilQ secretin is formed by TsaP. We have previously reported that in *N. meningitidis*, which also encodes a TsaP homolog, the secretin structure contains the inner and peripheral ring but that the spikes are absent [105]. Similarly, the spikes, but not the peripheral ring, are lost in the *N. gonorrhoeae* $\Delta pilP$ and $\Delta pilF$ mutants, whereas the spikes are still made in the $\Delta pilW$ and $\Delta pilC$ mutants [105]. Immunoblotting of whole cell extracts and of isolated membranes from the $\Delta pilP$, $\Delta pilF$, $\Delta pilW$ and $\Delta pilC$ mutants demonstrated that they contained similar levels of TsaP as the WT and that TsaP associated with the OM as in WT (Figure 25). Because loss of the peripheral ring is only observed in the $\Delta tsaP$ mutant and the tight association of TsaP with the OM depends on PilQ and occurs in the absence of the spikes, we suggest that TsaP forms, or is part of, the peripheral ring.

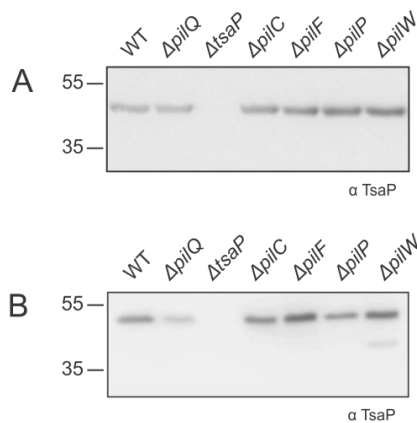


Figure 25 TsaP levels are reduced in membranes of the $\Delta pilQ$ strain, but not in the membranes of the $\Delta pilC$, $\Delta pilF$, $\Delta pilP$ and $\Delta pilW$ strains

(A) Immunoblot analysis of equal amounts of total cell extracts of the *N. gonorrhoeae* WT, $\Delta pilQ$, $\Delta tsaP$, $\Delta pilC$, $\Delta pilF$, $\Delta pilP$ and $\Delta pilW$ strains using α -TsaP, antibodies. (B) Immunoblot analysis of membranes isolated from the *N. gonorrhoeae* WT, $\Delta pilQ$, $\Delta tsaP$, $\Delta pilC$, $\Delta pilF$, $\Delta pilP$ and $\Delta pilW$ strains using the α -TsaP antibody.

4.2.7 TsaP homologs are specifically found in bacteria encoding T4aPS

As mentioned, TsaP homologs are widespread in Gram-negative bacteria. Based on our studies in *N. gonorrhoeae*, we hypothesized that TsaP homologs may also be important for T4P function in these bacteria. To test this hypothesis, we set-out to determine whether TsaP homologs are specifically present in bacteria containing T4aPS. In Neisseriales, *tsaP* is not located in the vicinity of genes associated with T4PS. Synteny analysis of homologs of *tsaP* also did not reveal the presence of genes encoding proteins of T4PS in close proximity. Genes of T4PS are often found in operons, but e.g. genes encoding pilotins are generally found separated from other T4PS genes. To test whether there is a correlation between the occurrence of T4PS in a genome and the presence of a TsaP homolog the reciprocal BlastP method [182] was performed with 6 marker proteins whose presence is indicative of T4aPS (PilQ, PilF, PilT, PilM, PilN, and PilO). When 4 of the 6 proteins were identified within a genome, this genome was considered to contain a T4aP system. Divergent T4aP systems in more phylogenetically distant organisms might not be identified due to the stringent thresholds needed to distinguish between T4aP and T2SS. Therefore, we focused on 450 genomes available for proteobacteria. The presence of genes encoding the T4aP diagnostic proteins and TsaP homologs in the different genomes is given in the supplementary Table 46. The distribution of the TsaP homologs and the representatives of T4P systems, as identified by reciprocal blast analysis, is shown in Figure 26. Using reciprocal BlastP analysis, 4 of the 6 T4aPS diagnostic genes were found in 171 of the 450 genomes. In 155 of these 171 genomes, genes encoding TsaP homologs were identified. Only 1 TsaP homolog was detected in the remaining 279 genomes. This demonstrated a strong link between the presence of TsaP and the presence of a T4PS. Three other LysM domain containing proteins (MltD, a membrane-bound lytic murein transglycosylase D, AmiC, the N-acetylmuramoyl-L-alanine amidase and FimV, the peptidoglycan-binding protein) were also included in our analysis (see supplementary Table 46). No relation was found between the presence of MltD or AmiC and the presence of T4PS. FimV homologs could be identified in 114 of the 171 genomes encoding a T4PS and in 23 of the 279 genomes that did not encode a T4PS, demonstrating that although not as strongly as observed for TsaP, also the presence of a FimV homolog correlated with presence of T4PS. Many bacteria that contain a T4PS contain both a TsaP and a FimV homolog. We were unable to find representative proteins and thresholds suitable to reliably identify T4bPS and T2SS using the reciprocal BlastP method, and therefore we manually screened genomes that did not encode a T4aPS, but encoded

either a T4bPS or a T2SS for the presence of a TsaP homolog. No homologs of TsaP were identified on the R64 plasmid or in the genomes of enteropathogenic *E. coli* and of *Aggregatibacter actinomycetemcomitans*, which encode T4bPS or in the genomes of *Klebsiella spp.* and *Yersinia enterocolitica* which contain a T2SS, but not a T4aPS (Table 45). Therefore, we conclude that a strong correlation exists between the presence of TsaP homologs and T4aPS, but that this correlation does not seem to exist for TsaP and T4bPS or T2SS.

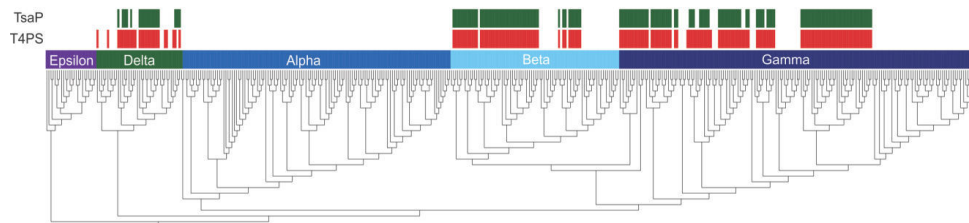


Figure 26 Identification of genes encoding TsaP homologs and T4aPS related genes in different genomes

Reciprocal Blast analysis was performed for six proteins representative for T4aPS (PilQ, PilT, PilF, PilM, PilN and PilO), as well as for TsaP to identify the different proteins in 450 proteobacterial genomes. Results were plotted on the 16S RNA phylogenetic tree. Colored boxes indicate the presence of a TsaP ortholog or the presence of at least 4 of the 6 proteins representative for T4aPS. [The shown phylogenetic tree was generated, using the ITOL website, according to the results of the reciprocal BlastP analysis which was performed by Dr. S. Huntley]

Table 45 Nomenclature of TsaP homologs and ATPase and secretin proteins of T4P assembly systems and T2SS of different organisms

Organism	Type IV pili			TsaP homolog	T2SS	
	Assembly ATPase	Secretin	Retraction ATPase		Secretion ATPase	Secretin
<i>Neisseria gonorrhoeae</i> ¹	PilF	PilQ	PilT	NGFG_01788		
<i>Neisseria meningitidis</i> ²	PilF	PilQ	PilT, PilU	NMC0101		
<i>Ralstonia solanacearum</i> ³	PilF	PilQ	PilT, PilU	RSc0069		
<i>Methylobacillus flagellatus</i> ⁴	PilF	PilQ	PilT, PilU	Mfla_0188		
<i>Azoarcus spp.</i> ⁵	PilF	PilQ	PilT, PilU	azo0098		
<i>Methylococcus capsulatus</i> ⁶	PilB	PilQ	PilT, PilU	MCA2842		
<i>Dichelobacter nodosus</i> ⁷	PilB	PilQ	PilT, PilU	DNO_0155		
enteropathogenic <i>Escherichia coli</i> ⁸	HofB	HofQ	-	-		
Plasmid R64 ⁹	PilQ	PilN	-	-		
<i>Aggregatibacter actinomycetemcomitans</i> ¹⁰	TadA	RcpA	-	-		
<i>Shewanella putrefaciens</i> ¹¹	PilB	PilQ	PilT, PilU	Sputcn32_0025	GspE	GspD
<i>Pseudomonas aeruginosa</i> ¹²	PilB	PilQ	PilT, PilU	PA0020	XcpR	XcpQ
<i>Legionella pneumophila</i> ¹³	PilB	PilQ	PilT	lpg2596	LspE	LspD
<i>Vibrio cholerae</i> ¹⁴	PilB	PilQ	PilT, PilU	VC0047	GspE	GspD
<i>Xanthomonas campestris</i> ¹⁵	PilB	PilQ	PilT, PilU	XCC3750	XpsE	XpsD
<i>Myxococcus xanthus</i> ¹⁶	PilB	PilQ	PilT	MXAN_3001	GspE	GspD
<i>Klebsiella oxytoca</i> ¹⁷	-	-	-	-	PuE	PuD
<i>Yersinia enterocolitica</i> ¹⁸	-	-	-	-	GspE	GspD

¹*Neisseria gonorrhoeae* MS11, ²*Neisseria meningitidis* Fam18, ³*Ralstonia solanacearum* GMI1000, ⁴*Methylobacillus flagellatus* KT, ⁵*Azoarcus sp.* BH72, ⁶*Methylococcus capsulatus* str. Bath, ⁷*Dichelobacter nodosus* VCS1703A, ⁸*Escherichia coli* O104:H4 str. C227-11, ¹⁰*Aggregatibacter actinomycetemcomitans* D11S-1, ¹¹*Shewanella putrefaciens* CN-32, ¹²*Pseudomonas aeruginosa* PAO1, ¹³*Legionella pneumophila* subsp. *pneumophila* str. Philadelphia I, ¹⁴*Vibrio cholerae* O1 biovar El Tor str. N16961, ¹⁵*Xanthomonas campestris* pv. *Campestris* str. ATCC 33913, ¹⁶*Myxococcus xanthus* DK1612, ¹⁷*Klebsiella oxytoca* KCTC 1686, ¹⁸*Yersinia enterocolitica* subsp. *enterocolitica* 8081, ¹⁹*Burkholderia pseudomallei* K96243

4.3 Analysis of TsaP domains and their function

4.3.1 Domain prediction

Studies of the secretin ring of *N. gonorrhoeae* embedded in OM sheets showed that the PilQ-secretin ring is surrounded by a peripheral structure. Previous experiments revealed that a conserved protein, named TsaP, forms this peripheral ring structure or at least is part of it. To characterize TsaP in more detail, BlastP analysis and sequence alignment were performed and showed that TsaP homologs are conserved over the whole length of TsaP (Figure 18). These data together with recent RaptorX structure prediction analysis, gave more information about putative domains of TsaP. The *in silico* analysis identified two β -sheet rich domains next to the N-terminal located LysM domain, which most likely resulted from sequence duplication. These two domains show 18 % and 15 % sequence identity to the C-terminal domain of FlgT of *Vibrio spp.* FlgT is a periplasmic protein, forming the H-ring of the flagella system of *Vibrio spp.* Recently, Martinez *et al.* and Terashima *et al.* could show that the H-ring stabilizes the basal body structure that anchors the flagellum [201, 202]. The crystal structure of FlgT revealed that the C-terminal domain is made of seven β -strands, where six of the seven strands are arranged in a core β -barrel structure [202, 203]. RaptorX structure prediction, using TsaP and TsaP_{MX} sequences, showed that the β -sheet rich domains form beta-barrel structures similar to the C-terminal domain of FlgT (Figure 27), facilitating outer membrane insertion. In addition, a linker region that connects the two FlgT-like domains was identified only in *Neisseria spp.* Therefore, we conclude that TsaP can be divided into four domains (Figure 28); (i) the LysM domain, (ii) FlgT domain 1, (iii) FlgT domain 2 and (iv) a linker region that is only found in *Neisseria spp.*

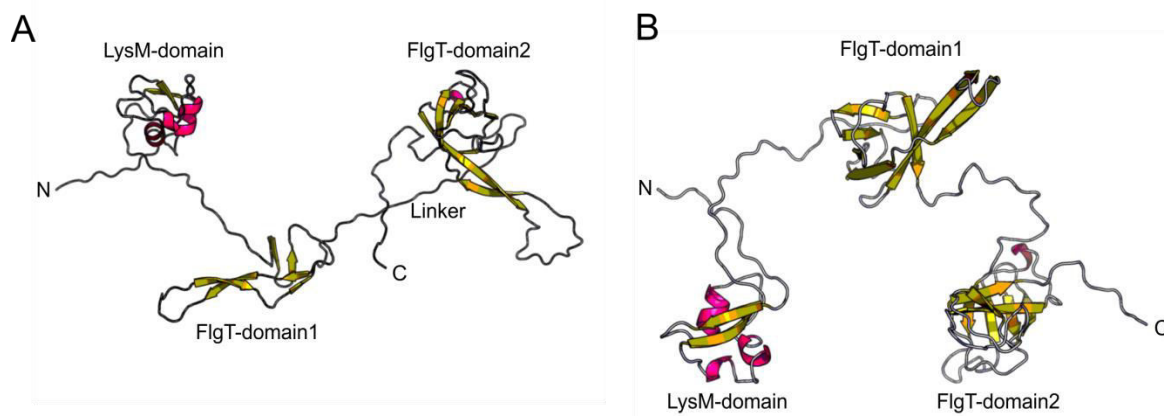


Figure 27 Model prediction for TsaP and TsaP_{MX}

Side view on the structural ribbon model of TsaP from *Neisseria gonorrhoeae* (A) and *Myxococcus xanthus* (B). The structures have been modeled using the RaptorX prediction software. Identified domains are indicated.

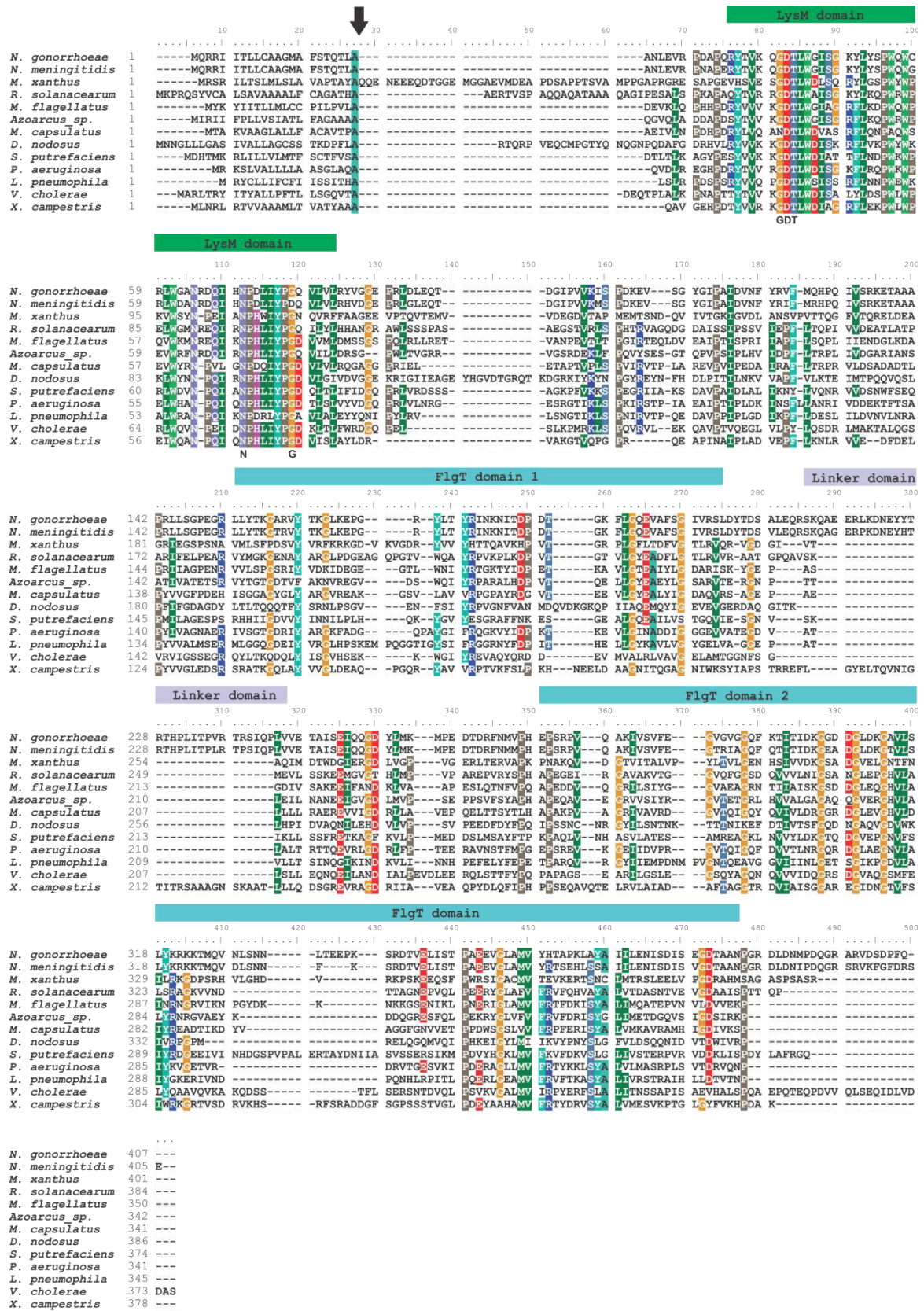


Figure 28 Domain architecture of Tsap

Tsap homologs described in table 46 (supplementary data) were aligned. Colored residues indicate <50 % conservation. The putative signal sequence cleavage site is indicated with a black arrow. The LysM domain is indicated with a green box. Residues (G40, D41, T42, N70 and G77), that are highly conserved in LysM domains are indicated in bold below the alignment. The FlgT domains are indicated with blue boxes and the neisserial linker domain is indicated by purple box.

4.3.2 Lack of the gonococcal linker domain of TsaP affects surface assembly of T4P

To clarify the role of each TsaP domain in *N. gonorrhoeae*, we aimed to prepare domain deletion mutants, analyze the colony morphology of those mutants and monitor the secretin structures in their native lipid environment. To examine the contribution of the linker region to surface assembled T4P and to the secretin structure, an in-frame chromosomal deletion of amino acids S213-V245 of *tsaP* was constructed in the WT strain (*tsaPΔS213-V245*). Moreover, a *tsaPΔS213-V245* complementation strain was generated by the ectopic insertion of a copy of *tsaP* under control of the *lac* promoter (*tsaPΔS213-V245/tsaP⁺*) [18]. Unless otherwise indicated, the *tsaPΔS213-V245/tsaP⁺* strain was grown in the presence of 1 mM IPTG. In addition, it was aimed to generate a markerless *tsaPΔlysM* (*tsaPΔA33-R83*) mutant in the WT strain. Following mutagenesis, approximately 50.000 colonies were isolated and screened to identify those with a *tsaPΔA33-R83* mutation. Unfortunately, a *tsaPΔA33-R83* mutation could not be confirmed. In a next step, a *tsaPΔA33-R83* strain was generated by complementing a Δ *tsaP* strain by an ectopic insertion of a copy of *tsaPΔA33-R83* under control of the *lac* promoter (Δ *tsaP/tsaPΔA33-R83⁺*). A total of 10 colonies showed chromosomal integration of the *tsaPΔA33-R83⁺* complementation construct. Western blot analysis on whole cell extracts of these 10 mutant revealed that 9 mutants had a restored full-length TsaP. This indicates that the complementation construct integrated in 90 % of the cases into the original loci, restoring the Δ *tsaP* mutation, which was generated by insertion duplication mutagenesis. Only one Δ *tsaP/tsaPΔA33-R83⁺* strain showed correct insertion in the neisserial complementation site (data not shown).

On agar plates, gonococci assembling T4P on their cell surface form small, compact colonies with a sharp edge. Non-piliated cells form flat colonies with a larger diameter and a “fuzzy” edge [177]. To further understand the function of TsaP, the WT, Δ *pilQ*, *tsaPΔS213-V245*, *tsaPΔS213-V245/tsaP⁺* and Δ *tsaP/tsaPΔA33-R83⁺* strains were analyzed on agar plates. WT and the Δ *pilQ* mutant showed colony morphologies corresponding to piliated and non-piliated cells, respectively. The *tsaPΔS213-V245* mutant and the *tsaPΔS213-V245/tsaP⁺* and Δ *tsaP/tsaPΔA33-R83⁺* strains grown in the absence of IPTG showed colony morphologies matching that of non-piliated cells. Importantly, in the presence of IPTG, the *tsaPΔS213-V245/tsaP⁺* and Δ *tsaP/tsaPΔA33-R83⁺* strain showed a colony morphology matching that of piliated cells (Figure 29). Since we hypothesize that the LysM domain is involved in anchoring the secretin complex, the piliated colony morphology of the Δ *tsaP/tsaPΔA33-R83⁺* strain was unexpected. To exclude re-recombination of the ectopic *tsaPΔA33-R83⁺* into the original *tsaP* loci immunoblot analysis of the induced strain need to be carried out. Thus, deletion of the linker region (S213-V245) resulted in loss of the piliated colony morphology.

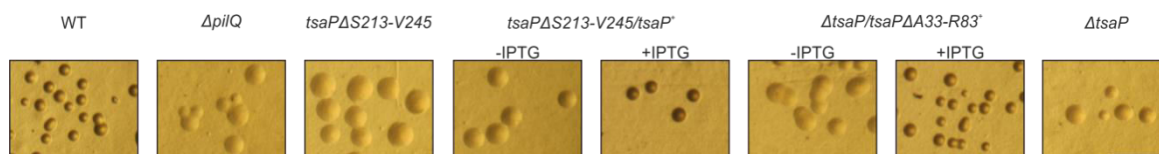


Figure 29 The linker domain of TsaP is important for T4P-dependent colony morphology

The indicated *N. gonorrhoeae* strains were incubated at 37 °C for 24 h on GCB plates. The scale bar equals 1 mm.

Because the gonococcal TsaP mutant is deficient in surface exposed T4P, we asked whether surface exposed T4P were detectable in the *tsaPΔS213-V245* and Δ *tsaP/tsaPΔA33-R83*⁺ mutants. In a next step, WT, *tsaPΔS213-V245*, *tsaPΔS213-V245/tsaP*⁺ and Δ *tsaP/tsaPΔA33-R83*⁺ cells were negatively stained for subsequent EM analysis. In WT, the *tsaPΔS213-V245/tsaP*⁺ and the Δ *tsaP/tsaPΔlysM*⁺, single and bundled T4P were observed. In addition, the Δ *tsaP/tsaPΔA33-R83*⁺ showed single and bundled T4P and additional T4P filled membrane protrusions as observed in the Δ *tsaP* background strain. In contrast, no surface assembled T4P were observed in the *tsaPΔS213-V245* mutant, suggesting that this deletion might affect the peripheral secretin structure.

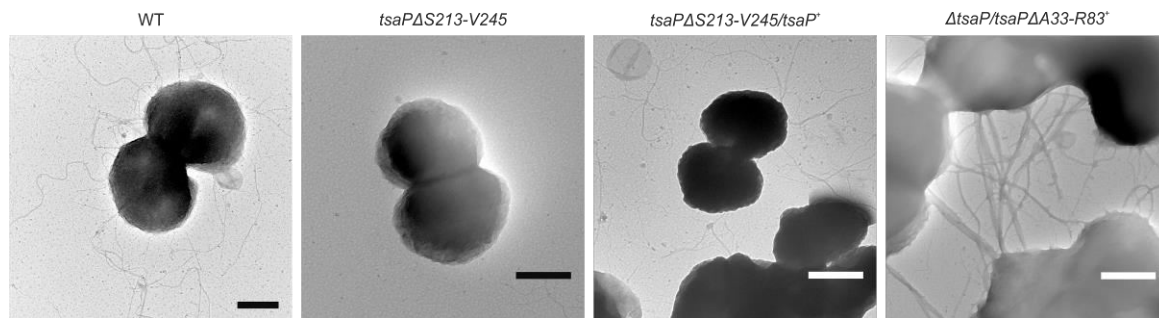


Figure 30 Deletion of the gonococcal TsaP-linker domain leads to the loss of surface exposed T4P in *N. gonorrhoeae*

EM analysis of WT, *tsaPΔS213-V245*, *tsaPΔS213-V245/tsaP*⁺ and Δ *tsaP/tsaPΔA33-R83*⁺ strains grown in the presence of 1 mM IPTG. Cells were applied to carbon-coated copper grids, washed twice with double distilled water and subsequently stained with uranyl acetate before investigation via EM. Scale bar equals 500 nm. [The EM analysis was performed together with A-L Henche, MPI-Marburg]

4.3.3 The peripheral structure of the secretin complex is lost in the *tsaPΔS213-V245* mutant

In order to determine whether the deletion of the gonococcal TsaP-linker and the LysM domain affected the structure of the secretin complex in its native OM environment, OMs isolated from the *tsaPΔS213-V245*, *tsaPΔS213-V245/tsaP*⁺ and Δ *tsaP/tsaPΔA33-R83*⁺ strains were studied by transmission EM followed by single particle averaging [105]. A comparison of the projection maps of the secretin complexes obtained from membranes of the *tsaPΔS213-V245* (Figure 31B), *tsaPΔS213-V245/tsaP*⁺ (Figure 31C) and Δ *tsaP/tsaPΔA33-R83*⁺ (Figure 31D) strains with projection maps obtained from WT membranes (Figure 31A), showed that the peripheral ring and the spikes are lost in the *tsaPΔS213-V245* mutant, and that they are recovered in the *tsaPΔS213-V245/tsaP*⁺ strain. The structures observed in membranes of the *tsaPΔS213-V245* mutant strongly resemble the structure of the isolated PilQ complex (Figure 16B). The structure observed in membranes of the Δ *tsaP/tsaPΔA33-R83*⁺ strain resembles the structure of the WT complex. Loss of the peripheral structure in the *tsaPΔS213-V245* mutant, combined with the observations that this region is only found in *Neisserial spp.*, suggest that this TsaP domain might interact with the SBR-region of PilQ which is also found only in *Neisserial spp.*

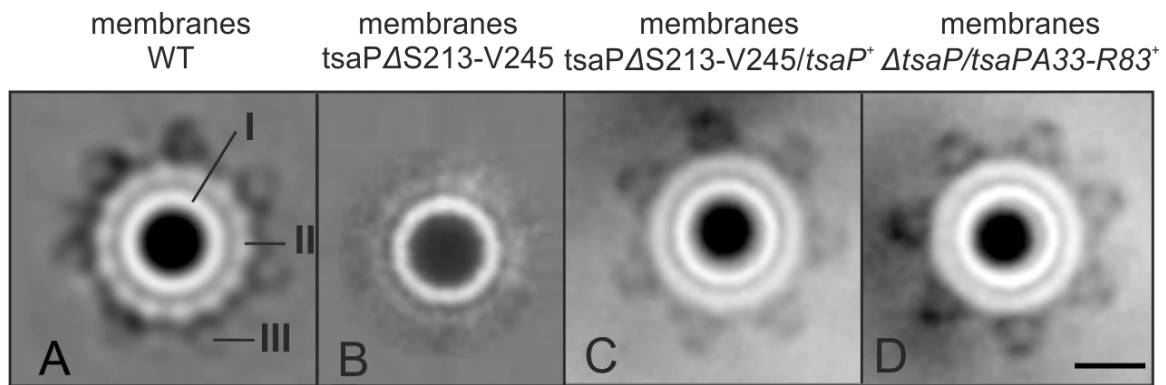


Figure 31 Projection maps of single particle electron microscopy analysis of the PilQ complex from *N. gonorrhoeae*

Projection maps of class averages of single particle EM images obtained from membranes isolated from (A) the WT, (B) the *tsaP* Δ S213-V245 strain, (C) the *tsaP* Δ S213-V245/*tsaP*⁺ and (D) the Δ *tsaP*/*tsaPA*33-R83⁺ grown in the presence of 1 mM IPTG. I, II and III indicate the inner ring, the peripheral ring and the spikes respectively. Scale bar, 10 nm. [The EM analysis and single particle electron microscopy analysis was performed by D.A. Semchonok, Rijksuniversiteit Groningen]

4.4 Interaction of TsaP with other components of the type IV pili system

4.4.1 Identification of protein-protein interaction between TsaP and PilQ using a bacterial adenylate cyclase two-hybrid system

The process of assembly of pili is complicated: it requires the cooperative action of a group of proteins which span both the inner and outer membranes in bacteria. In September 2012, Berry *et al.* determined the structure of PilQ, which is part of the machinery forming a channel between both membranes [150]. Using bioinformatic studies, they suggested that the N-terminal regions of T4P-dependent secretins generally contain one or two putative domains (named B1/B2), predicted to be rich in β -sheets and characteristically different from the α/β domains observed in T2SS and T3SS secretins. Mapping sequence conservation on to the structure of the B2 domain implicated that there is a highly conserved patch, forming a binding site to another unidentified T4P biogenesis protein [150]. Since we could show that localization, membrane integration and/or stability of TsaP is PilQ dependent, we hypothesize that TsaP would bind to the highly conserved patch of the B2 domain. To identify protein-protein interaction of TsaP and PilQ, fragments of TsaP and PilQ were tested *in vivo*, using the bacterial adenylate cyclase two-hybrid (BACTH) system. This system is based on the interaction-mediated reconstitution of the adenylate cyclase activity in *E. coli*. One limitation of this system is that cAMP needs to be produced in the cytoplasm, precluding the analysis of proteins that have no cytoplasmic domain. For this reason, signal sequence truncated versions of TsaP and PilQ were generated. For TsaP and PilQ, 12 different plasmids were generated by cloning the full-length, the N-terminus and the C-terminus of the corresponding gene into appropriate BACTH vectors to create fusions with the N- or C-termini of T18 and T25. All the possible pairs of T18 and T25 plasmids, 144 in total, were co-transformed in the *E. coli* strain BTH101. Functional complementation between T18 and T25 was determined by plating transformants on selective LB/X-Gal/IPTG plates and observing the coloration of the colonies after 48 h of growth at 30 °C. In the absence of functional complementation between T18 and T25 the colonies are white, while they are blue when functional complementation occurs. The PilQ fragment fusions were apparently and for an unknown reason toxic, and could not be scored as it yielded no microscopic colonies even after prolonged incubation. Out of the 144 T18/T25 plasmid combinations, four yielded colored colonies,

indicating protein-protein interactions (Figure 32). In summary, using the BACTH system it could be shown that TsaP might self-interact forming oligomers.

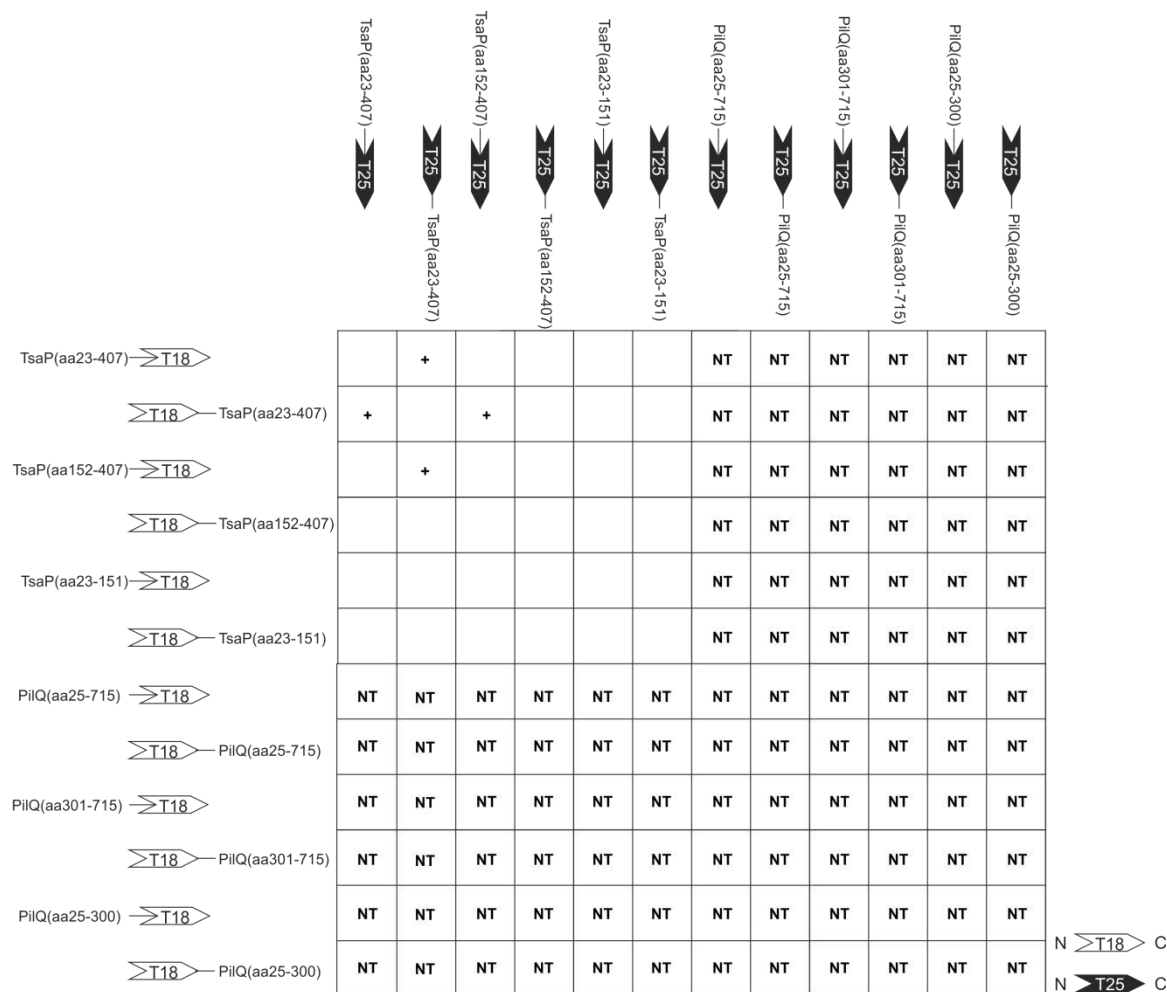


Figure 32 Binary interactions between TsaP and PilQ of *N. gonorrhoeae* using a bacterial adenylate cyclase two-hybrid (BACTH) system

Full-length and protein domains of TsaP and PilQ, indicated by the amino acids, were fused to both the N- and C-termini of the *B. pertussis* adenylylase fragments T18 and T25 respectively. All possible T18 + T25 plasmid combination, 144 in total were co-transformed in *E. coli* strain BTH101 and plated on LB-agar plates supplemented with X-gal and IPTG. Functional complementation between the T18 and T25 fragments, which occurs only upon interaction of the hybrid proteins, triggers expression of the *lacZ* gene and yields blue colonies. +, pairs that yielded colored colonies; NT, this combination could not be tested because no colonies were obtained even after prolonged incubation.

4.4.2 PilQ(B1/B2) can be purified as a stable dimer

Since the fusions of full-length PilQ and the truncated PilQ-fragments to the T18 and T25 fragment were for an unknown reason toxic within the bacterial adenylate cyclase two-hybrid system it was aimed to test for protein-protein interaction using heterologous overexpressed and purified proteins. As PilQ contains a type I signal sequence, the first 21 amino acids were removed to prevent secretion of the protein upon overexpression in *E. coli*. In 2012 Berry *et al.* could show that overexpression of the B1-domain of *N. meningitidis* result in low protein yields and/or poor stability

of the protein [150]. To improve the protein yields and stability of the B1/B2 domain, HA-PilQ(B1/B2) was fused to the MARTX toxin cysteine protease domain (CPD) of *V. cholerae*, which is was shown to improve protein stability and solubility [204]. After overexpression, HA-PilQ(B1/B2)-CPD-His₁₀ could be purified in pure and high amounts using a two step protocol as described in chapter 3.4.12. HA-PilQ(B1/B2)-CPD-His₁₀ elutes from the Ni²⁺-affinity column at an imidazole concentration of 200 mM. The elution profile is shown in Figure 33A. Each elution fraction was analyzed by 12 % SDS/PAGE. HA-PilQ(B1/B2)-CPD-His₁₀ migrates on SDS/PAGE gels at a position corresponding to the calculated size of 55 kDa (Figure 33B). Fractions C1-C11 were pool and loaded on a size exclusion volume. The elution profile showed one distinct peak at an elution volume of 70 ml (see Figure 34A). Correlating the elution volume of the observed protein peak (600 mAU) with commercially available molecular weight standards showed that this peak correspond to a molecular mass of 109 kDa, which is in

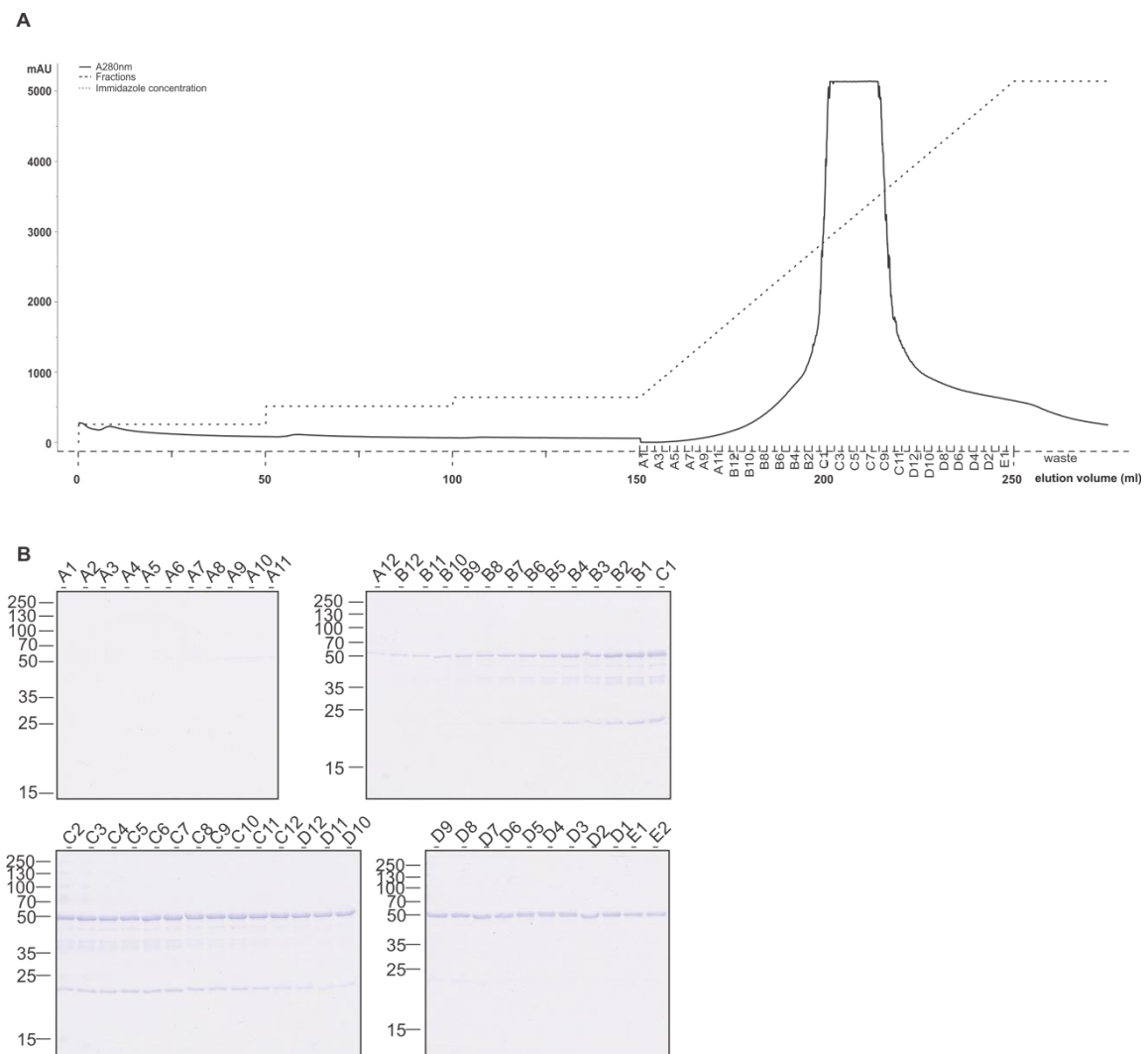


Figure 33 Ni²⁺-affinity purification of HA-PilQ(B1B2)-CPD-His₁₀

(A) Elution profile of Ni²⁺-affinity chromatography. The protein was detected at 280 nm and is indicated by the solid line. The imidazole concentration is indicated by the dashed line. The intensity is given in mAU. The collected fractions are labeled as indicated. (B) 12 % SDS/PAGE with elution fractions from the Ni²⁺-affinity chromatography. The labeling of the lanes corresponds to the labeling of the elution fractions shown in (A). Molecular masses are indicated on the left site. PilQ(B1/B2) migrates at a position corresponding to a molecular mass of 55 kDa.

agreement with the calculate mass of a dimeric HA-PilQ(B1/B2)-CPD-His₁₀. The different elution fractions were analyzed by SDS/PAGE and TsaP was detected in fractions B10-B8 corresponding to a dimeric structure of HA-PilQ(B1/B2)-CPD-His₁₀ (Figure 34B).

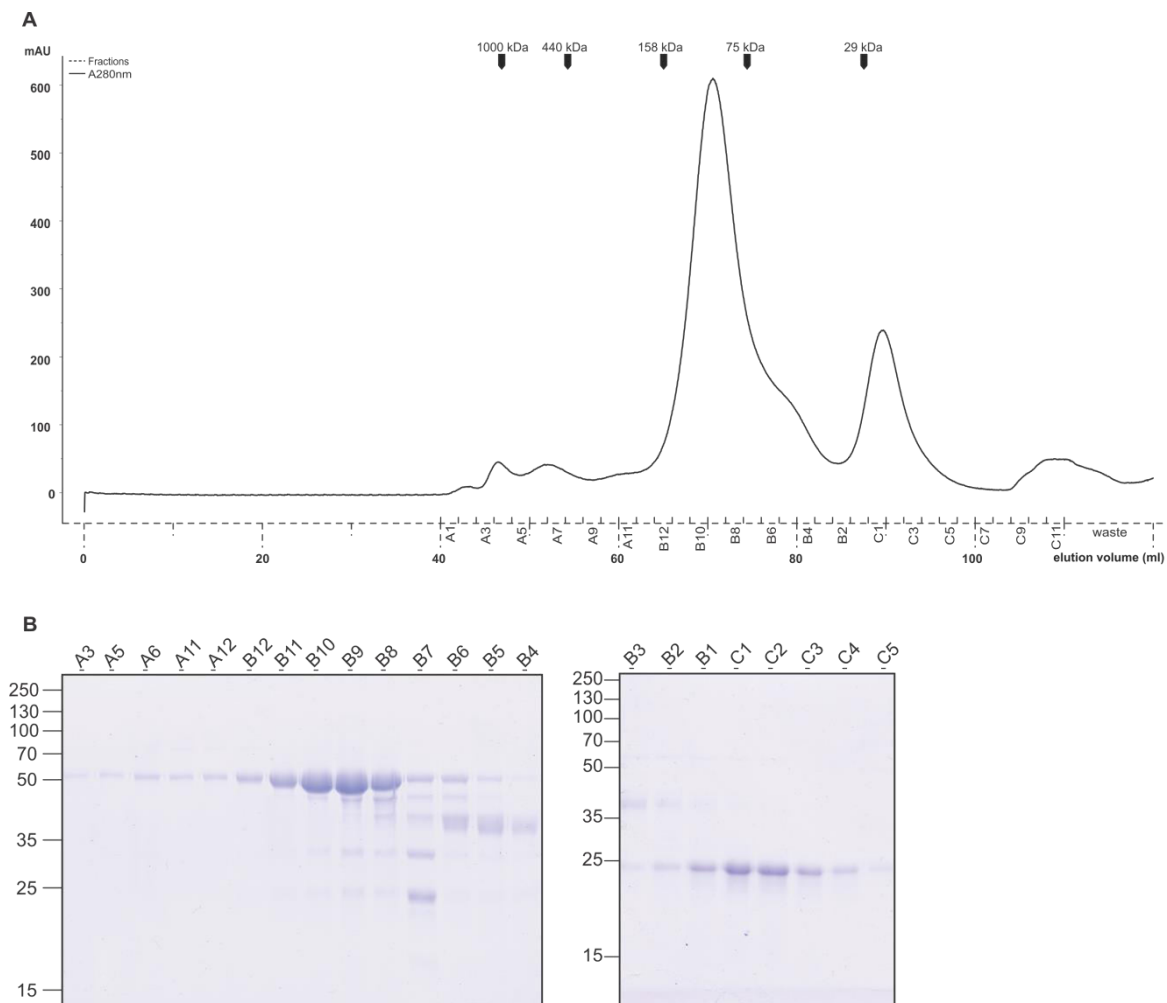


Figure 34 Size exclusion chromatography of HA-PilQ(B1/B2)-CPD-His₁₀

(A) PilQ(B1/B2) eluted as a dimer from the Superdex 200 HiLoad 16/60 gel filtration column. The protein was detected at 280 nm and is indicated by the solid line. (B) HA-PilQ(B1/B2)-CPD-His₁₀ was essentially pure as assayed by Coomassie staining of a 12 % SDS/PAGE of the purified protein. The labeling of the lanes corresponds to the labeling of the elution fractions shown in (C). The position of various markers for both the gel filtration and the SDS/PAGE are indicated.

4.4.3 TsaPΔLysM forms a SDS stable multimer

In order to test for protein-protein interaction between PilQ and TsaP, it was decided to heterologously express and purify a truncated version of TsaP. As TsaP contains a type I signal sequence and a flexible LysM domain, which might interfere in the interaction assay, the first 83 amino acids were removed. Similarly to the overexpressed and purified full length TsaP (see paragraph 4.2.3). TsaPΔA33-R83 was cloned under the T7 promoter. After overexpression in *E. coli* BL21 (DE3) star, His₁₀-TsaPΔA33-R83 could be purified to homogeneity in high amounts using a two step protocol as described in chapter 3.4.11. The first step in His₁₀-TsaPΔA33-R83 purification was an immobilized metal ion affinity chromatography (IMAC). The elution profile, shown in Figure 35A,

indicates that the protein elutes from the Ni^{2+} -affinity column at an imidazole concentration of 350 mM. Each elution fraction was analyzed by 12 % SDS/PAGE. His₁₀-TsaPΔA33-R83 migrates on SDS/PAGE gels at a position corresponding to the calculated size of 37 kDa (Figure 35B). Surprisingly, a SDS stable complex, which just migrated into the running gel could be observed in the fractions containing the His₁₀-TsaPΔA33-R83 protein. This migration behavior has been seen before only for large and stable complexes, like secretin complexes. In a next step the fractions C10-D2 were pooled and analyzed by size exclusion chromatography. The elution profile, shown in Figure 36A, showed peaks at elution volumes of 42 ml, 52 ml and 80 ml. Correlating the elution volume of the observed protein peaks with commercially available molecular weight standards showed that the peak eluting at 80 ml correspond to a molecular mass of 44 kDa, which is in agreement with the calculate mass of

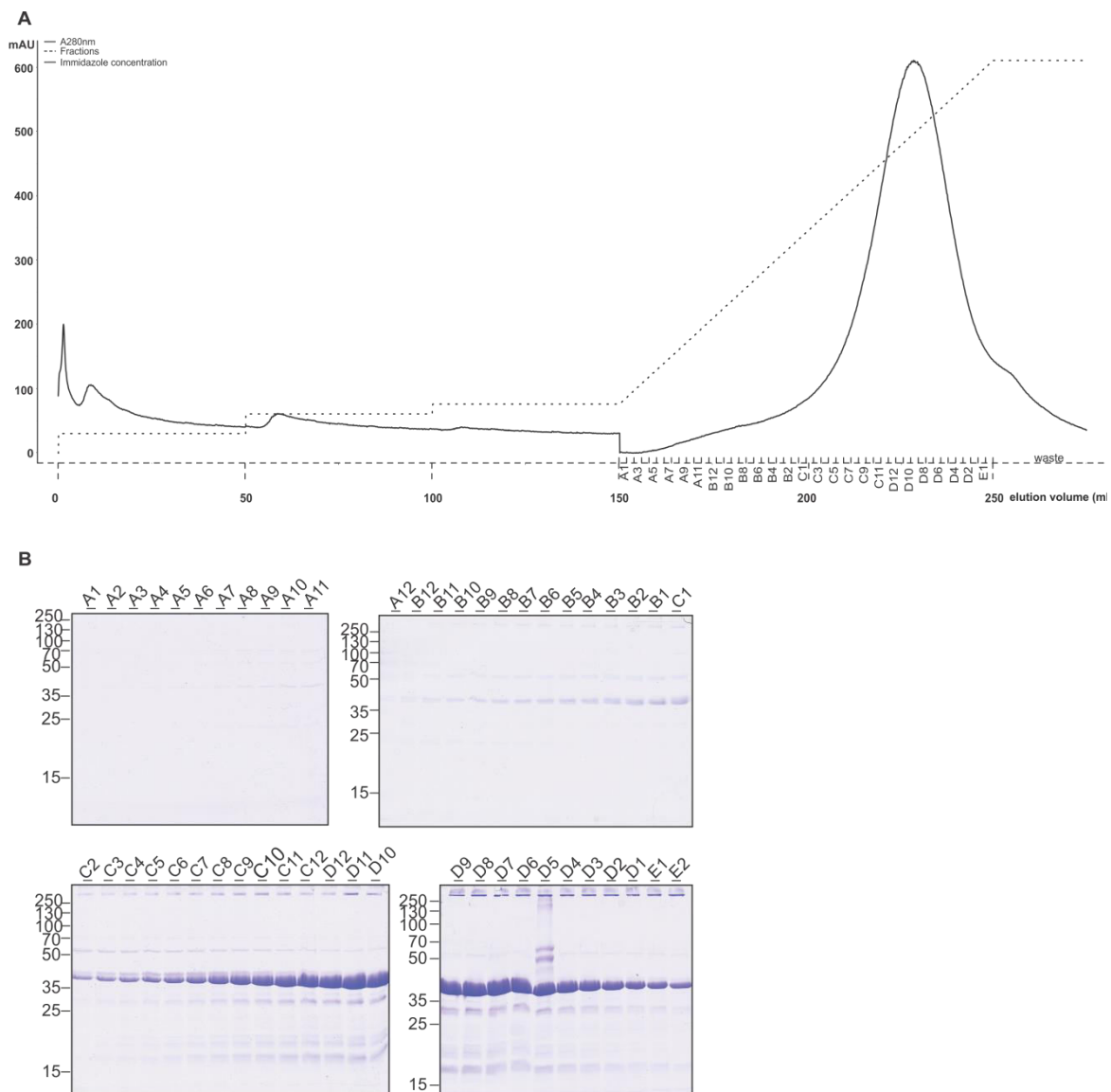


Figure 35 Ni^{2+} -affinity purification of His₁₀-TsaPΔA33-R83

(A) Elution profile of Ni^{2+} -affinity chromatography. The protein was detected at 280 nm and is indicated by the solid line. The imidazole concentration is indicated by the dashed line. The intensity is given in mAU. The collected fractions are labeled as indicated. (B) 12 % SDS/PAGE with elution fractions from the Ni^{2+} -affinity chromatography. The labeling of the lanes corresponds to the labeling of the elution fractions shown in (A). Molecular masses are indicated on the left site. His₁₀-TsaPΔA33-R83 migrates at a position corresponding to a molecular mass of 37 kDa.

a monomer. Since the resolution of the size exclusion chromatography column is limited, molecular masses of proteins eluting at 42 ml and 52 ml cannot be determined. The different elution fractions were analyzed by SDS/PAGE and $\text{TsaP}\Delta\text{A33-R83}$ was detected in each of the fractions (Figure 36D). In addition, the peaks observed at 42 ml and 52 ml contained next to $\text{His}_{10}\text{-TsaP}\Delta\text{A33-R83}$ also the SDS-stable complex. Because of the limited resolution of the size exclusion chromatography column, it was not possible to distinguish between a high molecular complex and aggregated protein.

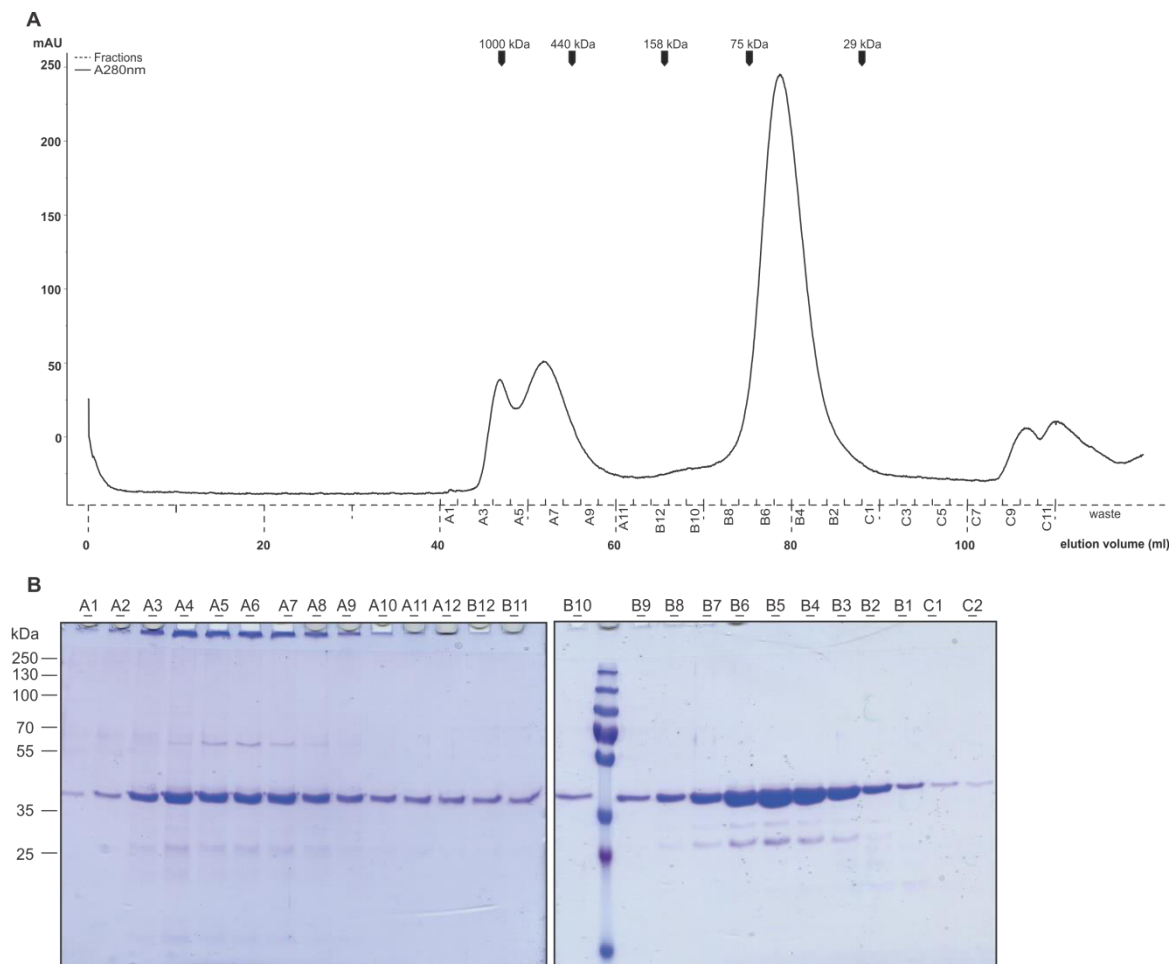


Figure 36 Size exclusion chromatography of $\text{His}_{10}\text{-TsaP}\Delta\text{A33-R83}$

(A) $\text{His}_{10}\text{-TsaP}\Delta\text{A33-R83}$ eluted as a monomer from the Superdex 200 HiLoad 16/60 gel filtration column. The protein was detected at 280 nm and is indicated by the solid line. (B) $\text{His}_{10}\text{-TsaP}\Delta\text{A33-R83}$ was essentially pure as assayed by Coomassie staining of a 12 % SDS/PAGE of the purified protein. The labeling of the lanes corresponds to the labeling of the elution fractions shown in (C). The position of various markers for both the gel filtration and the SDS/PAGE are indicated.

In order to verify the molecular masses of the peaks detected at 42 ml and 52 ml and to determine the size of the SDS stable complex, the elution fractions B5, A6, A4 and A2 were analyzed by Blue native PAGE (BN/PAGE). BN/PAGE is a method that was developed for separation of protein complexes in the range of 10 kDa and 10 MDa under non-denaturing conditions [205]. The results of the BN/PAGE are shown in Figure 37A. To ensure appropriate molecular mass estimation of the proteins in the different fractions, a protein standard composed of eight proteins, with known masses, was used. Plotting the molecular masses and the relative mobility of the standard proteins as a function of each other allows calculation of the molecular masses of the analyzed protein.

Fitting the relative mobility of the analyzed proteins to the mobility of the standard proteins revealed that the different size exclusion chromatography fractions contain protein complexes with molecular masses of 50 kDa, 70 kDa, 153 kDa, 245 kDa, 712 kDa and >1236 kDa. To exclude that the protein complex that just migrated into the BN/PAGE gel (Figure 37A) is formed by aggregated protein, a second BN/PAGE gel analysis with longer migration time was performed. Since the high molecular weight complex of >1236 kDa is able to migrate further into the gel, protein aggregation was excluded (Figure 37B). MS analysis (performed by J. Kahnt) identified that the formed protein complexes are composed of His₁₀-TsaPΔA33-R83. Therefore, it is concluded that His₁₀-TsaPΔLysM forms different oligomers which result in the formation an SDS stable complex.

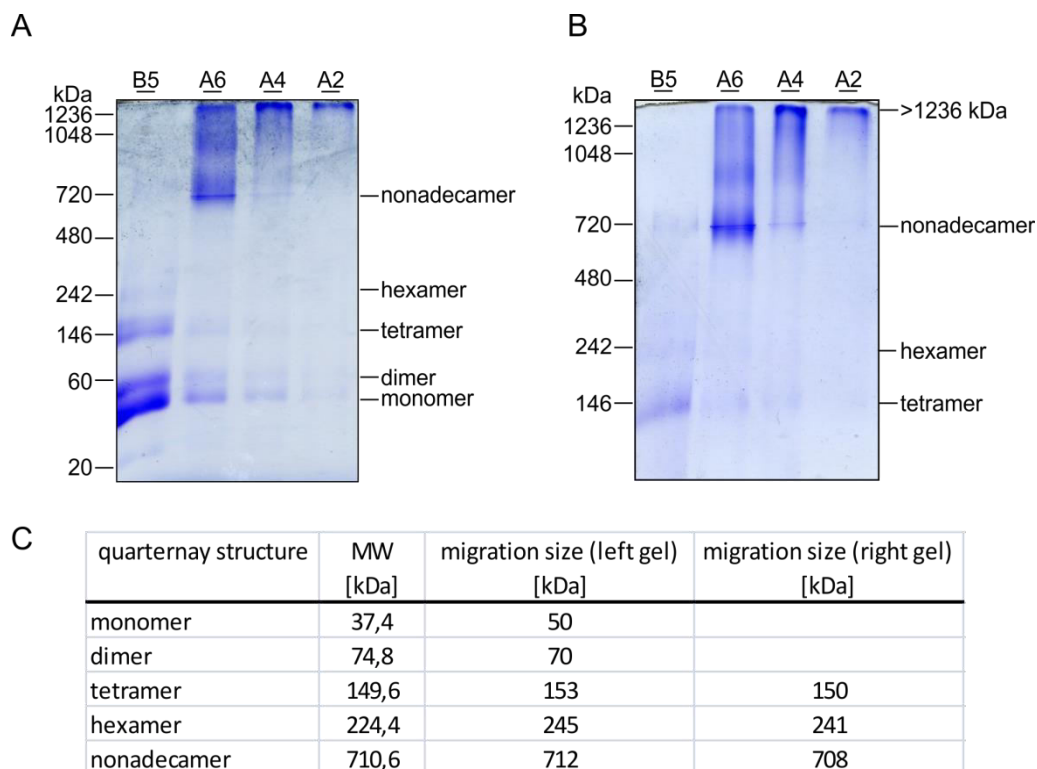


Figure 37 Blue Native PAGE analysis of His₁₀-TsaPΔA33-R83

(A) BN/PAGE with 5-13 % acrylamide gradient gel. (B) BN/PAGE with 5-13 % acrylamide gradient gel with a longer migration time than in (A). Molecular masses and His₁₀-TsaPΔA33-R83 quaternary structures are indicated on the left and right side, respectively. The labeling of each lane corresponds to the different size exclusion chromatography fractions. (C) Comparison of the calculated His₁₀-TsaPΔA33-R83 quaternary structures and the molecular masses seen in BN/PAGE.

4.4.4 PilQ_{MX} and TsaP_{MX} can be purified as stable dimers

To investigate direct protein-protein interactions for TsaP and PilQ of *N. gonorrhoeae* and other organisms, it was aimed to additionally test for interaction between PilQ_{MX} and TsaP_{MX} of *M. xanthus*. PilQ_{MX}(aa20-656) and TsaP_{MX} were cloned by Dr. Carmen Friedrich into the pET24b⁺ and pMal-c2x overexpression vector, respectively and the resulting overexpression constructs were introduced into *E. coli* Rosetta 2 (DE3). After overexpression, His₆-PilQ_{MX}(aa20-656) and MalE-TsaP_{MX} could be purified using a two step protocol as described in chapter 3.5.15 and 3.5.16. Size exclusion chromatography of His₆-PilQ_{MX}(aa20-656) showed an elution profile with one distinct peak at an

elution volume of 67 ml (Figure 38A). Correlation of the elution volume with commercially available size standards revealed that an elution volume of 67 ml correspond to a molecular mass of 140 kDa. Taking into account that the calculated mass of His₆- PilQ_{MX}(aa20-656) is 70 kDa, indicates that His₆- PilQ_{MX}(aa20-656) forms dimers. Analysis of the different elution fractions by SDS/PAGE showed that PilQ_{MX} was detected in each of the fractions (Figure 38B).

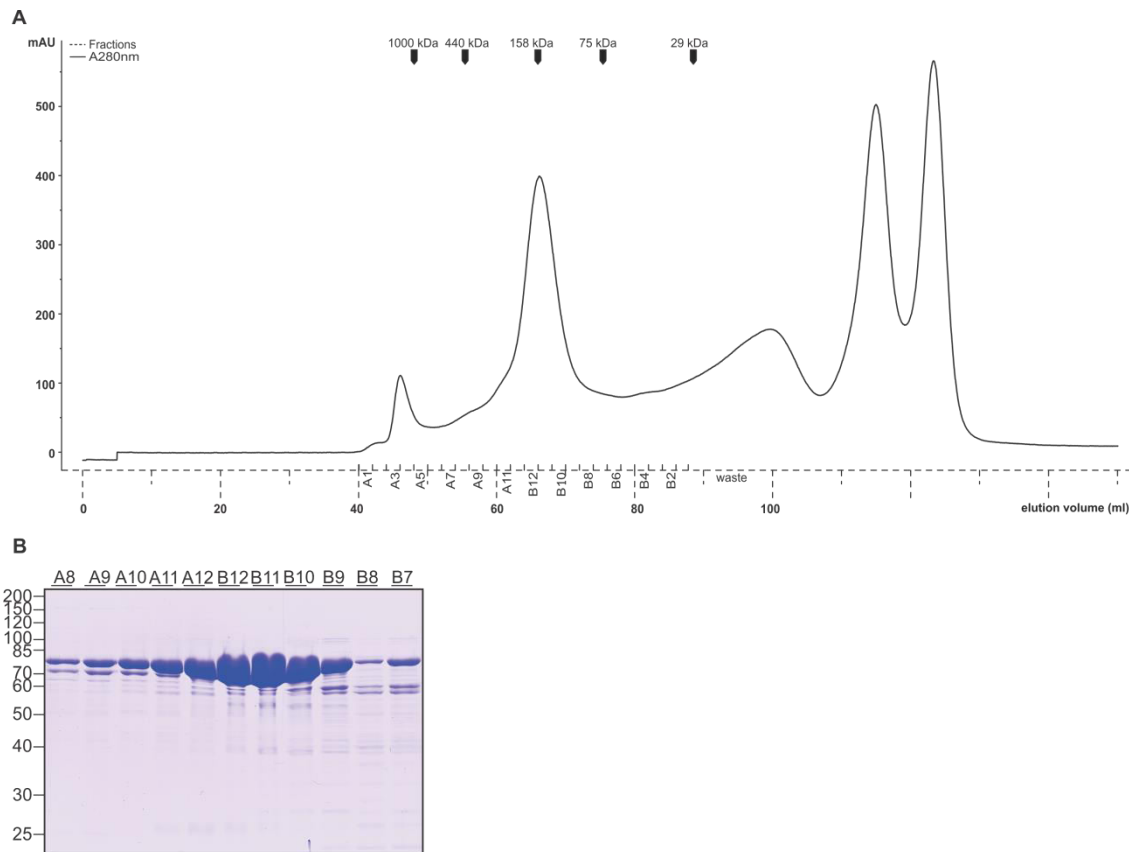


Figure 38 Size exclusion chromatography of His₆- PilQ_{MX}(aa20-656)

(A) His₆- PilQ_{MX}(aa20-656) eluted as a dimer from the SD200 gel filtration column. The protein was detected at 280 nm and is indicated by the solid line. (B) His₆- PilQ_{MX}(aa20-656) was essentially pure as assayed by Coomassie staining of a 12 % SDS/PAGE of the purified protein. The labeling of the lanes corresponds to the labeling of the elution fractions shown in (C). The position of various markers for both the gel filtration and the SDS/PAGE are indicated.

Analysis of purified MalE-TsaP_{MX} by size exclusion chromatography showed an elution profile with an increasing mAU signal at A₂₈₀nm at an elution volume of 42 ml. Overlap of the increasing signal with a dominant peak of 1400 mAU at an elution volume 65 ml leads to the formation of a shoulder (Figure 39A). Due to resolution limitation of the size exclusion chromatography column is it not possible to determine the molecular mass of the shoulder, which starts at 42 ml and overlap with the dominant peak at an elution volume of approximately 58 ml kDa. In contrast, the shoulder eluting at 65 ml corresponds to a molecular mass of 169 kDa. Taking into account that the calculated mass of MalE-TsaP_{MX} is 84,5 kDa, our data indicate that MalE-TsaP_{MX} forms dimers. Analysis of the different elution fractions by SDS/PAGE showed that MalE-TsaP_{MX} was detected in each of the fractions (Figure 39B).

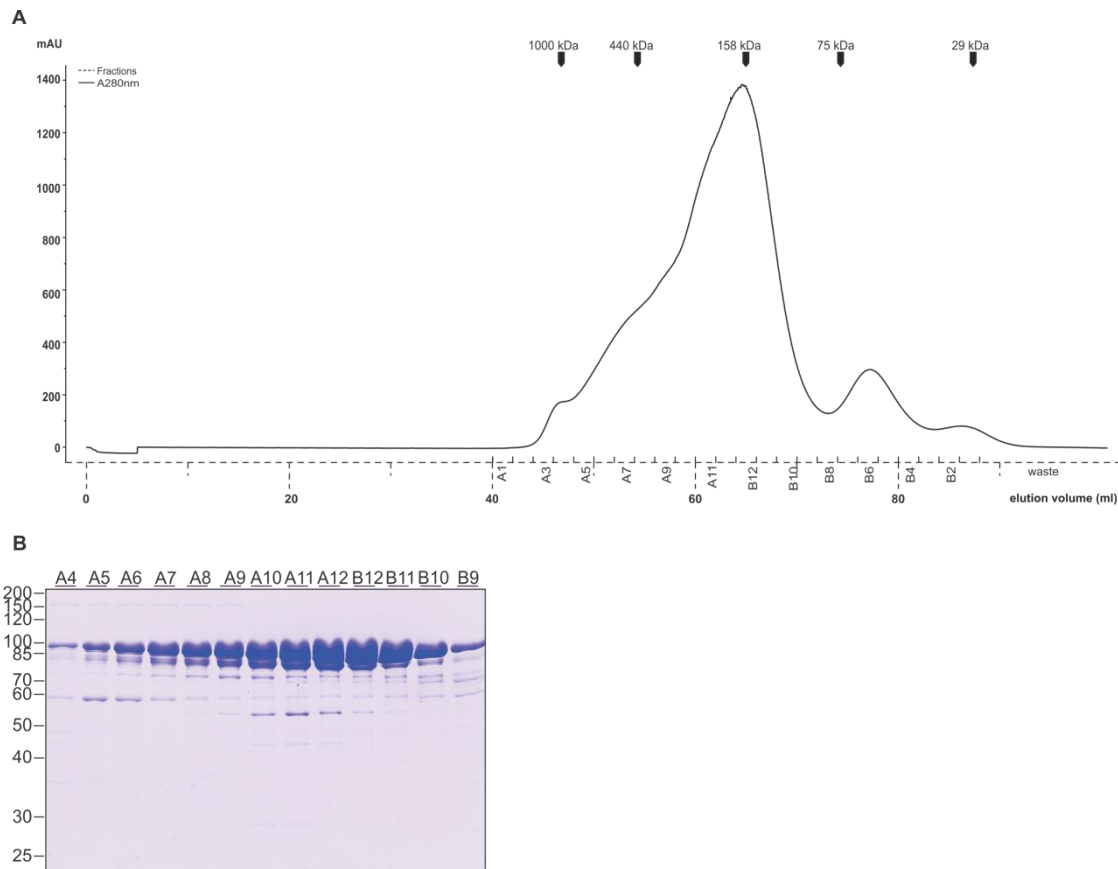


Figure 39 Size exclusion chromatography of MalE-TsaP_{MX}

(A) MalE-TsaP_{MX} eluted as a dimer from the SD200 gel filtration column. The protein was detected at 280 nm and is indicated by the solid line. (B) MalE-TsaP_{MX} was essentially pure as assayed by Coomassie staining of a 12 % SDS/PAGE of the purified protein. The labeling of the lanes corresponds to the labeling of the elution fractions shown in (C). The position of various markers for both the gel filtration and the SDS/PAGE are indicated.

4.4.5 Identification of protein-protein interaction between TsaP and PilQ

In order to determine whether TsaP directly interacts with PilQ via the B2 domain, TsaP Δ A33-R83 and PilQ(B1/B2) of *N. gonorrhoeae* as well as TsaP_{MX} and PilQ_{MX}(aa20-656) of *M. xanthus* were purified. PilQ(B1/B2), TsaP_{MX} and PilQ_{MX}(aa20-656) could be purified as stable dimers, where as TsaP Δ A33-R83 eluted at a volume corresponding to a monomer and a high molecular weight complex. As an alternative method to the BACTH system, size exclusion chromatography (SEC) of mixed proteins was used. TsaP Δ A33-R83 and PilQ(B1/B2) as well as TsaP_{MX} and PilQ_{MX}(aa20-656) were mixed and analyzed by SEC. Comparing the elution profile of the TsaP Δ A33-R83/PilQ mixture with the elution profiles of the single proteins, a peak at 7.5 ml appeared (see Figure 40). This peak elutes with an apparent molecular mass of >400 kDa. SEC analysis of the TsaP_{MX}-PilQ_{MX} complex showed that free TsaP and free PilQ_{MX}(aa20-656) elute as dimers with apparent molecular masses of 169 kDa and 140 kDa, respectively, which correspond well with the theoretical masses of 84,5 kDa and 70 kDa. Apparent TsaP-PilQ complexes elute at a molecular mass of >400 kDa, respectively (Figure 41).

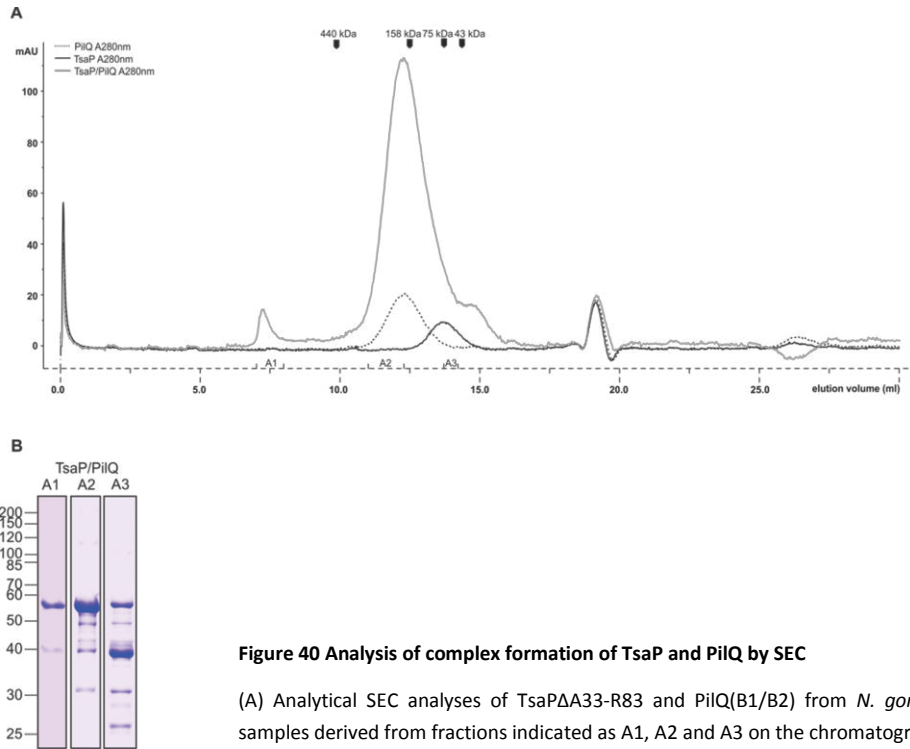


Figure 40 Analysis of complex formation of TsaP and PilQ by SEC

(A) Analytical SEC analyses of TsaP Δ A33-R83 and PilQ(B1/B2) from *N. gonorrhoeae*. (B) SDS-PAGE of samples derived from fractions indicated as A1, A2 and A3 on the chromatograms

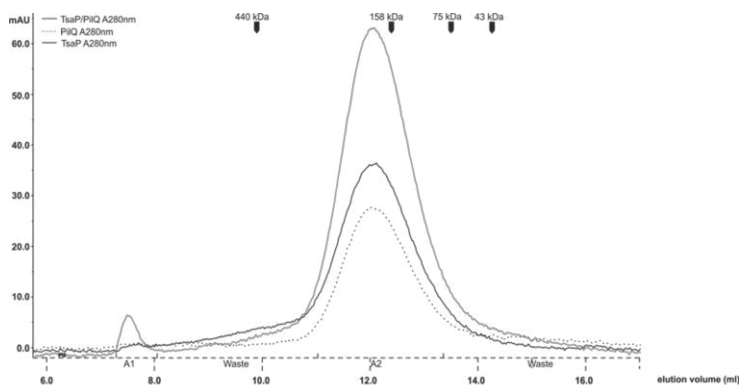
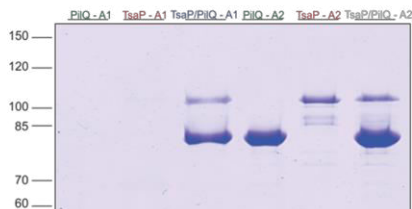


Figure 41 Analysis of complex formation of TsaP and PilQ by SEC

(A) Analytical SEC analyses of TsaP and PilQ(aa20-656) from *M. xanthus*. (B) SDS-PAGE of samples derived from fractions indicated as A1, A2 and A3 on the chromatograms



In order to obtain structural data relevant to understand the formation of the high molecular weight complex observed during TsaP Δ A33-R83 purification and in TsaP/PilQ interaction assay, EM was performed. Negatively staining of the A6 fraction of the size exclusion chromatography during TsaP Δ A33-R83 purification showed ring like particles (Figure 42A). Measurements showed that these

rings have a diameter of 19.6 ± 2.2 nm, similar to the peripheral ring of the secretin complex, seen in its native lipid environment. These data indicate that TsaP forms higher oligomers, which assemble into a ring that could form the peripheral ring structure around the PilQ secretin ring.

Analysis of the high molecular weight fraction of the interaction assay, using TsaP and PilQ of *N. gonorrhoeae*, showed neither formation of ring-like particles nor other complexes. In contrast, the high molecular weight fraction of the interaction assay, using the proteins of *Myxococcus*, showed a double ring structure (Figure 42B and Figure 42C). Measurements of this structure revealed that these rings have a diameter of 14.7 ± 1.4 nm and 18.3 ± 1.4 nm. Comparison of the double ring structure, seen in the high molecular weight fraction of the interaction assay, and the secretin complex structure of *N. gonorrhoeae* in its native lipid environment, revealed that the formed complexes have similar sizes. Because the PilQ_{MX}(aa20-656) construct does not only consist of the B1/B1 domain but also includes part of the N0 domain, lead to the suggestion that the B2 domain of the HA-PilQ(B1/B2)-CPD-His₁₀ might not be accessible for interacting with TsaP. However, these data indicate that the double ring structure formed by TsaP_{MX} and PilQ_{MX}(aa20-656), might be mediated via the interaction of TsaP and the B2 domain of PilQ.

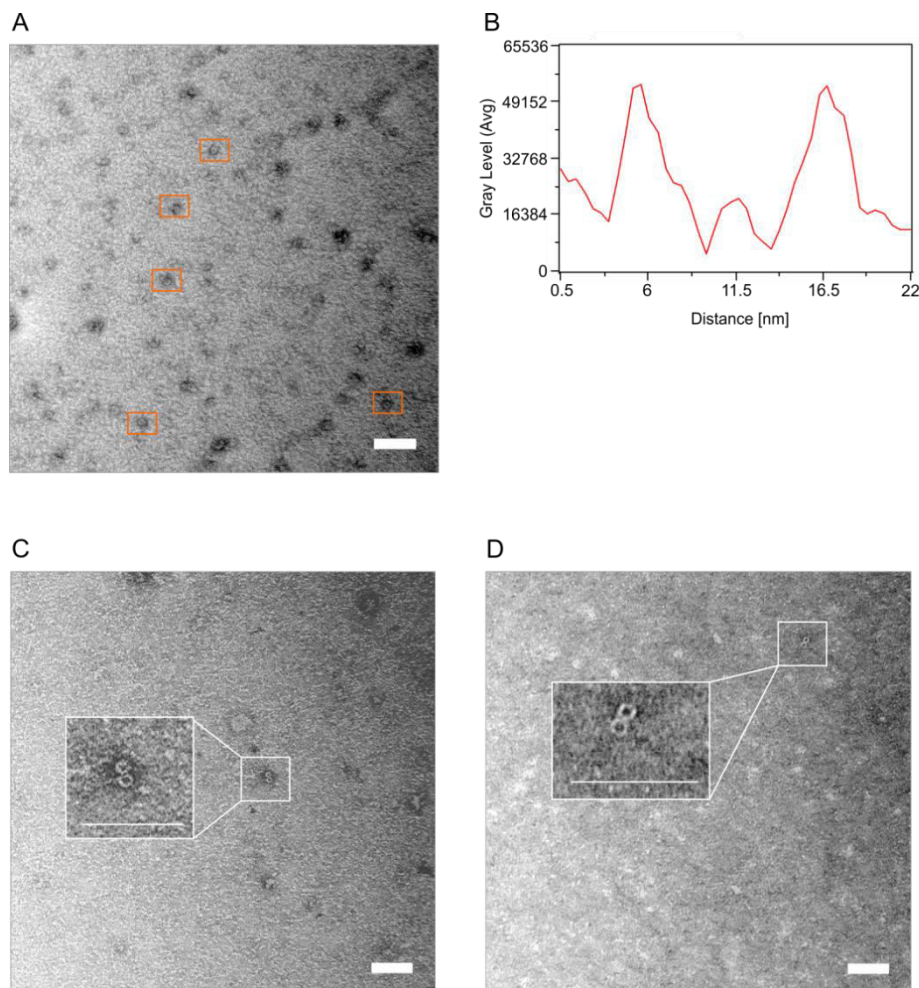


Figure 42 EM analysis of TsaP Δ A33-R83 and the high molecular weight complex of the TsaP/PilQ interaction assay

(A) Elution fractions of the TsaP Δ A33-R83 purification were applied to carbon coated copper grids and negatively stained with 2 % uranyl acetate. TsaP Δ A33-R83 particles are indicated by red boxes. The scale bar equals 100 nm. (B) Stain density across the diameter of a TsaP Δ A33-R83 particle. (C/D) High molecular weight elution fraction of the TsaP/PilQ interaction assay using TsaP_{MX} and PilQ_{MX}(aa20-656) of *M. xanthus*. [The EM analysis was performed together with A-L. Henche, MPI-Marburg]

5. Discussion

5.1 Analysis of the Gonococcal Genetic Island

Operons are the transcriptional unit in prokaryotes, allowing coordinated regulation of groups of genes that predominantly encode functionally linked proteins [206, 207]. To gain more insights of how genes of the type IV secretion system of *N. gonorrhoeae* are transcribed, transcriptional mapping was performed for genes essential for DNA secretion in *N. gonorrhoeae*.

Using this approach, we revealed that they are encoded within different operons. The first operon encoded by the relaxase *Tral*, the putative coupling protein *TraD* and the two hypothetical proteins *Yaf* and *Yaa* is transcribed divergently from the rest of the T4SS genes. Analysis of the expression levels of *tral* and *traD* revealed an increased transcription level of *traD* and *tral* in piliated *N. gonorrhoeae* strains, leading to the hypothesis that secretion might be regulated by the DNA processing genes encoded in this operon. The second (*ItgX-traF*) and third operon (*traH-yeh*) encode in total 22 proteins, including channel subunits, the energizing ATPase *TraC*, components of the pilus, which together are involved in the formation of the mating pair formation complex. The end region (*exp1-parA*) of the GGI encodes 36 open reading frames. Several of these genes encode proteins with homology to DNA processing and modifying proteins, however most genes encode for proteins with unknown function. However, the last operon (*parA-yfa*) within the GGI encodes the DNA partitioning proteins *ParA* and *ParB*. Downstream of this operon locates a repeated sequence, which may function as the centromer-like *parS* site, to which the partitioning protein *ParB* could bind. *ParB-ParS* binding and interaction of the nucleoprotein complex is important during DNA secretion, suggesting that these nucleoproteins may be involved in the recruitment to the secretion system as it was shown for *A. tumefaciens* [208]. The RT-PCR analysis additionally demonstrated that the *parA*, *parB*, *yfeB* and *yfb* genes are not encoded in the same operon, although they are often found genetically linked to *ssbB* [183]. In a next step, it was aimed to determine if the operon, containing the *ssbB*, *topB*, *yeh*, *yegB* and *yegA* genes is expressed, even though it is not essentially involved in T4SS dependent secretion. We next determined if the expression levels of the *ssbB* and *topB* genes might be influenced by the piliation state, like it was shown for *tral* and *traD*. The results, revealed no differences at the expression levels of the *ssbB* and *topB* genes between piliated and non-piliated cells. However, the expression level these two genes were significantly higher than the expression levels of *tral* and *traD*, indicating that the transcription of *ssbB* and *topB* is not regulated by the gonococcal piliation state. The exact role of this region remains to be elucidated.

To investigate if single stranded DNA that is secreted via the T4SS encoded within the GGI facilitates biofilm formation, biofilm formation of two different *N. gonorrhoeae* strains was examined by Dr. Maria Zweig. Strains initially used within this study were the *N. gonorrhoeae* MS11 WT strain and the MS11 Δ *traB* deletion strain. Biofilms were developed by growing cells of these two strains for 3 days in a continuous flow chamber system. Biofilm formation was imaged by Dr. Maria Zweig after 24, 48 and 72 hours. Quantification of biofilms showed that the deletion of *traB* affected biofilm formation. Complementation of the *traB* deletion by the WT *traB* gene demonstrated that the effects of the *traB* deletion on biofilm formation were indeed caused by the *traB* mutation, and were not the result of antigenic variation. A recent paper by Gloag *et al.* showed that eDNA is important in

coordinating bacterial movements during biofilm expansion of *P. aeruginosa* [209]. Since eDNA is important in coordinating bacterial movements, and the DNA secretion level is higher in piliated than in non-piliated *Neisseria* strains, suggests that T4P of *N. gonorrhoeae* bind the secreted ssDNA, which may serve as a signal for the formation of a complex network among cells, which is facilitated by the single stranded DNA, secreted via the T4SS.

5.2 The peptidoglycan-binding protein TsaP functions in surface assembly of type IV pili

Previous EM studies of PilQ in isolated membranes of *N. gonorrhoeae* showed that the native complex containing the PilQ secretin consists of an inner ring and an additional peripheral structure consisting of a peripheral ring with 14-fold symmetry and seven extending spikes [105]. Based on the structural similarity with purified PilQ of *N. meningitidis*, it was proposed that the inner ring is formed by PilQ and that the peripheral structure is formed by one or more unidentified proteins. In this study, we have identified TsaP, a 45.5 kDa protein with a signal sequence and an N-terminal LysM domain, as an essential component for the formation of the peripheral structure. TsaP was not found associated with solubilized and purified His₈-PilQ of *N. gonorrhoeae*; however, TsaP was, like PilQ, detected in isolated membranes and was difficult to solubilize and extract from these membranes by 7.5 M urea. Membrane integration or association of TsaP depended on the presence of PilQ, and the level of TsaP in isolated membranes was strongly reduced in a strain lacking PilQ. Comparison of the projection maps of native secretin complexes observed in OM sheets isolated from the WT and the $\Delta tsaP$ mutant showed that the peripheral structure was lost in the $\Delta tsaP$ mutant. Deletion of *tsaP* also resulted in loss of the colony morphology that corresponds to piliated cells. EM showed that T4P are still assembled in the $\Delta tsaP$ mutant, but are not displayed on the surface of cells. Rather, the assembled T4P are found in membrane protrusions. Importantly, the peripheral ring and the spikes around PilQ and the display of T4P on the cell surface were recovered in the $\Delta tsaP/tsaP^+$ complementation strain. The presence of TsaP homologs in different genomes is strongly linked to the occurrence of T4aP systems in these genomes. No TsaP homologs were identified in species that contain only a T2SS or a T4bPS. The strong link between the presence of TsaP and T4aPSs suggested that the TsaP homologs are also important for T4aP biogenesis in other species. Overall, the data demonstrate that the presence of TsaP is strongly linked to the presence of T4PSs and that TsaP is important for the surface assembly of T4aP in *N. gonorrhoeae*.

An important question remains whether the observed link between TsaP and PilQ is the result of a direct or indirect interaction. Several lines of evidences suggest that TsaP interacts directly with PilQ: (i) the peripheral ring around the inner PilQ secretin ring in OM sheets is lost in the *N. gonorrhoeae* $\Delta tsaP$ mutant (but not in the $\Delta pilC$, $\Delta pilW$, $\Delta pilP$, $\Delta pilE$, and $\Delta pilF$ mutants) and regained in the $\Delta tsaP/tsaP^+$ complementation strain; and (ii) TsaP associates with the OM of *N. gonorrhoeae* in a PilQ-dependent manner (but independent of PilC, PilW, PilP, and PilF). In addition to these indications Dr. Carmen Friedrich could show that, similar to *N. gonorrhoeae*, accumulation of the TsaP homolog in *M. xanthus* strongly depends on PilQ_{MX} and the pilotin Tgl, which is important for PilQ multimerization. These data indicate that TsaP_{MX} is specifically stabilized by PilQ_{MX} [175]. Furthermore, Dr. Carmen Friedrich could show the absence of TsaP_{MX} affects T4P-dependent motility; moreover localization of TsaP in *M. xanthus* specifically depends on PilQ and the pilotin Tgl,

but not the other proteins involved in T4P assembly and function (PilA_{MX}, PilB_{MX}, PilT_{MX}, PilC_{MX}, PilN_{MX}, PilO_{MX} or PilP_{MX}), indicating that TsaP specifically interacts with PilQ but not with any of the other tested T4P proteins [175]. Therefore, TsaP most likely directly interacts with PilQ.

Another important question is whether TsaP forms the peripheral ring or the spikes. We previously observed that in *N. meningitidis*, which also encodes a TsaP homolog, the spikes are absent [105], and the spikes were also not observed in images obtained from membranes of the *N. gonorrhoeae* $\Delta pilP$ and $\Delta pilF$ strains. The membranes of these strains, however, contain similar levels of TsaP as the WT. Because loss of the peripheral ring was only observed in the $\Delta tsaP$ mutant, we suggest that TsaP forms, or is part of, the peripheral ring. Derrick and coworkers recently solved the structures of the B2 and N0N1 domains of PilQ of *N. meningitidis* and modeled these structures on their 3D structure of full-length PilQ obtained by cryo-EM [150]. They also showed that the periplasmic domain of the IM lipoprotein PilP interacts with the N0 domain and identified a highly conserved patch on the B2 domain that could form a binding site for a T4PS protein [150]. The B2 domain is found in secretins of T4aPSs but not in secretins of T4bPSs or T2SSs. Because TsaP co-occurs with T4aP but not with secretins of T4bPSs or T2SSs, TsaP might bind to this conserved patch on the B2 domain. We propose that TsaP interacts directly with PilQ and is part of the peripheral structure of the secretin complex in *N. gonorrhoeae* and, based on the widespread occurrence of TsaP in genomes of organisms containing T4aPSs, that this peripheral structure is also formed in other organisms.

TsaP homologs contain a conserved N-terminal LysM domain. LysM domains bind PG and, in combination with a hydrolyzing domain (e.g., muramidase, glucosaminidase, or endopeptidase domain), can function in PG hydrolysis [158]; however, the LysM domain is not thought to be enzymatically active in PG hydrolysis. Bioinformatics analyses did not identify a PG hydrolyzing domain in TsaP. Consistently, we observed that purified TsaP binds to PG but we have not observed any PG hydrolysis. This suggests that TsaP is a PG-binding protein and functions in anchoring the secretin complex to the PG via the LysM domain. Phylogenomic analyses showed that the presence of the *tsaP* gene in a genome is strongly linked to the presence of genes for T4aP systems. A main functional difference between T4aPSs and T4bPSs and T2SSs is that T4aP retracts and generates high forces [210, 211]. To our knowledge, nothing is known about extension and possible retraction rates and forces for T4bPSs and T2SSs, but these rates and forces may well be much lower than observed for T4aPSs. Thus, TsaP might only be required for T4aPSs where higher rates of extension and retraction result in greater forces. Recently, FimV, a LysM domain containing protein of *P. aeruginosa*, was also shown to be involved in T4P assembly [155, 156]. FimV is a 919 aa IM protein with an N-terminal LysM domain, a transmembrane domain, and an unusually acidic C-terminal domain with tetratricopeptide repeats. Lack of FimV results in impaired T4P assembly, reduced levels of PilQ multimer formation, and lower levels of the PilMNOP proteins [156]. Similar to TsaP, the presence of FimV homologs in bacterial genomes is related to the presence of a T4PS. The *N. gonorrhoeae* $\Delta tsaP$ mutant displays membrane protrusions that are filled with multiple T4P. Similar membrane protrusions have been described for a $\Delta pilQ/\Delta pilT$ strain of *N. gonorrhoeae* [200]. These protrusions were only observed in the $\Delta pilQ/\Delta pilT$ double mutant, but not in the $\Delta pilQ$ mutant [200]. Koomey and coworkers [200] proposed that in the $\Delta pilQ$ mutant, depolymerization exceeds polymerization of pilin subunits, whereas in the $\Delta pilQ/\Delta pilT$ double mutant, polymerization exceeds

depolymerization. Because the membrane protrusions are observed in the $\Delta tsaP$ mutant even in the presence of PilT, pilin polymerization seems, contrary to the $\Delta pilQ$ mutant, not to be affected in the $\Delta tsaP$ mutant. Based on these comparisons, we speculate that the T4P-filled membrane protrusions formed in the absence of TsaP are either caused by (i) T4P that are stuck in the secretin ring and then push against the OM, resulting in the membrane protrusions, or (ii) misalignment of the IM/periplasmic and OM parts of the T4PS, resulting in the assembled T4P pushing against the OM. In both scenarios, the primary defect is likely caused by the lack of secretin attachment to the PG. We have previously shown that the PilQ secretin of *N. gonorrhoeae* interacts with other proteins in the OM to form a large multidomain complex. Here, we identified TsaP as a likely member of this complex and show that the occurrence of TsaP in bacterial genomes is strongly linked to the presence of T4aPSs. TsaP plays an important role in pilus biogenesis in the β -proteobacterium *N. gonorrhoeae*. TsaP most likely functions in anchoring the secretin to the PG to enable the secretin to withstand the forces during pilus extension and retraction. TsaP might also function in aligning the IM and OM components of the T4PS. T4P play an important role in the pathogenesis of many bacteria. Because TsaP is found in all bacteria that express T4aP and plays an important role in T4aP biogenesis, it might be an important future drug target.

5.3 Analysis of TsaP domains and their function

Previous experiments revealed that a conserved protein, named TsaP, forms this peripheral ring structure or at least is part of it. *In silico* analysis revealed that TsaP contains an N-terminal LysM domain and two β -sheet rich domains that are separated by a linker region, only found in *Neisseria spp.* The two β -sheet rich domains show 18 % and 15 % sequence identity to the C-terminal domain of FlgT of *Vibrio spp.*, respectively. FlgT was shown to be a periplasmic protein, whose C-terminus is made of seven β -strands forming a core β -barrel structure [203]. Studies by Martinez *et al.* and Terashima *et al.* could show that FlgT forms the H-ring of the flagella system of *Vibrio spp.*, which is involved in basal body formation [201, 202]. Since the flagella motor of *Vibrio alginolyticus* can achieve remarkably fast rotation and *flgT* deletion mutants release assembled flagella into the supernatant, FlgT might be required to hold the flagella base on the cell surface and function as a scaffold to form the T ring [201, 202]. Since it is suggested that FlgT might reinforce robustness of the complex and thereby protect it against physical breaking of the basal body, it is suggested that TsaP might perform a similar function as FlgT in the flagella system. Additional *in silico* analysis showed that FlgT of *Vibrio spp.* and the FlgT-like domains of TsaP structurally resemble the N-terminal domain of the F₁ α/β -subunit and FliI. Since these proteins form a ring structure through the tight interaction between the tandem wise arranged, β -barrel domains by forming inter-subunit β -sheets we hypothesize that TsaP molecules assemble around the secretin structure, forming the peripheral structure, which may be stabilized by a similar interaction through the two FlgT-like domains. Sequence alignment revealed that the two FlgT-like domains are separated by a linker region which is only present in *Neisseria spp.* Taking into consideration that PilQ of *Neisseria spp.* contains a small basic repeat region that is not found in other secretins [212], this region might interact with this linker region or is involved in spanning the linker region. In order to investigate the role of each domain, an in-frame chromosomal deletion of the linker region (*tsaP* Δ S213-V245) was constructed. In addition, it was aimed to generate a markerless *tsaP* Δ lysM (*tsaP* Δ A33-E83) mutant. However, no *tsaP* Δ A33-E83 mutation could be confirmed. Therefore, we hypothesized that the

deletion of the LysM domain would result in a full assembled T4P system whose secretin is not anchored to the peptidoglycan layer, if the LysM domain is involved in anchoring the secretin. If the system with special focus on the secretin complex is not anchored to the peptidoglycan layer, the high forces that are generated during assembly and retraction of the pilus fibers with approximately 1.500 pilin subunits per second [84] might result in partial tearing of the complex from the membrane, which would lead to death of the cell. To test this hypothesis, it was aimed to complement the $\Delta tsaP$ strain by an ectopic insertion of a copy of $tsaP\Delta A33-R83$ under the control of the *lac* promoter ($\Delta tsaP/tsap\Delta A33-R83^+$), as this construct also includes a resistance marker which would simplify the screening. Even though the screening showed several colonies with chromosomal integration of the $tsap\Delta A33-R83^+$ construct, immunoblot analysis revealed that in 90 % of the colonies, the $tsap\Delta A33-R83^+$ construct integrated into the original loci that result in full length *tsaP*. However, one of the screened colonies revealed that in one case the $tsap\Delta A33-R83$ construct integrated into the chromosomal complementation site between *aspC* and *lctP*. Mutational analysis of the LysM domain and the linker region revealed that only deletion of the linker region resulted in the loss of the colony morphology that corresponds to piliated cells. EM showed that no T4P are assembled in the $tsaP\Delta S213-V245$ mutant. In contrast, the $\Delta tsaP/tsap\Delta A33-R83^+$ mutant can form surface assembled T4P and additionally T4P filled membrane protrusions as observed for the $\Delta tsaP$ background strain. Comparison of the projection maps of native secretin complexes observed in OM sheets isolated from the WT, the $tsaP\Delta A33-E83$ strain, and $\Delta tsaP/tsap\Delta A33-R83^+$ strain showed that the peripheral structure was lost in the $tsaP\Delta S213-V245$ mutant. Importantly, the peripheral ring and the spikes around PilQ and the display of T4P on the cell surface were recovered in the $tsaP\Delta A33-E83/tsaP^+$ complementation strain. Since *Neisseria spp.* show high recombination rates of chromosomal regions, it cannot be excluded that the results seen for the $\Delta tsaP/tsap\Delta A33-R83^+$ strain are caused by re-recombination of the $tsap\Delta A33-R83^+$ construct into the original loci of the $\Delta tsaP$ strain. To exclude this possibility, immunoblot analysis of piliated $\Delta tsaP/tsap\Delta A33-R83^+$ are required.

We proposed that TsaP anchors the secretin to the PG and enables the secretin to withstand the forces generated during pilus extension and retraction. Here, we identified that TsaP contains apart from the LysM domain, two FlgT-like domains and a linker region, which is specific for *Neisseria spp.* We could show that the linker domain plays an important role in pilus biogenesis in the β -proteobacterium *N. gonorrhoeae*. If the FlgT-like domains would lead to a tight interaction between the tandemly arranged β -barrel domains by forming inter-subunit β -sheets, TsaP could form a ring like structure, surrounding the PilQ secretin complex. If the FlgT-domains are important for subunit-subunit interaction by forming inter-subunit β -sheets, the deletion of the linker region could lead to hindered inter-subunit formation and by this disable the ring formation by TsaP.

5.4 Interaction of TsaP with other components of the type IV pili system

The process of type IV pili assembly is complicated: it requires the cooperative action of a group of proteins that span both the inner and outer membranes in bacteria. Previously we could identify a protein, which we named TsaP, whose localization, membrane integration and/or stability is PilQ dependent. In addition, we hypothesize that TsaP forms a ring structure, by inter-subunit formation of the β -sheets that are present in the FlgT-like domains, around PilQ. In September 2012, Berry

et al. identified a highly conserved patch of PilQ, named B2, which might form a binding site to another unidentified T4P biogenesis protein [150]. To investigate if TsaP would bind to the highly conserved patch of the B2 domain of PilQ, fragments of TsaP and PilQ were tested for interaction *in vivo* using the bacterial adenylate cyclase two-hybrid system and were heterologously overexpressed and purified. Since this system is limited by the cytoplasmic cAMP production, the used TsaP and PilQ fragments lack the signal sequence. Since the PilQ fragment fusions were apparently and for an unknown reason toxic, this assay only showed that TsaP might self-interact.

In order to test for protein-protein interaction between PilQ and TsaP, we heterologously express and purify PilQ as well as a truncated version of TsaP, since the LysM domain might affect interaction between the two proteins. As we suggest that TsaP interacts with the recently identified B2 domain of PilQ, we adopted a cloning and expression strategy where HA-PilQ(B1/B2)-CPD-His₁₀ and His₁₀-TsaPΔA33-R83 were overproduced. Overexpression of HA-PilQ(B1/B2)-CPD-His₁₀ results in the formation of large amounts of soluble protein in *E. coli* BL21 star. Analyzing the purified protein by size exclusion chromatography revealed that the B1/B2 domain of PilQ of *Neisseria gonorrhoeae* forms stable homodimers, which is in agreement with the dimerization of the PilQ NON1 domains of *N. meningitidis* [150] and the secretin XcpQ of the T2SS of *P. aeruginosa* [213]. Overexpression of His₁₀-TsaPΔA33-R83 results in the formation of large amounts of soluble protein in *E. coli* BL21 star. SDS/PAGE analysis of the fraction obtained after Ni²⁺-affinity chromatography and size exclusion chromatography revealed a SDS-stable protein complex that just entered the running gel, apart from a protein band corresponding to the calculated size of 37 kDa. This migration behavior on SDS/PAGE has been observed previously only for large stable complexes. As this SDS-stable complex elutes in the void volume of the Superdex 200 HiLoad 16/60 column, no difference can be seen between a high molecular weight complex and aggregated protein. To differentiate between these two possibilities and to analyze the oligomerization state of purified His₁₀-TsaPΔA33-R83, different fractions after the size exclusion chromatography were analyzed by BN/PAGE. Correlation of the relative mobility of the analyzed protein fractions with a protein standard composed of eight proteins revealed that His₁₀-TsaPΔA33-R83 forms different quaternary structures. Importantly, MS analysis demonstrated that all oligomeric structures are solely formed by His₁₀-TsaPΔA33-R83, indicating that the purified protein forms the SDS-stable complex, excluding the possibility of contamination. Remarkably, the quaternary structures identified by BN/PAGE also revealed a nonadecamer of His₁₀-TsaPΔA33-R83. This is in contrast to the 14-fold symmetry of the peripheral structure detected in its native lipid environment [105]. However, mutational analysis of components of the T4P system followed by analysis of the secretin structure in its native lipid environment showed that the number of protein copies in the peripheral ring increase from 14 to 19 in *pilP* and *pilE* mutants [105], leading to the suggestion that the symmetry of this protein depends on components of the membrane platform formed by PilM/PilN/PilO/PilP. Recently, Karupiah *et al.* could show that after formation of a complex consisting of PilM/PilN/PilO, this complex is capable of binding the major pilin subunit, resulting in a T-shaped complex [148]. Overall, the deletion of parts of this complex leads to changes in symmetry [144]; while the stability of these proteins depends on each other [105]. Therefore, the connection between the secretin in the outer membrane and components in the inner membrane is disturbed as soon as one component is missing. If the interaction of PilQ to the membrane platform complex is lost, TsaP can arrange and interact with PilQ in a different way. If more components are required to receive a 14-fold symmetry, the

nodadecamer seen in BN/PAGE analysis can be explained by lack of these components. EM analysis of the fractions containing the high molecular weight complex revealed a ring-like structure with a diameter of 19.6 ± 2.2 nm, similar to the peripheral ring of the secretin complex, observed in its native lipid environment. These data indicate that TsaP assembles into higher oligomers, forming a ring that may become the peripheral ring structure around the PilQ secretin ring.

In order to determine if TsaP directly interacts with PilQ via the B2 domain, TsaP Δ A33-R83 and PilQ(B1/B2) of *N. gonorrhoeae* as well as TsaP_{MX} and PilQ_{MX}(aa20-656) of *M. xanthus* were purified. Overexpression of His₆-PilQ_{MX}(aa20-656) and MalE-TsaP_{MX} leads to the formation of large amounts of soluble protein. Analysis of the purified proteins by size exclusion chromatography revealed that both proteins of *M. xanthus* form stable homodimers. As an alternative method to the BACTH system, size exclusion chromatography (SEC) of mixed proteins was used. For this, either TsaP Δ A33-R83 and PilQ(B1/B2) or TsaP_{MX} and PilQ_{MX}(aa20-656) were mixed and analyzed by SEC. The elution profile of the TsaP Δ A33-R83/PilQ or TsaP_{MX}/PilQ_{MX}(aa20-656) mixture revealed the formation of a high molecular weight complex eluting at approximately 7.5 ml, compared to the profile of the individual proteins. It is worth noting, that variation of TsaP:PilQ(aa20-656) ratios leads to the suggestion that the height and with this the amount of the high molecular weight complex detected by SEC might be PilQ dependent. EM analysis of these high molecular weight fractions of the interaction assay, revealed that only TsaP_{MX}/PilQ_{MX}(aa20-656) form a double ring structure, with a diameter of 14.7 ± 1.4 nm and 18.3 ± 1.4 nm. This double ring structure exhibits similar sizes compared with the secretin complex structure of *N. gonorrhoeae* in its native lipid environment. The fact that the PilQ_{MX}(aa20-656) construct does not only consist of the B1/B2 domain but also contains part of the N0 domain, leads to the suggestion that the B2 domain of the HA-PilQ(B1/B2)-CPD-His₁₀ might not be accessible for TsaP to interact with. However, these data indicate that the secretin complexes of *N. gonorrhoeae* and *M. xanthus* are formed by PilQ and TsaP, whose interaction might be dependent of the B2 domain of PilQ.

5.5. Conclusion

In conclusion, the major part of this work describes the discovery of TsaP, a protein that functions in surface assembly of T4P. T4P are well studied, ubiquitous and versatile bacterial cell surface structures found in many bacteria, and involved in different processes like adhesion to host cells, biofilm formation, motility and DNA uptake. T4P play an important role in the pathogenesis of many bacteria. TsaP was identified as a protein that interacts with the secretin, most likely via the B2-domain of PilQ and show that the presence of homologs of TsaP in bacterial genomes is strictly linked to the presence of genes involved in T4P assembly, and functionally characterized TsaP in the β -proteobacterium *Neisseria gonorrhoeae*. Our results show that TsaP is a peptidoglycan binding outer membrane bound protein that is involved in the surface assembly of T4P. Protein purification revealed that TsaP forms SDS-stable ring structures with the size similar to the peripheral ring of the secretin complex. Interaction assays using heterologous overexpressed proteins of *N. gonorrhoeae* and *M. xanthus* suggested a possible interaction of these proteins. Whether this interaction is mediated via the B2 domain of PilQ remains to be elucidated. Because we propose that TsaP is a novel ubiquitous protein that functions to anchor the secretin complex to the peptidoglycan and in

that way aligns the secretin to inner membrane components, TsaP might be an important future drug target.

6. Literature

1. Ligon, B.L., *Albert Ludwig Sigismund Neisser: discoverer of the cause of gonorrhoea*. Semin Pediatr Infect Dis, 2005. 16(4): p. 336-41.
 2. Morse, S.A., *The biology of the gonococcus*. CRC Crit Rev Microbiol, 1978. 7(2): p. 93-189.
 3. Merz, A.J. and M. So, *Interactions of pathogenic neisseriae with epithelial cell membranes*. Annu Rev Cell Dev Biol, 2000. 16: p. 423-57.
 4. Organization, W.H., *Global action plan to control the spread and impact of antimicrobial resistance in Neisseria gonorrhoeae*. 2013.
 5. Post, D.M., et al., *Biochemical and functional characterization of membrane blebs purified from Neisseria meningitidis serogroup B*. J Biol Chem, 2005. 280(46): p. 38383-94.
 6. Connell, T.D., D. Shaffer, and J.G. Cannon, *Characterization of the repertoire of hypervariable regions in the Protein II (opa) gene family of Neisseria gonorrhoeae*. Mol Microbiol, 1990. 4(3): p. 439-49.
 7. Dempsey, J.A., et al., *Physical map of the chromosome of Neisseria gonorrhoeae FA1090 with locations of genetic markers, including opa and pil genes*. J Bacteriol, 1991. 173(17): p. 5476-86.
 8. Stern, A., et al., *Opacity genes in Neisseria gonorrhoeae: control of phase and antigenic variation*. Cell, 1986. 47(1): p. 61-71.
 9. Ward, M.J., P.R. Lambden, and J.E. Heckels, *Sequence analysis and relationships between meningococcal class 3 serotype proteins and other porins from pathogenic and non-pathogenic Neisseria species*. FEMS Microbiol Lett, 1992. 73(3): p. 283-9.
 10. Suker, J., I.M. Feavers, and M.C. Maiden, *Structural analysis of the variation in the major outer membrane proteins of Neisseria meningitidis and related species*. Biochem Soc Trans, 1993. 21(2): p. 304-6.
 11. Griffiss, J.M., et al., *Lipooligosaccharides: the principal glycolipids of the neisserial outer membrane*. Rev Infect Dis, 1988. 10 Suppl 2: p. S287-95.
 12. Dehio, C., S.D. Gray-Owen, and T.F. Meyer, *Host cell invasion by pathogenic Neisseriae*. Subcell Biochem, 2000. 33: p. 61-96.
 13. Elkins, C., et al., *Species-specific uptake of DNA by gonococci is mediated by a 10-base-pair sequence*. J Bacteriol, 1991. 173(12): p. 3911-3.
 14. Duffin, P.M. and H.S. Seifert, *DNA uptake sequence-mediated enhancement of transformation in Neisseria gonorrhoeae is strain dependent*. J Bacteriol, 2010. 192(17): p. 4436-44.
 15. Goodman, S.D. and J.J. Scocca, *Factors influencing the specific interaction of Neisseria gonorrhoeae with transforming DNA*. J Bacteriol, 1991. 173(18): p. 5921-3.
-

16. Hamilton, H.L., K.J. Schwartz, and J.P. Dillard, *Insertion-duplication mutagenesis of neisseria: use in characterization of DNA transfer genes in the gonococcal genetic island*. J Bacteriol, 2001. 183(16): p. 4718-26.
 17. Dillard, J.P. and H.S. Seifert, *A variable genetic island specific for Neisseria gonorrhoeae is involved in providing DNA for natural transformation and is found more often in disseminated infection isolates*. Mol Microbiol, 2001. 41(1): p. 263-77.
 18. Hamilton, H.L., et al., *Neisseria gonorrhoeae secretes chromosomal DNA via a novel type IV secretion system*. Mol Microbiol, 2005. 55(6): p. 1704-21.
 19. Fronzes, R., P.J. Christie, and G. Waksman, *The structural biology of type IV secretion systems*. Nat Rev Microbiol, 2009. 7(10): p. 703-14.
 20. d'Enfert, C., C. Chapon, and A.P. Pugsley, *Export and secretion of the lipoprotein pullulanase by Klebsiella pneumoniae*. Mol Microbiol, 1987. 1(1): p. 107-16.
 21. Voulhoux, R., et al., *Involvement of the twin-arginine translocation system in protein secretion via the type II pathway*. EMBO J, 2001. 20(23): p. 6735-41.
 22. Veenendaal, A.K., C. van der Does, and A.J. Driessen, *The protein-conducting channel SecYEG*. Biochim Biophys Acta, 2004. 1694(1-3): p. 81-95.
 23. Johnson, S., et al., *Expression, limited proteolysis and preliminary crystallographic analysis of IpaD, a component of the Shigella flexneri type III secretion system*. Acta Crystallogr Sect F Struct Biol Cryst Commun, 2006. 62(Pt 9): p. 865-8.
 24. Filloux, A., *The underlying mechanisms of type II protein secretion*. Biochim Biophys Acta, 2004. 1694(1-3): p. 163-79.
 25. Nunn, D.N. and S. Lory, *Components of the protein-excretion apparatus of Pseudomonas aeruginosa are processed by the type IV prepilin peptidase*. Proc Natl Acad Sci U S A, 1992. 89(1): p. 47-51.
 26. Cisneros, D.A., G. Pehau-Arnaudet, and O. Francetic, *Heterologous assembly of type IV pili by a type II secretion system reveals the role of minor pilins in assembly initiation*. Mol Microbiol, 2012. 86(4): p. 805-18.
 27. Cisneros, D.A., et al., *Minor pseudopilin self-assembly primes type II secretion pseudopilus elongation*. EMBO J, 2012. 31(4): p. 1041-53.
 28. Hardie, K.R., et al., *The secretin-specific, chaperone-like protein of the general secretory pathway: separation of proteolytic protection and piloting functions*. Mol Microbiol, 1996. 22(5): p. 967-76.
 29. Shevchik, V.E., J. Robert-Baudouy, and G. Condemine, *Specific interaction between OutD, an Erwinia chrysanthemi outer membrane protein of the general secretory pathway, and secreted proteins*. EMBO J, 1997. 16(11): p. 3007-16.
 30. Lu, C., et al., *Hexamers of the type II secretion ATPase GspE from Vibrio cholerae with increased ATPase activity*. Structure, 2013. 21(9): p. 1707-17.
-

31. Shiue, S.J., et al., *XpsE oligomerization triggered by ATP binding, not hydrolysis, leads to its association with XpsL*. EMBO J, 2006. 25(7): p. 1426-35.
 32. Py, B., L. Loiseau, and F. Barras, *An inner membrane platform in the type II secretion machinery of Gram-negative bacteria*. EMBO Rep, 2001. 2(3): p. 244-8.
 33. Abendroth, J., et al., *The X-ray structure of the type II secretion system complex formed by the N-terminal domain of EpsE and the cytoplasmic domain of EpsL of Vibrio cholerae*. J Mol Biol, 2005. 348(4): p. 845-55.
 34. Sandkvist, M., et al., *Interaction between the autokinase EpsE and EpsL in the cytoplasmic membrane is required for extracellular secretion in Vibrio cholerae*. EMBO J, 1995. 14(8): p. 1664-73.
 35. Cascales, E. and P.J. Christie, *The versatile bacterial type IV secretion systems*. Nat Rev Microbiol, 2003. 1(2): p. 137-49.
 36. de la Cruz, F., et al., *Conjugative DNA metabolism in Gram-negative bacteria*. FEMS Microbiol Rev, 2010. 34(1): p. 18-40.
 37. Lawley, T.D., et al., *F factor conjugation is a true type IV secretion system*. FEMS Microbiol Lett, 2003. 224(1): p. 1-15.
 38. Woodall, C.A., *DNA transfer by bacterial conjugation*. Methods Mol Biol, 2003. 235: p. 61-5.
 39. Zhu, J., et al., *The bases of crown gall tumorigenesis*. J Bacteriol, 2000. 182(14): p. 3885-95.
 40. Segal, G. and H.A. Shuman, *How is the intracellular fate of the Legionella pneumophila phagosome determined?* Trends Microbiol, 1998. 6(7): p. 253-5.
 41. Vogel, J.P., et al., *Conjugative transfer by the virulence system of Legionella pneumophila*. Science, 1998. 279(5352): p. 873-6.
 42. Hofreuter, D., S. Odenbreit, and R. Haas, *Natural transformation competence in Helicobacter pylori is mediated by the basic components of a type IV secretion system*. Mol Microbiol, 2001. 41(2): p. 379-91.
 43. Weiss, A.A., F.D. Johnson, and D.L. Burns, *Molecular characterization of an operon required for pertussis toxin secretion*. Proc Natl Acad Sci U S A, 1993. 90(7): p. 2970-4.
 44. Frost, L.S., et al., *Mobile genetic elements: the agents of open source evolution*. Nat Rev Microbiol, 2005. 3(9): p. 722-32.
 45. Gomis-Ruth, F.X., et al., *The bacterial conjugation protein TrwB resembles ring helicases and F1-ATPase*. Nature, 2001. 409(6820): p. 637-41.
 46. Guglielmini, J., et al., *The repertoire of ICE in prokaryotes underscores the unity, diversity, and ubiquity of conjugation*. PLoS Genet, 2011. 7(8): p. e1002222.
 47. Guglielmini, J., F. de la Cruz, and E.P. Rocha, *Evolution of conjugation and type IV secretion systems*. Mol Biol Evol, 2013. 30(2): p. 315-31.
 48. Cascales, E. and P.J. Christie, *Definition of a bacterial type IV secretion pathway for a DNA substrate*. Science, 2004. 304(5674): p. 1170-3.
-

49. Bhattya, M., J.A. Laverde Gomez, and P.J. Christie, *The expanding bacterial type IV secretion lexicon*. Res Microbiol, 2013. 164(6): p. 620-39.
 50. Fronzes, R., et al., *Structure of a type IV secretion system core complex*. Science, 2009. 323(5911): p. 266-8.
 51. Chandran, V., et al., *Structure of the outer membrane complex of a type IV secretion system*. Nature, 2009. 462(7276): p. 1011-5.
 52. Rivera-Calzada, A., et al., *Structure of a bacterial type IV secretion core complex at subnanometre resolution*. EMBO J, 2013. 32(8): p. 1195-204.
 53. Low, H.H., et al., *Structure of a type IV secretion system*. Nature, 2014. 508(7497): p. 550-3.
 54. Trokter, M., et al., *Recent advances in the structural and molecular biology of type IV secretion systems*. Curr Opin Struct Biol, 2014. 27C: p. 16-23.
 55. Pena, A., et al., *The hexameric structure of a conjugative VirB4 protein ATPase provides new insights for a functional and phylogenetic relationship with DNA translocases*. J Biol Chem, 2012. 287(47): p. 39925-32.
 56. Arechaga, I., et al., *ATPase activity and oligomeric state of TrwK, the VirB4 homologue of the plasmid R388 type IV secretion system*. J Bacteriol, 2008. 190(15): p. 5472-9.
 57. Wallden, K., et al., *Structure of the VirB4 ATPase, alone and bound to the core complex of a type IV secretion system*. Proc Natl Acad Sci U S A, 2012. 109(28): p. 11348-53.
 58. Hare, S., et al., *Identification, structure and mode of action of a new regulator of the Helicobacter pylori HP0525 ATPase*. EMBO J, 2007. 26(23): p. 4926-34.
 59. Hare, S., et al., *A large domain swap in the VirB11 ATPase of Brucella suis leaves the hexameric assembly intact*. J Mol Biol, 2006. 360(1): p. 56-66.
 60. Hoppner, C., et al., *VirB1 orthologs from Brucella suis and pKM101 complement defects of the lytic transglycosylase required for efficient type IV secretion from Agrobacterium tumefaciens*. J Bacteriol, 2004. 186(5): p. 1415-22.
 61. Berger, B.R. and P.J. Christie, *Genetic complementation analysis of the Agrobacterium tumefaciens virB operon: virB2 through virB11 are essential virulence genes*. J Bacteriol, 1994. 176(12): p. 3646-60.
 62. Paranchych, W. and L.S. Frost, *The physiology and biochemistry of pili*. Adv Microb Physiol, 1988. 29: p. 53-114.
 63. Clarke, M., et al., *F-pili dynamics by live-cell imaging*. Proc Natl Acad Sci U S A, 2008. 105(46): p. 17978-81.
 64. Jakubowski, S.J., V. Krishnamoorthy, and P.J. Christie, *Agrobacterium tumefaciens VirB6 protein participates in formation of VirB7 and VirB9 complexes required for type IV secretion*. J Bacteriol, 2003. 185(9): p. 2867-78.
 65. Sagulenko, E., et al., *Role of Agrobacterium VirB11 ATPase in T-pilus assembly and substrate selection*. J Bacteriol, 2001. 183(20): p. 5813-25.
-

66. Bradley, D.E., *Morphological and serological relationships of conjugative pili*. Plasmid, 1980. 4(2): p. 155-69.
 67. Moore, D., et al., *The Escherichia coli K-12 F plasmid gene traX is required for acetylation of F pilin*. J Bacteriol, 1993. 175(5): p. 1375-83.
 68. Eisenbrandt, R., et al., *Conjugative pili of IncP plasmids, and the Ti plasmid T pilus are composed of cyclic subunits*. J Biol Chem, 1999. 274(32): p. 22548-55.
 69. Eisenbrandt, R., et al., *Maturation of IncP pilin precursors resembles the catalytic Dyad-like mechanism of leader peptidases*. J Bacteriol, 2000. 182(23): p. 6751-61.
 70. Lai, E.M., et al., *Biogenesis of T pili in Agrobacterium tumefaciens requires precise VirB2 propilin cleavage and cyclization*. J Bacteriol, 2002. 184(1): p. 327-30.
 71. Dominguez, N.M., K.T. Hackett, and J.P. Dillard, *XerCD-mediated site-specific recombination leads to loss of the 57-kilobase gonococcal genetic island*. J Bacteriol, 2011. 193(2): p. 377-88.
 72. Salgado-Pabon, W., et al., *A novel relaxase homologue is involved in chromosomal DNA processing for type IV secretion in Neisseria gonorrhoeae*. Mol Microbiol, 2007. 66(4): p. 930-47.
 73. Salgado-Pabon, W., et al., *Increased Expression of the Type IV Secretion System in Piliated Neisseria gonorrhoeae Variants*. Journal of Bacteriology, 2010. 192(7): p. 1912-1920.
 74. Emilia Pachulec, K.S., Tobias Bender, Eva-Maria Heller, Wilmara Salgado-Pabon, Shelly K. Schmoller, Katelynn L. Woodhams, Joseph P. Dillard and Chris van der Does, *Functional analysis of the Gonococcal Genetic Island of Neisseria Gonorrhoeae* submitted to PLoS One, 2014.
 75. Ramsey, M.E., K.L. Woodhams, and J.P. Dillard, *The Gonococcal Genetic Island and Type IV Secretion in the Pathogenic Neisseria*. Front Microbiol, 2011. 2: p. 61.
 76. Zola, T.A., et al., *Type IV secretion machinery promotes ton-independent intracellular survival of Neisseria gonorrhoeae within cervical epithelial cells*. Infect Immun, 2010. 78(6): p. 2429-37.
 77. Woodhams, K.L., et al., *Prevalence and detailed mapping of the gonococcal genetic island in Neisseria meningitidis*. J Bacteriol, 2012. 194(9): p. 2275-85.
 78. Zweig, M.A., et al., *Secreted single-stranded DNA is involved in the initial phase of biofilm formation by Neisseria gonorrhoeae*. Environ Microbiol, 2013.
 79. Proft, T. and E.N. Baker, *Pili in Gram-negative and Gram-positive bacteria - structure, assembly and their role in disease*. Cell Mol Life Sci, 2009. 66(4): p. 613-35.
 80. Jarrell, K.F. and S.V. Albers, *The archaellum: an old motility structure with a new name*. Trends Microbiol, 2012. 20(7): p. 307-12.
 81. Nudleman, E. and D. Kaiser, *Pulling together with type IV pili*. J Mol Microbiol Biotechnol, 2004. 7(1-2): p. 52-62.
-

82. Peabody, C.R., et al., *Type II protein secretion and its relationship to bacterial type IV pili and archaeal flagella*. Microbiology, 2003. 149(Pt 11): p. 3051-72.
 83. Skerker, J.M. and H.C. Berg, *Direct observation of extension and retraction of type IV pili*. Proc Natl Acad Sci U S A, 2001. 98(12): p. 6901-4.
 84. Merz, A.J., M. So, and M.P. Sheetz, *Pilus retraction powers bacterial twitching motility*. Nature, 2000. 407(6800): p. 98-102.
 85. Shahapure, R., et al., *The archaellum: a rotating type IV pilus*. Mol Microbiol, 2014. 91(4): p. 716-23.
 86. Barken, K.B., et al., *Roles of type IV pili, flagellum-mediated motility and extracellular DNA in the formation of mature multicellular structures in Pseudomonas aeruginosa biofilms*. Environ Microbiol, 2008. 10(9): p. 2331-43.
 87. Jurcisek, J.A. and L.O. Bakaletz, *Biofilms formed by nontypeable Haemophilus influenzae in vivo contain both double-stranded DNA and type IV pilin protein*. J Bacteriol, 2007. 189(10): p. 3868-75.
 88. Luke, N.R., et al., *Contribution of Moraxella catarrhalis type IV pili to nasopharyngeal colonization and biofilm formation*. Infect Immun, 2007. 75(12): p. 5559-64.
 89. Lang, E., et al., *Identification of neisserial DNA binding components*. Microbiology, 2009. 155(Pt 3): p. 852-62.
 90. Jonsson, A.B., G. Nyberg, and S. Normark, *Phase variation of gonococcal pili by frameshift mutation in pilC, a novel gene for pilus assembly*. EMBO J, 1991. 10(2): p. 477-88.
 91. Jonsson, A.B., M. Rahman, and S. Normark, *Pilus biogenesis gene, pilC, of Neisseria gonorrhoeae: pilC1 and pilC2 are each part of a larger duplication of the gonococcal genome and share upstream and downstream homologous sequences with opa and pil loci*. Microbiology, 1995. 141 (Pt 10): p. 2367-77.
 92. Rahman, M., et al., *PilC of pathogenic Neisseria is associated with the bacterial cell surface*. Mol Microbiol, 1997. 25(1): p. 11-25.
 93. Rudel, T., et al., *Role of pili and the phase-variable PilC protein in natural competence for transformation of Neisseria gonorrhoeae*. Proc Natl Acad Sci U S A, 1995. 92(17): p. 7986-90.
 94. Rudel, T., I. Scheurerpflug, and T.F. Meyer, *Neisseria PilC protein identified as type-4 pilus tip-located adhesin*. Nature, 1995. 373(6512): p. 357-9.
 95. Freitag, N.E., H.S. Seifert, and M. Koomey, *Characterization of the pilF-pilD pilus-assembly locus of Neisseria gonorrhoeae*. Mol Microbiol, 1995. 16(3): p. 575-86.
 96. Dupuy, B. and A.P. Pugsley, *Type IV prepilin peptidase gene of Neisseria gonorrhoeae MS11: presence of a related gene in other piliated and nonpiliated Neisseria strains*. J Bacteriol, 1994. 176(5): p. 1323-31.
 97. Parge, H.E., et al., *Structure of the fibre-forming protein pilin at 2.6 Å resolution*. Nature, 1995. 378(6552): p. 32-8.
-

98. Jakovljevic, V., et al., *PilB and PilT are ATPases acting antagonistically in type IV pilus function in Myxococcus xanthus*. J Bacteriol, 2008. 190(7): p. 2411-21.
 99. Tonjum, T., et al., *Identification and characterization of pilG, a highly conserved pilus-assembly gene in pathogenic Neisseria*. Mol Microbiol, 1995. 16(3): p. 451-64.
 100. Collins, R.F., M. Saleem, and J.P. Derrick, *Purification and three-dimensional electron microscopy structure of the Neisseria meningitidis type IV pilus biogenesis protein PilG*. J Bacteriol, 2007. 189(17): p. 6389-96.
 101. Carbonnelle, E., et al., *A systematic genetic analysis in Neisseria meningitidis defines the Pil proteins required for assembly, functionality, stabilization and export of type IV pili*. Mol Microbiol, 2006. 61(6): p. 1510-22.
 102. Karuppiah, V. and J.P. Derrick, *Structure of the PilM-PilN inner membrane type IV pilus biogenesis complex from Thermus thermophilus*. J Biol Chem, 2011. 286(27): p. 24434-42.
 103. Sampaleanu, L.M., et al., *Periplasmic domains of Pseudomonas aeruginosa PilN and PilO form a stable heterodimeric complex*. J Mol Biol, 2009. 394(1): p. 143-59.
 104. Tammam, S., et al., *Characterization of the PilN, PilO and PilP type IVa pilus subcomplex*. Mol Microbiol, 2011. 82(6): p. 1496-514.
 105. Jain, S., et al., *Structural characterization of outer membrane components of the type IV pilus system in pathogenic Neisseria*. PLoS One, 2011. 6(1): p. e16624.
 106. Haas, R. and T.F. Meyer, *The repertoire of silent pilus genes in Neisseria gonorrhoeae: evidence for gene conversion*. Cell, 1986. 44(1): p. 107-15.
 107. Wolfgang, M., et al., *PilT mutations lead to simultaneous defects in competence for natural transformation and twitching motility in piliated Neisseria gonorrhoeae*. Mol Microbiol, 1998. 29(1): p. 321-30.
 108. Wolfgang, M., et al., *Suppression of an absolute defect in type IV pilus biogenesis by loss-of-function mutations in pilT, a twitching motility gene in Neisseria gonorrhoeae*. Proc Natl Acad Sci U S A, 1998. 95(25): p. 14973-8.
 109. Kurre, R., et al., *PilT2 enhances the speed of gonococcal type IV pilus retraction and of twitching motility*. Mol Microbiol, 2012. 86(4): p. 857-65.
 110. Winther-Larsen, H.C., et al., *Neisseria gonorrhoeae PilV, a type IV pilus-associated protein essential to human epithelial cell adherence*. Proc Natl Acad Sci U S A, 2001. 98(26): p. 15276-81.
 111. Helaine, S., et al., *PilX, a pilus-associated protein essential for bacterial aggregation, is a key to pilus-facilitated attachment of Neisseria meningitidis to human cells*. Mol Microbiol, 2005. 55(1): p. 65-77.
 112. Helaine, S., et al., *3D structure/function analysis of PilX reveals how minor pilins can modulate the virulence properties of type IV pili*. Proc Natl Acad Sci U S A, 2007. 104(40): p. 15888-93.
-

113. Wolfgang, M., et al., *The comP locus of Neisseria gonorrhoeae encodes a type IV prepilin that is dispensable for pilus biogenesis but essential for natural transformation*. Mol Microbiol, 1999. 31(5): p. 1345-57.
 114. Cehovin, A., et al., *Specific DNA recognition mediated by a type IV pilin*. Proc Natl Acad Sci U S A, 2013. 110(8): p. 3065-70.
 115. Carbonnelle, E., et al., *Type IV pilus biogenesis in Neisseria meningitidis: PilW is involved in a step occurring after pilus assembly, essential for fibre stability and function*. Mol Microbiol, 2005. 55(1): p. 54-64.
 116. Strom, M.S. and S. Lory, *Structure-function and biogenesis of the type IV pili*. Annu Rev Microbiol, 1993. 47: p. 565-96.
 117. Nunn, D.N. and S. Lory, *Product of the Pseudomonas aeruginosa gene pilD is a prepilin leader peptidase*. Proc Natl Acad Sci U S A, 1991. 88(8): p. 3281-5.
 118. Strom, M.S., D. Nunn, and S. Lory, *Multiple roles of the pilus biogenesis protein pilD: involvement of pilD in excretion of enzymes from Pseudomonas aeruginosa*. J Bacteriol, 1991. 173(3): p. 1175-80.
 119. Thanassi, D.G., J.B. Bliska, and P.J. Christie, *Surface organelles assembled by secretion systems of Gram-negative bacteria: diversity in structure and function*. FEMS Microbiol Rev, 2012. 36(6): p. 1046-82.
 120. Kim, S.R. and T. Komano, *The plasmid R64 thin pilus identified as a type IV pilus*. J Bacteriol, 1997. 179(11): p. 3594-603.
 121. Craig, L., M.E. Pique, and J.A. Tainer, *Type IV pilus structure and bacterial pathogenicity*. Nat Rev Microbiol, 2004. 2(5): p. 363-78.
 122. Craig, L., et al., *Type IV pilin structure and assembly: X-ray and EM analyses of Vibrio cholerae toxin-coregulated pilus and Pseudomonas aeruginosa PAK pilin*. Mol Cell, 2003. 11(5): p. 1139-50.
 123. Giltner, C.L., Y. Nguyen, and L.L. Burrows, *Type IV pilin proteins: versatile molecular modules*. Microbiol Mol Biol Rev, 2012. 76(4): p. 740-72.
 124. Craig, L., et al., *Type IV pilus structure by cryo-electron microscopy and crystallography: implications for pilus assembly and functions*. Mol Cell, 2006. 23(5): p. 651-62.
 125. Ramphal, R., et al., *Role of pili in the adherence of Pseudomonas aeruginosa to injured tracheal epithelium*. Infect Immun, 1984. 44(1): p. 38-40.
 126. Kirn, T.J., et al., *Delineation of pilin domains required for bacterial association into microcolonies and intestinal colonization by Vibrio cholerae*. Mol Microbiol, 2000. 35(4): p. 896-910.
 127. Biais, N., et al., *Force-dependent polymorphism in type IV pili reveals hidden epitopes*. Proc Natl Acad Sci U S A, 2010. 107(25): p. 11358-63.
-

128. Hobbs, M. and J.S. Mattick, *Common components in the assembly of type 4 fimbriae, DNA transfer systems, filamentous phage and protein-secretion apparatus: a general system for the formation of surface-associated protein complexes*. Mol Microbiol, 1993. 10(2): p. 233-43.
 129. Nunn, D., S. Bergman, and S. Lory, *Products of three accessory genes, pilB, pilC, and pilD, are required for biogenesis of Pseudomonas aeruginosa pili*. J Bacteriol, 1990. 172(6): p. 2911-9.
 130. Chiang, P., M. Habash, and L.L. Burrows, *Disparate subcellular localization patterns of Pseudomonas aeruginosa Type IV pilus ATPases involved in twitching motility*. J Bacteriol, 2005. 187(3): p. 829-39.
 131. Iyer, L.M., et al., *Evolutionary history and higher order classification of AAA+ ATPases*. J Struct Biol, 2004. 146(1-2): p. 11-31.
 132. Rivas, S., et al., *TrwD, a protein encoded by the IncW plasmid R388, displays an ATP hydrolase activity essential for bacterial conjugation*. J Biol Chem, 1997. 272(41): p. 25583-90.
 133. Aukema, K.G., et al., *Functional dissection of a conserved motif within the pilus retraction protein PilT*. J Bacteriol, 2005. 187(2): p. 611-8.
 134. Chiang, P., et al., *Functional role of conserved residues in the characteristic secretion NTPase motifs of the Pseudomonas aeruginosa type IV pilus motor proteins PilB, PilT and PilU*. Microbiology, 2008. 154(Pt 1): p. 114-26.
 135. Satyshur, K.A., et al., *Crystal structures of the pilus retraction motor PilT suggest large domain movements and subunit cooperation drive motility*. Structure, 2007. 15(3): p. 363-76.
 136. Whitchurch, C.B., et al., *Characterisation of a Pseudomonas aeruginosa twitching motility gene and evidence for a specialised protein export system widespread in eubacteria*. Gene, 1991. 101(1): p. 33-44.
 137. Biais, N., et al., *Cooperative retraction of bundled type IV pili enables nanonewton force generation*. PLoS Biol, 2008. 6(4): p. e87.
 138. Abendroth, J., et al., *The three-dimensional structure of the cytoplasmic domains of EpsF from the type 2 secretion system of Vibrio cholerae*. J Struct Biol, 2009. 166(3): p. 303-15.
 139. Kolappan, S. and L. Craig, *Structure of the cytoplasmic domain of TcpE, the inner membrane core protein required for assembly of the Vibrio cholerae toxin-coregulated pilus*. Acta Crystallogr D Biol Crystallogr, 2013. 69(Pt 4): p. 513-9.
 140. Karuppiah, V., et al., *Structure and oligomerization of the PilC type IV pilus biogenesis protein from Thermus thermophilus*. Proteins, 2010. 78(9): p. 2049-57.
 141. Takhar, H.K., et al., *The platform protein is essential for type IV pilus biogenesis*. J Biol Chem, 2013. 288(14): p. 9721-8.
 142. Wu, S.S., J. Wu, and D. Kaiser, *The Myxococcus xanthus pilT locus is required for social gliding motility although pili are still produced*. Mol Microbiol, 1997. 23(1): p. 109-21.
-

143. Ayers, M., et al., *PilM/N/O/P proteins form an inner membrane complex that affects the stability of the Pseudomonas aeruginosa type IV pilus secretin*. J Mol Biol, 2009. 394(1): p. 128-42.
 144. Friedrich, C., I. Bulyha, and L. Sogaard-Andersen, *Outside-in assembly pathway of the type IV pilus system in Myxococcus xanthus*. J Bacteriol, 2014. 196(2): p. 378-90.
 145. Rumszauer, J., C. Schwarzenlander, and B. Averhoff, *Identification, subcellular localization and functional interactions of PilMNOWQ and PilA4 involved in transformation competency and pilus biogenesis in the thermophilic bacterium Thermus thermophilus HB27*. FEBS J, 2006. 273(14): p. 3261-72.
 146. van den Ent, F., L.A. Amos, and J. Lowe, *Prokaryotic origin of the actin cytoskeleton*. Nature, 2001. 413(6851): p. 39-44.
 147. van den Ent, F. and J. Lowe, *Crystal structure of the cell division protein FtsA from Thermotoga maritima*. EMBO J, 2000. 19(20): p. 5300-7.
 148. Karupiah, V., et al., *Structure and assembly of an inner membrane platform for initiation of type IV pilus biogenesis*. Proc Natl Acad Sci U S A, 2013. 110(48): p. E4638-47.
 149. Georgiadou, M., et al., *Large-scale study of the interactions between proteins involved in type IV pilus biology in Neisseria meningitidis: characterization of a subcomplex involved in pilus assembly*. Mol Microbiol, 2012. 84(5): p. 857-73.
 150. Berry, J.L., et al., *Structure and assembly of a trans-periplasmic channel for type IV pili in Neisseria meningitidis*. PLoS Pathog, 2012. 8(9): p. e1002923.
 151. Ast, V.M., et al., *Expression of the ExeAB complex of Aeromonas hydrophila is required for the localization and assembly of the ExeD secretion port multimer*. Mol Microbiol, 2002. 44(1): p. 217-31.
 152. Strozen, T.G., et al., *Involvement of the GspAB complex in assembly of the type II secretion system secretin of Aeromonas and Vibrio species*. J Bacteriol, 2011. 193(9): p. 2322-31.
 153. Howard, S.P., et al., *Interactions between peptidoglycan and the ExeAB complex during assembly of the type II secretin of Aeromonas hydrophila*. Mol Microbiol, 2006. 59(3): p. 1062-72.
 154. Li, G. and S.P. Howard, *ExeA binds to peptidoglycan and forms a multimer for assembly of the type II secretion apparatus in Aeromonas hydrophila*. Mol Microbiol, 2010. 76(3): p. 772-81.
 155. Semmler, A.B., et al., *Identification of a novel gene, fimV, involved in twitching motility in Pseudomonas aeruginosa*. Microbiology, 2000. 146 (Pt 6): p. 1321-32.
 156. Wehbi, H., et al., *The peptidoglycan-binding protein FimV promotes assembly of the Pseudomonas aeruginosa type IV pilus secretin*. J Bacteriol, 2011. 193(2): p. 540-50.
 157. Garvey, K.J., M.S. Saedi, and J. Ito, *Nucleotide sequence of Bacillus phage phi 29 genes 14 and 15: homology of gene 15 with other phage lysozymes*. Nucleic Acids Res, 1986. 14(24): p. 10001-8.
-

158. Buist, G., et al., *LysM, a widely distributed protein motif for binding to (peptido)glycans*. Mol Microbiol, 2008. 68(4): p. 838-47.
 159. Bateman, A. and M. Bycroft, *The structure of a LysM domain from E. coli membrane-bound lytic murein transglycosylase D (MltD)*. J Mol Biol, 2000. 299(4): p. 1113-9.
 160. Steen, A., et al., *Cell wall attachment of a widely distributed peptidoglycan binding domain is hindered by cell wall constituents*. J Biol Chem, 2003. 278(26): p. 23874-81.
 161. Bitter, W., et al., *Formation of oligomeric rings by XcpQ and PilQ, which are involved in protein transport across the outer membrane of Pseudomonas aeruginosa*. Mol Microbiol, 1998. 27(1): p. 209-19.
 162. Nouwen, N., et al., *Domain structure of secretin PulD revealed by limited proteolysis and electron microscopy*. EMBO J, 2000. 19(10): p. 2229-36.
 163. Burghout, P., et al., *Structure and electrophysiological properties of the YscC secretin from the type III secretion system of Yersinia enterocolitica*. J Bacteriol, 2004. 186(14): p. 4645-54.
 164. Chami, M., et al., *Structural insights into the secretin PulD and its trypsin-resistant core*. J Biol Chem, 2005. 280(45): p. 37732-41.
 165. Guilvout, I., et al., *Genetic dissection of the outer membrane secretin PulD: are there distinct domains for multimerization and secretion specificity?* J Bacteriol, 1999. 181(23): p. 7212-20.
 166. Nouwen, N., et al., *Secretin PulD: association with pilot PulS, structure, and ion-conducting channel formation*. Proc Natl Acad Sci U S A, 1999. 96(14): p. 8173-7.
 167. Reichow, S.L., et al., *Structure of the cholera toxin secretion channel in its closed state*. Nat Struct Mol Biol, 2010. 17(10): p. 1226-32.
 168. Korotkov, K.V., et al., *Crystal structure of the N-terminal domain of the secretin GspD from ETEC determined with the assistance of a nanobody*. Structure, 2009. 17(2): p. 255-65.
 169. Spreter, T., et al., *A conserved structural motif mediates formation of the periplasmic rings in the type III secretion system*. Nat Struct Mol Biol, 2009. 16(5): p. 468-76.
 170. Hodgkinson, J.L., et al., *Three-dimensional reconstruction of the Shigella T3SS transmembrane regions reveals 12-fold symmetry and novel features throughout*. Nat Struct Mol Biol, 2009. 16(5): p. 477-85.
 171. Opalka, N., et al., *Structure of the filamentous phage pIV multimer by cryo-electron microscopy*. J Mol Biol, 2003. 325(3): p. 461-70.
 172. Collins, R.F., et al., *Three-dimensional structure of the Neisseria meningitidis secretin PilQ determined from negative-stain transmission electron microscopy*. J Bacteriol, 2003. 185(8): p. 2611-7.
 173. Swanson, J., *Studies on gonococcus infection. II. Freeze-fracture, freeze-etch studies on gonococci*. J Exp Med, 1972. 136(5): p. 1258-71.
 174. Black, W.J., et al., *Characterization of Neisseria gonorrhoeae protein II phase variation by use of monoclonal antibodies*. Infect Immun, 1984. 45(2): p. 453-7.
-

175. Siewering, K., et al., *Peptidoglycan-binding protein TsaP functions in surface assembly of type IV pili*. Proc Natl Acad Sci U S A, 2014. 111(10): p. E953-61.
 176. Pachulec, E. and C. van der Does, *Conjugative plasmids of Neisseria gonorrhoeae*. PLoS One, 2010. 5(4): p. e9962.
 177. Dillard, J.P., *Genetic Manipulation of Neisseria gonorrhoeae*. Curr Protoc Microbiol, 2011. Chapter 4: p. Unit4A 2.
 178. Moll, A., et al., *DipM, a new factor required for peptidoglycan remodelling during cell division in Caulobacter crescentus*. Mol Microbiol, 2010. 77(1): p. 90-107.
 179. Hancock, R.E. and H. Nikaido, *Outer membranes of gram-negative bacteria. XIX. Isolation from Pseudomonas aeruginosa PAO1 and use in reconstitution and definition of the permeability barrier*. J Bacteriol, 1978. 136(1): p. 381-90.
 180. Kahnt, J., et al., *Profiling the outer membrane proteome during growth and development of the social bacterium Myxococcus xanthus by selective biotinylation and analyses of outer membrane vesicles*. J Proteome Res, 2010. 9(10): p. 5197-208.
 181. Bubendorfer, S., et al., *Specificity of motor components in the dual flagellar system of Shewanella putrefaciens CN-32*. Mol Microbiol, 2012. 83(2): p. 335-50.
 182. Huntley, S., et al., *Comparative genomic analysis of fruiting body formation in Myxococcales*. Mol Biol Evol, 2011. 28(2): p. 1083-97.
 183. Jain, S., et al., *Characterization of the single stranded DNA binding protein SsbB encoded in the Gonococcal Genetic Island*. PLoS One, 2012. 7(4): p. e35285.
 184. Whitchurch, C.B., et al., *Extracellular DNA required for bacterial biofilm formation*. Science, 2002. 295(5559): p. 1487.
 185. Moscoso, M., E. Garcia, and R. Lopez, *Biofilm formation by Streptococcus pneumoniae: role of choline, extracellular DNA, and capsular polysaccharide in microbial accretion*. J Bacteriol, 2006. 188(22): p. 7785-95.
 186. Thomas, V.C., et al., *Regulation of autolysis-dependent extracellular DNA release by Enterococcus faecalis extracellular proteases influences biofilm development*. J Bacteriol, 2008. 190(16): p. 5690-8.
 187. Rice, K.C., et al., *The cidA murein hydrolase regulator contributes to DNA release and biofilm development in Staphylococcus aureus*. Proc Natl Acad Sci U S A, 2007. 104(19): p. 8113-8.
 188. Lappann, M., et al., *A dual role of extracellular DNA during biofilm formation of Neisseria meningitidis*. Mol Microbiol, 2010. 75(6): p. 1355-71.
 189. Steichen, C.T., et al., *The Neisseria gonorrhoeae biofilm matrix contains DNA, and an endogenous nuclease controls its incorporation*. Infect Immun, 2011. 79(4): p. 1504-11.
 190. Frye, S.A., et al., *Topology of the outer-membrane secretin PilQ from Neisseria meningitidis*. Microbiology, 2006. 152(Pt 12): p. 3751-64.
-

191. Collins, R.F., et al., *Analysis of the PilQ secretin from Neisseria meningitidis by transmission electron microscopy reveals a dodecameric quaternary structure*. J Bacteriol, 2001. 183(13): p. 3825-32.
 192. Collins, R.F., et al., *Structure of the Neisseria meningitidis outer membrane PilQ secretin complex at 12 Å resolution*. J Biol Chem, 2004. 279(38): p. 39750-6.
 193. Koster, M., et al., *The outer membrane component, YscC, of the Yop secretion machinery of Yersinia enterocolitica forms a ring-shaped multimeric complex*. Mol Microbiol, 1997. 26(4): p. 789-97.
 194. Balasingham, S.V., et al., *Interactions between the lipoprotein PilP and the secretin PilQ in Neisseria meningitidis*. J Bacteriol, 2007. 189(15): p. 5716-27.
 195. Hu, Y., et al., *Proteome analysis of Neisseria meningitidis serogroup strains C associated with outbreaks in China*. Biomed Environ Sci, 2010. 23(4): p. 251-8.
 196. van der Does, C., et al., *SecA is an intrinsic subunit of the Escherichia coli preprotein translocase and exposes its carboxyl terminus to the periplasm*. Mol Microbiol, 1996. 22(4): p. 619-29.
 197. Swim, S.C., et al., *Strain distribution in extents of lysozyme resistance and O-acetylation of gonococcal peptidoglycan determined by high-performance liquid chromatography*. Infect Immun, 1983. 42(2): p. 446-52.
 198. de Souza, A.L. and A.C. Seguro, *Two centuries of meningococcal infection: from Vieusseux to the cellular and molecular basis of disease*. J Med Microbiol, 2008. 57(Pt 11): p. 1313-21.
 199. Remis, J.P., et al., *Bacterial social networks: structure and composition of Myxococcus xanthus outer membrane vesicle chains*. Environ Microbiol, 2013.
 200. Wolfgang, M., et al., *Components and dynamics of fiber formation define a ubiquitous biogenesis pathway for bacterial pili*. EMBO J, 2000. 19(23): p. 6408-18.
 201. Martinez, R.M., et al., *Role of FlgT in anchoring the flagellum of Vibrio cholerae*. J Bacteriol, 2010. 192(8): p. 2085-92.
 202. Terashima, H., et al., *The flagellar basal body-associated protein FlgT is essential for a novel ring structure in the sodium-driven Vibrio motor*. J Bacteriol, 2010. 192(21): p. 5609-15.
 203. Terashima, H., et al., *Insight into the assembly mechanism in the supramolecular rings of the sodium-driven Vibrio flagellar motor from the structure of FlgT*. Proc Natl Acad Sci U S A, 2013. 110(15): p. 6133-8.
 204. Shen, A., et al., *Simplified, enhanced protein purification using an inducible, autoprocessing enzyme tag*. PLoS One, 2009. 4(12): p. e8119.
 205. Wittig, I., H.P. Braun, and H. Schagger, *Blue native PAGE*. Nat Protoc, 2006. 1(1): p. 418-28.
 206. Overbeek, R., et al., *The use of gene clusters to infer functional coupling*. Proc Natl Acad Sci U S A, 1999. 96(6): p. 2896-901.
-

207. Salgado, H., et al., *Operons in Escherichia coli: genomic analyses and predictions*. Proc Natl Acad Sci U S A, 2000. 97(12): p. 6652-7.
 208. Atmakuri, K., et al., *Agrobacterium ParA/MinD-like VirC1 spatially coordinates early conjugative DNA transfer reactions*. EMBO J, 2007. 26(10): p. 2540-51.
 209. Gloag, E.S., et al., *Self-organization of bacterial biofilms is facilitated by extracellular DNA*. Proc Natl Acad Sci U S A, 2013. 110(28): p. 11541-6.
 210. Clausen, M., et al., *High-force generation is a conserved property of type IV pilus systems*. J Bacteriol, 2009. 191(14): p. 4633-8.
 211. Maier, B., et al., *Single pilus motor forces exceed 100 pN*. Proc Natl Acad Sci U S A, 2002. 99(25): p. 16012-7.
 212. Tonjum, T., et al., *Structure and function of repetitive sequence elements associated with a highly polymorphic domain of the Neisseria meningitidis PilQ protein*. Mol Microbiol, 1998. 29(1): p. 111-24.
 213. Douzi, B., et al., *Deciphering the Xcp Pseudomonas aeruginosa type II secretion machinery through multiple interactions with substrates*. J Biol Chem, 2011. 286(47): p. 40792-801.
-

V Supplementary Data

Table 46 is only part of the printed version and not of the electronic version of the thesis.

Tabelle 46 ist nur Bestandteil der gedruckten Version, jedoch kein Bestandteil der Online-Veröffentlichung.

Table 46 Reciprocal blast analysis of the 450 genomes of proteobacteria

The table describes the outcomes of the reciprocal blast analysis of 450 genomes. The table depicts for each organism its name, superkingdom, phylum and class, and whether or not a T4PS was identified. For all analyzed proteins, the names of the first (outSubj) and second (retSubj) blast and the respective E-value are depicted. It is also depicted whether, based on the criteria, the protein was identified. The first sign identifies whether a protein was identified that fit the criteria in the initial blast (outSubj) of the protein (no = -, yes = +). The second sign indicates whether the reblast of the identified protein against the original genome (retSubj) identified the initial protein (no = -, yes = +). [The table was generated according to the reciprocal blast analysis which was performed by Dr. S. Huntley]

VI Acknowledgments

The current page (acknowledgments) contains personal data, thus is not part of the electronic version of the thesis.

Diese Seite (Danksagung) enthält persönliche Daten. Sie ist deshalb nicht Bestandteil der Online-Veröffentlichung.

VII Curriculum Vitae

The current page (CV) contains personal data, thus is not part of the electronic version of the thesis.

Diese Seite (Lebenslauf) enthält persönliche Daten. Sie ist deshalb nicht Bestandteil der Online-Veröffentlichung.

The current page (CV) contains personal data, thus is not part of the electronic version of the thesis.

Diese Seite (Lebenslauf) enthält persönliche Daten. Sie ist deshalb nicht Bestandteil der Online-Veröffentlichung.

VIII Erklärung

Hiermit versichere ich, dass ich die vorliegende Dissertation mit dem Titel

„One ring to rule them all: Identification and characterization of the type IV pili secretin associated protein Tsap and analysis of the type IV secretion system of *Neisseria gonorrhoeae*“

selbstständig verfasst, keine anderen als die im Text angegebenen Hilfsmittel verwendet und sämtliche Stellen, die im Wortlaut oder dem Sinn nach anderen Werken entnommen sind, mit Quellenangaben kenntlich gemacht habe.

Die Dissertation wurde in der jetzigen oder einer ähnlichen Form noch bei keiner anderen Hochschule eingereicht und hat noch keinen sonstigen Prüfungszwecken gedient.

Marburg,

Ort, Datum

Katja Siewering
